TECHNICAL REPORT

SHOCK-TUBE STUDIES OF N^+ AND O^+ RECOMBINATION RADIATION IN THE VACUUM ULTRAVIOLET

By: Paul V. Marrone, Walter H. Wurster and John E. Stratton

CAL No. AG-1729-A-7

Prepared for:

National Aeronautics and Space Administration
Fluid Physics Branch, Research Division
Office of Advanced Research and Technology
Washington, D.C. 20456

FINAL REPORT
Contract No. NASr-119
Study of Reentry Radiation and Airflow
June 1968

CORNELL AERONAUTICAL LABORATORY, INC.
OF CORNELL UNIVERSITY, BUFFALO, N. Y. 14221

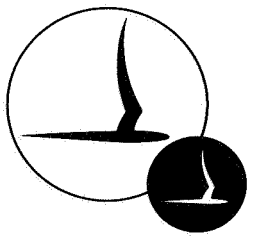

CORNELL AERONAUTICAL LABORATORY, INC.
BUFFALO, NEW YORK 14221

SHOCK-TUBE STUDIES OF N^+ AND O^+ RECOMBINATION RADIATION IN THE VACUUM ULTRAVIOLET

FINAL REPORT

CAL REPORT NO. AG-1729-A-7

CONTRACT NO. NASr-119

STUDY OF REENTRY RADIATION AND AIRFLOW

JUNE 1968

Prepared For:

NATIONAL AERONAUTICS AND SPACE ADMINISTRATION
WASHINGTON, D.C. 20546

PREPARED BY: Paul V. Marrone
Paul V. Marrone

Walter H. Wurster
Walter H. Wurster

John E. Stratton
John E. Stratton

APPROVED BY: Charles E Treanor
Charles E. Treanor, Assistant Head
Aerodynamic Research Department

FOREWORD

A research program to determine the nonequilibrium flow field and optical radiation associated with high-speed entry vehicles was initiated at the Cornell Aeronautical Laboratory in June 1962. This program has been supported throughout by the National Aeronautics and Space Administration Headquarters, Washington, D. C., under Contract NASr-119. Early in the program, considerable effort was directed toward the investigation of equilibrium and nonequilibrium shock layer flow, vibrational relaxation phenomena at high temperatures and shock wave structure. The results of these studies have been documented in previous publications which are listed chronologically below.

A table of equilibrium conditions behind normal shock waves in air, applicable to bow-shock conditions during Apollo reentry, is presented in publication 1. The details of the research work on vibration-dissociation coupling that was performed under this contract are given in Pubs. 1, 3, and 8 and were reported in an invited paper at the American Physical Society meeting (Pub. 5). Diffusion of dissociated species and vibrationally excited species behind shock waves is described in Pubs. 4 and 6. The theoretical work related to calculation of vibrational transition probabilities using time-dependent wave functions is described in Pubs. 10 and 12. A method of calculating 3-dimensional flow fields using the inverse technique is reported in Pub. 11. A numerical integration technique that was developed under this contract and which was especally useful for calculation of chemically reacting flows is given in Pub. 7.

Since 1965, the emphasis of the research program has been directed toward the development of a capability to obtain experimental measurements of vacuum-ultraviolet radiation from shock-heated gases at high temperature. The present report documents this last phase of the program and also serves as the final report for contract NASr-119. The development of the experimental facility described in this report was discussed in two presentations, Pubs. 9 and 13.

Reports and Papers Published Under Contract NASr-119

1. Treanor, C. E., "Vibrational Relaxation Effects in Dissociation Rate-Constant Measurements," CAL Report AG-1729-A-1 (August 1962).

2. Marrone, P. V., "Normal Shock Waves in Air: Equilibrium Composition and Flow Parameters for Velocities from 26,000 to 50,000 ft/sec," CAL Report AG-1729-A-2 (August 1962).

3. Treanor, C. E. and Marrone, P. V., "Vibration and Dissociation Coupling Behind Strong Shock Waves." Proceedings of the AFOSR-GE Symposium on Dynamics of Manned Lifting Planetary Entry. Philadelphia, October 1962. John Wiley & Son, New York 1963.

4. Gibson, W. E., "The Effect of Ambient Dissociation and Species Diffusion on Nonequilibrium Shock Layers." IAS Paper No. 63-70. Presented at 31st IAS Annual Meeting, New York. January 1963.

5. Treanor, C. E., "Structure of Shock Waves in Chemically Reacting Gases." Paper S2, Bulletin of APS, Vol. 8, Number 5, p. 440, 1963. Presented at American Physical Society Meeting, Buffalo, New York, June 1963.

6. Gibson, W. E. and Buckmaster, J. D., "The Effect of Species Diffusion and Heat Conduction on Nonequilibrium Flows Behind Strong Shocks." CAL Report AG-1729-A-3 (October 1963); also AIAA Journal, Vol. 2, No. 10, pp. 1681-1688 (October 1964).

7. Treanor, C. E., "A Method for the Numerical Integration of Coupled First-Order Differential Equations with Greatly Different Time Constants." CAL Report AG-1729-A-4 (January 1964); also Mathematics of Computation, Vol. 20, No. 93, pp. 39-45 (January 1966).

8. Treanor, C. E., "Coupling of Vibration and Dissociation in Gasdynamic Flows." AIAA Paper No. 65-29. Presented at AIAA 2nd Aerospace Sciences Meeting, New York. January 1965.

9. Wurster, W. H., "Shock Tube Spectroscopy in the Vacuum Ultraviolet." Presented at the 5th International Shock Tube Symposium, Naval Ordnance Lab., Silver Springs, Maryland. April 1965.

10. Treanor, C. E., "Vibrational Energy Transfer in High Energy Collisions." CAL Report AG-1729-A-5 (May 1965), also NASA CR-291 (August 1965); also J. Chem. Phys. Vol. 43, No. 2, p. 532 (15 July 1965).

11. Joss, W. W., "Application of the Inverse Technique in the Flow Over a Blunt Body at Angle of Attack." CAL Report AG-1729-A-6 (December 1965); also NASA CR-445 (April 1966).

12. Treanor, C. E., "Transition Probabilities for the Forced Harmonic Oscillator." J. Chem. Phys. Vol. 44, No. 5, pp. 2220-2221 (1 March 1966).

13. Wurster, W. H., "Measurements of the Radiation From Shock-Heated Nitrogen and Argon at Wavelengths Below 1200Å." Presented at 3rd Meeting on Interdisciplinary Aspects of Radiative Transfer; Radiation Coupled Flows." Lockheed Palo Alto Research Laboratory, February 1967.

ABSTRACT

Spectrally resolved vacuum ultraviolet radiation measurements of the continuum arising from the recombination of electrons with N^+ and O^+ ions have been made using a high-purity shock tube to generate the radiating source. Mixtures of neon and nitrogen or oxygen were used as the test gas, with the radiation observed behind the reflected-shock wave at temperatures of 11,000°K to 13,000°K. Since the radiation under investigation occurs at wavelengths less than 1100Å, the use of windows is precluded. An explosively driven windowless plunger couples the shock tube to a vacuum ultraviolet spectrometer which has three bare stainless-steel photomultipliers as detectors. The development of the plunger-detector system is described in detail. Discussions of the problems encountered in an experiment of this type are presented. In particular, the problems of purity level of the gas handling system, the long ionization relaxation times involved with N_2 and O_2 heavily diluted with neon, the gasdynamics of the windowless plunger and the effects of nonequilibrium on the state of the gas are considered in some detail.

Experiments were performed for both N_2 - Ne and O_2 - Ne mixtures wherein the shocked gas ranged from optically thin to blackbody conditions for the VUV wavelength range. Photoionization cross sections for both N and O were obtained and are shown to compare favorably with theoretical calculations. The results demonstrate the usefulness of this shock-tube technique for absolute spectral radiation measurements in the windowless region of the vacuum ultraviolet.

TABLE OF CONTENTS

I. INTRODUCTION

Interest in the radiative properties of the shock-heated air comprising the gas-cap of vehicles entering the earth's atmosphere at high velocities has provided a stimulus for research in quantitative spectroscopy of the optically active species involved. For suborbital entry speeds, the radiation is dominated by the molecular species of the heated air; and, in general, the energy associated with the radiation is not significant relative to the convective heat loads sustained by the vehicle. However, at entry velocities associated with return from lunar and planetary missions (11 to 20 km/sec), the flow in the gas-cap region of a blunt vehicle will reach high pressure and temperature levels. Equilibrium temperatures in excess of 10,000°K are encountered, the molecular species are almost completely dissociated, and the shocked gas is composed chiefly of atoms, ions and electrons. The emission spectrum is now dominated by line radiation and the continua resulting from the recombination of ions and electrons. Such recombination to the ground states of oxygen and nitrogen atoms gives rise to radiation in the vacuum ultraviolet region of the spectrum at wavelengths below 1200 angstroms. Coupled with the attendant shift of the blackbody spectrum to shorter wavelengths at these higher temperatures, this portion of the spectrum becomes a significant feature of gas-cap radiation in superorbital entry.

Computation of the radiative heating to a high speed vehicle involves a consideration of several complex physical processes including emission in the vacuum-ultraviolet region, radiative cooling and reabsorption in the shock layer around the vehicle, and an assessment of the importance of radiation in coupling to the convective heat load. There have been numerous theoretical predictions of this high speed radiation heat transfer utilizing gasdynamic and radiative transport models with varying degrees of complexity (Refs 1-8). In general, these studies have shown that the contribution at wavelengths below about 1500Å (both atomic lines and recombination continuum) is the predominant radiative transfer mechanism at higher gas-cap temperatures. Solutions of the coupled problem including radiation cooling and self-absorption indicate that the shocked gas layer will be cooled near the vehicle surface. Subsequently,

the high absorption coefficients at low wavelengths (i.e. $\lambda < 1500\text{Å}$) may significantly reduce the vacuum ultraviolet radiation heat loads below early estimates. For short path lengths (i.e. near the shock front) the radiative flux toward the vehicle surface is dominated by the vacuum-ultraviolet portion of the spectrum. At longer path lengths (nearer the body surface) the highly self-absorbed VUV radiation is diminished and the optically thin visible radiation increases in importance.

A proper evaluation of the theoretical predictions is a comparison with experimental radiation measurements at high temperatures. Experimental studies have been reported in which the wavelength-integrated radiation from shock-heated air has been measured, using thin-film total radiation gauges (Refs 9-12). In these cases, check with theory may be affected by the assumed values of absorption coefficients used in the analyses for radiation in the VUV region. Experiments to determine radiation at very short wavelengths are of necessity complex, since most window materials will not transmit below a certain cutoff wavelength. Lithium-fluoride, for example, has a useful short wavelength cutoff of approximately 1100Å, while a sapphire window, as used in the experiment described in Refs 9 and 10, has a 1700Å cutoff limit. A novel gas window technique has been used in conjunction with a stagnation point total radiation cavity gauge (Ref 11) in which the lower cutoff bound has been extended down to 880Å with the use of krypton as the window gas. The wavelength-integrated experiments described in Ref 12 use a windowless technique for reflected shock measurements, wherein a thin-film gauge views the total radiation from the shocked gas through an aperture until an expansion-plume flow impinges upon the detecting element.

A ballistic-range technique using a neon-nitrogen mixture as the test gas was described in Ref 13. The detector used in this study was a photomultiplier coated with sodium-salicylate to convert the VUV radiation to visible light. Wavelength-integrated radiation data down to approximately 575Å (the neon photoionization edge) was obtained from the gas-cap surrounding small blunt models.

The wavelength-integrated shock-tube radiation measurements are

in adequate agreement with calculated predictions (see, for example, Refs 8 and 11) which use accepted theoretical absorption coefficients for the transitions included in the analyses. However, the determination of spectral features and the identification of the radiating species are necessary to obtain experimental values of the absorption coefficients for the radiation at short wavelengths. Spectrally resolved vacuum ultraviolet nitrogen absorption measurements have been reported, Ref 14, employing a shock tube technique. These experiments were performed in the lithium-fluoride window region (i.e. $\lambda > 1050\text{Å}$) and used neon and argon as the carrier gas with the addition of a few percent of nitrogen. However, these absorption measurements of vibrationally excited nitrogen were obtained at very early times after reflected shock arrival, prior to dissociation and ionization. Recently, some spectrally resolved measurements of the nitrogen atomic ion recombination continuum (in the wavelength range 970Å - 1150Å) have been reported (Ref 15), where the radiation source was a constricted-arc argon-plasma generator with a small percentage of nitrogen added.

It is the purpose of this report to discuss a shock-tube experimental study designed to obtain spectrally resolved radiation emission data of the nitrogen and oxygen atomic ion recombination continuum at wavelengths below 1150Å, at temperatures between 11,000°K and 13,000°K. The shock tube is used to provide a short-lived source of a shocked gas in thermal equilibrium. As mentioned earlier, an experiment of this type involves a windowless coupling of the detector system (in this experiment, a vacuum ultraviolet spectrometer) to the radiation source. This is accomplished through the use of a quick-opening, explosively driven plunger, which opens the spectrometer momentarily to the reflected-shock processed gas, and then closes, resealing the spectrometer from the shock tube. Experimental results are given in the form of absorption coefficients or photoionization cross-sections for the continua under study.

The remainder of this report is divided into four main sections. Section II presents the analysis and calculations used to predict the operating region for the shock-tube experiments, wherein the shocked gas ranges from blackbody to optically thin conditions for the nitrogen-neon and oxygen-neon

mixtures used as the test gas.

The experimental apparatus is discussed in Section III. The shock tube, loading system and quick-opening plunger window will be described. In particular, the VUV spectrometer, detectors and calibration system are discussed in some detail, since it is this detecting system that is the cornerstone of the experiment designed to yield spectrally resolved radiation data in this windowless regime.

Section IV presents the results of the experiments, and discusses some of the problem areas encountered during the course of the study. Included are visible-radiation data obtained behind incident and reflected shock waves, and a determination of the shock-tube test times together with the induction times required to obtain equilibrium conditions in a test gas highly diluted with neon. Experiments using various gaseous windows in the plunger to selectively absorb radiation of certain wavelengths are also described. The radiation data in the VUV regime are presented for both optically thick and optically thin shocked-gas conditions.

The final part of the report (Section V), presents the analysis of the data and gives the experimentally determined photoionization cross-sections and a comparison with other measurements. Sources of possible errors and a general discussion of shock-tube measurements of this type are presented.

II. ANALYSIS

Prior to initiation of the experimental shock tube program, it was necessary to calculate the shock-tube operating region, i.e., the values of the important shock tube parameters such as shock speed, initial test gas pressure, composition of the test gas mixtures, driver pressure, etc. These computations are required to yield the proper range of reflected shock temperatures and atom densities enabling meaningful radiation measurements to be obtained. It is required that high temperatures ($> 10,000°K$) be generated in the reflected shock region so that the test gas under study (i.e., oxygen or nitrogen) will dissociate and ionize. Extremely strong shock waves are required to obtain these conditions in the pure gases, and in addition, preliminary calculations indicated that the gases would be always optically thick in the wavelength range of interest ($\lambda < 1100$ Å). A rare-gas diluent can be used both to obtain high temperatures at moderate shock speeds, and to lower the number density of the atomic species under study so as to obtain optically thin gas conditions. There is a requirement that this diluent gas be optically inactive in the wavelength range of interest. As seen in Figure 1, xenon, krypton and argon could absorb radiation in the wavelength range under study, Ref. 16. The gas chosen as the diluent in the present series of experiments was neon, with a photoionization edge at 580 Å. This choice leaves a relatively clear spectral range for this investigation (700 Å to 1100 Å). The remainder of this Section of the report is divided into two parts. First, calculations for the emissivity of the recombination continua are discussed, as a function of temperature and number density. Secondly, the results of an equilibrium shock wave computer program for various neon-nitrogen or neon-oxygen dilutions are presented in conjunction with the emissivity calculations. This yields an operating-region graph giving continua emissivity as a function of wavelength for different values of initial test gas pressure and reflected shock temperature.

II. A. EMISSIVITY CALCULATIONS

The radiation under investigation arises from the recombination of an electron and atomic ion to the ground states of the nitrogen and oxygen atoms:

$$N^+ + e \longrightarrow N + h\nu \qquad \lambda < 1130\,\text{Å}$$
$$O^+ + e \longrightarrow O + h\nu \qquad \lambda < 911\,\text{Å} \tag{1}$$

The recombination transitions and energy levels involved are shown in Fig. 2 (see Refs. 17-19). Following the procedure of Ref. 17, the emissivity as a function of wavelength will be computed for various number densities and temperatures. Assuming thermodynamic equilibrium it is possible to apply theoretical photoionization cross-sections to calculate the rate of radiation due to the inverse recombination process. Thus, the radiation may be written as

$$I_\lambda = I_{BB_\lambda}\left(1 - e^{-\alpha_\lambda \ell}\right) = I_{BB_\lambda}\ \epsilon_\lambda \tag{2}$$

where I_{BB_λ} is the blackbody function at wavelength λ ; α_λ is the absorption coefficient, ℓ is the optical path length and ϵ_λ is defined as the emissivity. Substituting for α_λ ,

$$\alpha_\lambda = \sigma_\lambda\ n \tag{3}$$

these results,

$$I_\lambda = I_{BB_\lambda}\left(1 - e^{-\sigma_\lambda n \ell}\right), \tag{4}$$

where n is the atom number density and σ_λ is the photoionization cross-section.

For a given transition as shown in Fig. 2, the longest wavelength radiation is referred to as the photoionization edge or cutoff, indicating the minimum electron energy required for such a transition. Recombination with electrons of greater energy yields a continuum in the direction of

shorter wavelength radiations. Since the recombination transitions require nearly the same energy change (i. e. the various continuum edges are in close proximity in this wavelength regime), there is an overlapping of the continua at shorter wavelengths. This is shown schematically for nitrogen for example:

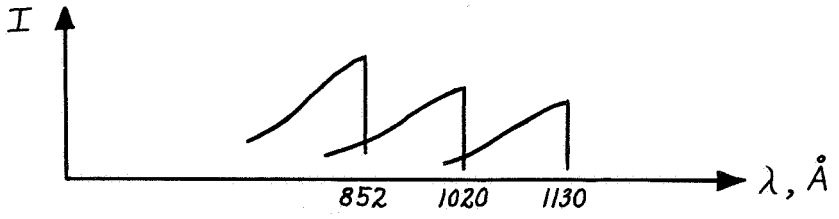

The shape of the various continua are determined by the wavelength dependence of the cross-sections for the particular transitions. Thus, the computation of the radiation at a given wavelength must account for the summation of these continua and Eq. (4) can be rewritten as

$$I_\lambda = I_{BB_\lambda} \left(1 - e^{-n\ell \sum_j X_j \sigma_{\lambda_j}}\right) . \tag{5}$$

Here, σ_{λ_j} is the wavelength-dependent photoionization cross-section for a particular transition, j, and X_j is the fraction of atomic species in energy level j from which the transition occurs. The term X_j is given as

$$X_j = \frac{g_j e^{-E_j/kT}}{\sum_j g_j e^{-E_j/kT}} , \tag{6}$$

where E_j is the energy of level j above the ground state, and g_j is the statistical weight of that level. Thus, for a given temperature T, and assumed values of σ_{λ_j}, the total emissivity as a function of wavelength can be calculated as a function of atomic number density (n) and path length (ℓ).

Nitrogen Calculations

A number of calculations were performed to cover the temperature range 10,500 °K to 13,000 °K. For example, at $T = 12,800$ °K, the X_j values are

Level	X_j
^4S	0.7425
^2D	0.2138
^2P	0.0436

indicating that 74% of the nitrogen atoms are in the ^4S ground state, while only 4% occupy the excited ^2P level. It may be expected, then, that the calculated emissivity of the continua resulting from ^2P transitions will be small, while the contribution to the overall emissivity from ^4S transitions will be substantial. To complete the calculation, values of the cross-sections, σ_{λ_j}, must be obtained. For the computations presented here, theoretical values were taken from Ref. 17. Figure 3, which is taken from that reference, gives these calculated photoionization cross-sections as a function of wavelength.

Figure 4a shows results from a calculation for ϵ_λ at $T = 12,800$ °K, $\ell = 7.62$ cm, the shock-tube diameter, and various values of atom number density in terms of a non-dimensionalized $(\rho/\rho_o)_N$, where ρ_o is ρ_{STP} (which is compatible with the output from the normal shock computer program to be discussed later). The product $(\rho/\rho_o)_N L_o = n_N$, where L_o is the Loschmidt number. Although the cross-section values used for the predominant ^2P transition(edge at 1130 Å) are comparable to the predominant ^4S transition values (edge at 852 Å), the small population of that excited state yields a small value for emissivity. Thus, for a given atom density, there is a wide range of ϵ_λ; a part of the continua wavelength region may be optically thick (i.e. $\lambda < 852$ Å) while another part of the spectrum may be optically thin. However, due to the steep slope of the blackbody curve at these wavelengths, the actual radiation fluxes from the different emissivity

plateaus may be comparable. This is seen from the calculations shown in Fig. 4b. Computations performed at lower temperatures showed similar trends, with the 1130 Å plateau region having lower ϵ_λ values due to the decreased population of the ^2P level at lower temperatures.

Oxygen Calculations

Similar computations were performed for oxygen, with the three lowest-lying levels being grouped (see Fig. 2).

Level	E_j (eV)	Statistical Wt.
$^3P_2$	0	5
$^3P_1$	.0196	3 } 9
$^3P_0$	.0281	1
^1D	1.9673	5
^1S	4.1896	1

At a temperature of 12, 500 °K for example, the X_j values are

Level	X_j
^3P	0.91598
^1D	0.08192
^1S	0.00208

indicating that 92% of the atoms are in the ^3P ground state. The values for σ_{λ_j} used in the calculation are again taken from Ref. 17 and shown in Fig. 5.

The results of a computation for T = 12, 500 °K, ℓ = 7.62 (the shock-tube diameter) and various values of $(\rho/\rho_o)_o$ are given in Fig. 6. Since the primary transitions arise from the heavily populated ground state for the oxygen atom, there is not the wide range of ϵ_λ as was evident in

the nitrogen calculations. Thus, for a given atom number density, the radiation will arise from a more uniformly (over the wavelength range of interest) thick or thin radiating gas. This in turn will reflect the strong blackbody dependence at these wavelengths.

II. B. NORMAL-SHOCK COMPUTER PROGRAM AND SHOCK-TUBE OPERATING REGION

It was also required to predict the shock-tube operating regime for these vacuum ultraviolet radiation experiments. That is, it was necessary to compute the range of shock velocities, and initial test gas mixes and pressures required to give the desired reflected shock temperature and atom number density. An equilibrium shock wave computer program developed at CAL (Ref. 20) was used to compute these values for neon-nitrogen and neon-oxygen mixes over a wide range of test gas pressures and mixtures. The species included Ne, Ne^+, e and N_2, N_2^+, N, N^+ or O_2, O_2^+, O, O^+, O^- with the thermodynamic properties of each species being described with a polynomial fit to tabulated values over a wide temperature range. Since the calculations were quite extensive, all of the results will not be shown here. Rather a few representative calculations will be presented to indicate the range of shock velocities, pressures, etc., required for the experiments. Figure 7 shows typical results for the neon-nitrogen calculations. It can be seen that shock velocities ranging from about 10,000 to 13,000 ft/sec are required to obtain reflected shock temperatures in the range of interest, and the test gas mixtures will generally be less than ten percent nitrogen in neon. Similar results for neon-oxygen mixtures are presented in Fig. 8.

For a constant reflected shock temperature, it was possible to obtain different values of atom density behind the reflected shock, (ρ/ρ_o) atom, as the mixture dilution and initial pressure were varied. These values of $(\rho/\rho_o)_N$ (or $(\rho/\rho_o)_O$) were then used with the emissivity computations presented earlier to give a curve of required shock-tube operating parameters as shown in Figs. 9 and 10 for typical nitrogen and oxygen test conditions.

Figure 9 presents the neon-nitrogen operating conditions for a reflected shock temperature of 12, 800 °K. The solid curves are calculated emissivities for the predominant continua edges (852 Å, 1020 Å and 1130 Å) as a function of $(\rho/\rho_o)_N$. The dotted lines using the right-hand abscissa indicate the values of $(\rho/\rho_o)_N$ obtained for a given test gas mixtures at various initial pressures. For example, 4 torr initial pressure of a 3% N_2/97% neon mixture predicts emissivity values of 1.0 at 852 Å, 0.7 at 1020 Å and 0.23 at 1130 Å. Thus, for a given mixture and p_1, a portion of the spectrum can be optically thick, while another may be optically thin. A 0.5% N_2/99.5% Ne mixture at a pressure of 3 torr will approach optically thin conditions at all wavelengths, while a 10% N_2/90% Ne mixture at 4 torr should yield blackbody conditions throughout the spectral range. By suitable variation of test gas mixture and pressure, a wide variation of spectral emissivity values can be obtained.

The oxygen-neon data is presented in Fig. 10 for a reflected shock temperature of 12, 500 °K. Again, the three main continua edges are shown at 666 Å, 732 Å and 911 Å. Due to the more nearly uniform spectral emissivity values, it may be possible to obtain optically thick or thin conditions throughout the spectral range with fewer test gas variations. For example, a 0.2% O_2/99.8% O_2/Ne mixture at 2 torr pressure will give low values of emissivity, while 4 torr of 4% O_2/96% Ne mixture will yield optically thick conditions throughout.

Figures 9 and 10 are typical of the operating region curves computed for the experimental series. These, in turn, were modified by practical considerations of shock tube operation which will be discussed in a later section. They include, however, poor shock tube operation at lower values of p_1 (the lowest initial pressures used were 2 torr), the problem of long ionization-induction times for very dilute mixtures, and the practicability of driving the extremely strong shock waves needed for the 10% N_2/90% Ne mixture (using a room-temperature hydrogen driver).

III. EXPERIMENTAL APPARATUS

In this section of the report a description is presented of the final configuration and components used to make the quantitative vacuum ultraviolet emission measurements. They consist primarily of the shock tube, the spectrometer and detector system, and the explosively driven plunger unit which couples the shock tube to the spectrometer in a windowless manner. In addition, the calibration procedures are also discussed, as is the method that was devised to provide correction factors which permit taking into account the effect of overlapping orders in the recorded data.

It should be emphasized that a considerable fraction of the contract effort was devoted to the development of the apparatus, and that a number of problems were encountered which determined the final experimental configuration. In general, it can be said that the application of conventional vacuum ultraviolet techniques, i.e., Ref. 21, to measurements of shock-heated gases is not straightforward, owing not only to the usual limitations of short testing times and low light levels, but also the instrinsic nature of the radiation source. Because the shock tube provides an equilibrium radiating source at high temperatures, by far the greatest amount of light lies at wavelengths longer than 2000 Å. Thus, measurements at wavelengths below 1200 Å must be made in the face of severe stray-light conditions. As will be shown, a study of the stray light problem showed that sodium salycilate-photomultiplier detectors, usually used in spectroscopy at these wavelengths, were unsuitable for quantitative radiation measurements using the shock tube.

For overall completeness and as guidelines for further shock tube experimentation in the vacuum ultraviolet, several of these developmental problems are also discussed in the last part of this section.

III. A. THE SHOCK TUBE FACILITY

The shock tube used in these studies was specifically designed for radiation measurements and has been described in earlier work (see Ref. 22 for example). However, the reflected-shock test section has been

redesigned for these vacuum-ultraviolet experiments. The tube has an internal diameter of three inches, with a driver 5 feet in length and a low pressure, or test section, thirty feet long. Room temperature hydrogen was used as the driver gas at pressures up to 2000 psi for the present series of experiments. The test gas consisted of neon with a few percent of N_2 or O_2 (and in some cases Ar) at pressures between 2 and 6 torr. The double-diaphragm technique was used to insure repeatability in the shock conditions and mild steel was used as the diaphragm material.

The shock wave speed was monitored over the last 12 feet of the test section with seven thin-film heat transfer gauges mounted along the tube wall. The first two intervals were three feet apart, while the last four intervals were 1.5 feet apart, the last station being 1.3 inches from the reflecting end wall. Megacycle timing counters were used to determine the shock velocity to better than $\pm$ 0.5%.

Between daily runs the shock-tube test section was thoroughly scrubbed with alcohol and hard-pumped overnight with a liquid-nitrogen trapped oil-diffusion pump. Pressure levels of $1\text{-}2 \times 10^{-5}$ torr (as indicated by an ionization gauge) were obtained in the test section prior to loading of the test gas. A shock tube experiment was never undertaken unless this pre-load pressure was less than 2×10^{-5} torr. The rate of pressure rise of the entire shock tube and gas-handling system was about 1μ/hour.

A Baratron differential pressure gauge, capable of measuring pressure in the 0 to 30 torr range with micron precision, was used to control and measure the initial test gas pressure in the shock tube. The test gases used in these experiments were supplied by Air Products and Chemicals, Inc., as their ultra-pure, zero gases. Analyses were procured for each gas cylinder, which showed the molecular concentration of each contaminant. The total hydrocarbon value was always $<$ 1 ppm, and the most abundant contaminant, helium or hydrogen was, in general, $<$ 5 ppm. Two types of test gas mixes were employed. Using the pure gases, mixtures of neon and the test gas (N_2, O_2 or Ar) were obtained using the shock tube loading and mixing manifold system. These mixtures, in

general, ran from about 0.5% to 10% of the test gas in neon. The system was flushed and pumped several times prior to the addition of the various pure gases. The mixture was stored in a disposable-cylinder reservoir at approximately 10 psig. The test gas mixture was discarded when this reservoir pressure approached 1 psig. In addition, the entire loading-mixing manifold was maintained at an overpressure of a few psi of neon to insure against possible contamination by leakage from the atmosphere. Alternately, premixed zero grade gases were obtained from Air Products and Chemicals, on the basis of the operation region calculations discussed earlier. These were procured in disposable cylinders of 50 standard liters (at approximately 300 psig) and 100 standard liters (at approximately 600 psig) and connected directly to the tube loading system. Several shock-tube runs were undertaken to check the radiation measurements obtained using the premixed gas as compared with those obtained using a test gas mixed in the tube manifold system. The vacuum ultraviolet measurements were consistent to within 10% for mixtures as dilute as 0.5% N_2 in neon. These results indicated that a high purity level was being maintained in both the loading and mixing manifold system.

The general instrumentation arrangement is shown in the schematic of the experimental system, Fig. 11. In addition to the three-channel vacuum ultraviolet spectrometer, other photomultiplier-filter combinations were used to monitor visible radiation. Approximately 6 feet from the reflecting end of the shock tube (i.e., 24 feet from the diaphragm station), two EMI 9558 photomultipliers were used to monitor the radiation from the hot gas behind the incident shock wave. One detector was used in conjunction with a narrow-band-pass blue filter (approximately $\Delta\lambda = 30$ Å) centered at 4270 Å, which recorded the 0, 1 transition of the N_2^+ (1-) system. The solid angle subtended by this blue system was determined by a 3-mm aperture at a sapphire window and another 3-mm aperture 4-1/2 inches away. This combination was used for both the O_2 and N_2 experiments, and also proved to be a sensitive monitor for possible nitrogen contamination for either pure neon or neon-oxygen experiments. The other incident radiation photomultiplier was used in conjunction with a red Optics Technology filter, OTS #706 centered at 7100 Å with a half width of 200 Å (observing primarily the $\Delta v = 2$ progression

of the N_2 (1+) system) for the N_2-Ne runs. This filter was changed for the O_2-Ne experiments, substituting an OTS #579 yellow filter centered at 5800 Å (covering 5600-6100 Å) observing primarily the $\Delta v = 0$ progression of the O_2^+ (1-) system. The solid angle subtended by this system was determined by a 3-mm aperture at a sapphire window, and a 1-mm aperture 3 inches away. Both of these photomultipliers were operated at 1000 volts using a Fluke No. 412B high voltage power supply. The output signals were displayed on Tektronix 502A oscilloscopes. At this same shock-tube station the output from a thin-film heat transfer gauge was also displayed, giving the sidewall temperature rise behind the incident shock (wall ΔT). These oscilloscopes were triggered from an upstream thin-film gauge.

The visible radiation was also monitored at the reflected-shock location, through a contoured sapphire window located 1/2-inch from the end wall of the shock tube. This viewing position was located directly opposite the sidewall orifice leading to the vacuum-ultraviolet spectrometer. Two Dumont K1430 photomultiplier tubes operating at 1500 volts viewed the reflected-shock radiation using a beam-splitter arrangement. One detector was used in conjunction with a similar blue (4270 Å) filter. The solid angle subtended was determined by a 0.5 mm aperture at the sapphire window and a 3 mm-diameter aperture located 4-1/4 inches away. The other detector was used with either a red or yellow filter. For the Ne-N_2 experiments, a Corning CS7-69 wide band red filter was used, peaking at about 8000 Å and covering the wavelength range of about 7800 Å-11, 000 Å. An OTS #589 yellow filter was used for the Ne-O_2 experiments, centered at 5900 Å and covering the range 5600 Å-6300 Å. The solid angle subtended by this system was determined by the 0.5 mm aperture at the window, and a 1 mm aperture 4-1/4 inches away. In addition, the sidewall ΔT output from the last thin-film gauge, located 0.8 inch upstream from the window aperture (or 1.3 inches from the endwall) was also monitored to obtain incident and reflected-shock arrival times. These outputs were also displayed on 502A oscilloscopes, triggered from an upstream thin-film gauge.

III. B. THE WINDOWLESS PLUNGER

The coupling of the vacuum ultraviolet spectrometer to the shock tube in a windowless manner has been accomplished using a quick acting plunger. A general schematic of this plunger arrangement is shown in Fig. 12. There is a 2.5 mm-diameter passage (4.5 mm in length) located 12 mm from the end wall of the shock tube leading to the plunger. The plunger separates the shock-tube wall from the entrance orifice (of 1 mm diameter) to the vacuum spectrometer. A slotted opening, 3 mm wide by 7 mm long, was machined through the plunger and acts as the window. Prior to a shock-tube experiment, the plunger is in a raised position such that this slot is above the shock tube and spectrometer orifices. The plunger body is sealed against these openings by small "O" rings encircling the orifices. Mounted atop the plunger is an explosively driven ram (Conax #1617-134-01 trigger assembly) which is triggered, through a time-delay generator, from an upstream thin-film gauge. This ram drives the plunger downward and, as the slot passes the orifices, momentarily exposes the spectrometer to the hot gas behind the reflected shock wave. The plunger continues its travel, coming to rest with the slot below the orifices, the plunger body again sealing the spectrometer from the shock tube. It may be noted that a new Conax trigger assembly is required for each shock-tube run.

During the initial series of experiments, the explosive ram was in direct contact with the upper surface of the plunger. Measurements showed that the spectrometer would be exposed to the shocked gas for approximately 80 μsecs. In an effort to increase this open time, two small pieces of 0.062-inch aluminum wire were placed between the ram and the plunger to act as energy-absorbing material. This arrangement was subsequently used for all later experiments. The full open time was increased to about 105 μsecs. Figure 13 shows the result of such a test. A 1P28 photomultiplier was placed outside of the sapphire window used for the monitor radiation, and a Tensor high-intensity lamp was used outside of the shock tube on the opposite side (in place of the spectrometer). The oscilloscope trace was triggered instantaneously with the initiation of the explosive ram. About 145 μsecs from the initiation, the window slot begins to open and is fully

open for 105 μsecs. The overall timing of these explosive rams has been extremely repeatable, ± 5 μsecs, and when triggered through a time delay generator, the plunger window thus permitted precise selective temporal viewing of the reflected-shock radiation. This has proven valuable for very dilute mixtures, where there was a slow approach to the final equilibrium state. Figure 14 shows an oscilloscope record from an actual shock tube experiment. The lower trace shows the visible reflected-shock radiation, and the upper trace shows the output from one of the detectors in the vacuum ultraviolet spectrometer. It is seen that the plunger window permits radiation to be viewed for a portion of the total test time, after which the spectrometer is resealed.

Another feature of the plunger assembly can be observed from the schematic shown in Fig. 12. The plunger itself is hollow and connected to a loading manifold, reservoir and vacuum pump located beneath the shock-tube test section. This enables the plunger to be utilized as either a vacuum window (i. e. the reservoir and plunger itself are evacuated), or as a gaseous window. This latter configuration would employ loading the reservoir and plunger with a gas at a specified pressure (for example, a pressure equal to that expected behind the reflected shock). With the proper selection of window gases, it may be expected that absorption of the radiation at selective wavelengths would occur. The use of argon as a window gas, for example, would tend to absorb all radiation below its photoionization edge at 780 Å. The results of several gaseous-window experiments will be discussed in Section IV of this report.

III. C. VACUUM-ULTRAVIOLET SPECTROMETER

The spectrometer and detector system used in the experiments was designed specifically for multichannel radiation measurements in the 700 to 1400 Å wavelength region. The multichannel approach was taken to permit the maximum amount of data to be obtained from a single shock-tube test. Initially, a ten-channel system utilizing sodium salicylate-photomultiplier detection was constructed and tested. However, as discussed in Section IIIE,

this approach was found unsuitable for these experiments. This led to the final design of a three-channel system, using the bare stainless steel photomultiplier tubes, which is described in this Section.

1. The Vacuum System

A general layout of the spectrograph is shown schematically in Fig. 15. The vacuum chamber is of welded steel construction consisting of a 42-inch length of 8"-diameter pipe with a 4-inch diameter entrance arm. Flanged ends are provided with "O" ring seals for affixing entrance slit, exit slit and grating mount assemblies. Dowel pin locators assure repeatable component alignment with minimum reassembly time when maintenance is required.

The inside surface and all baffles were painted with a zinc chromate epoxy primer and 3 M Black Velvet, a flat-black coating which has a low reflection coefficient, and produces a very porous surface, excellent for trapping stray light. It does, however, have the disadvantage of long initial pumping time which was greatly improved by back filling the spectrograph several times with helium when pumping was initiated.

The vacuum system consists of a Welch Duo Seal Mechanical pump, used both as a roughing pump and a backing pump for the 4-inch CVC oil diffusion pump. Both a CVC Multicoolant baffle and a Chevron baffle between the diffusion pump and main spectrograph chamber were used to minimize oil back streaming, thus preserving the cleanliness of the system.

Pressure levels were monitored with both an NRC 507 Ionization gauge and an Autovac Pirani-type gauge having provision for signaling a pressure rise above 0.1 torr. A coolant-water temperature sensor and a power-failure indicator were both incorporated in a control unit to initiate the closure of a gravity-operated gate valve which automatically isolated the spectrograph from the pumping system in the event of any malfunction. Continuous unattended pumping was thereby permitted.

Also shown in Fig. 15 is a fast-acting high-pressure ball valve which, during the shock-tube test, closes in about 0.5 second, and is triggered by the shock wave. This serves as a backup to the explosively driven plunger. In addition, because of the inherent danger of the high pressure hydrogen driver gas entering the spectrometer chamber by any electronic or other malfunction, an emergency vent to the roof was also provided, designed to open in the event that the spectrometer pressure exceeded one atmosphere. The spectrometer pressure after a test in most instances was of the order of a few microns pressure.

2. The Optical System

The spectrometer was designed to use a one meter focal length concave grating, which is mounted in a rotatable holder equipped with an electrically driven external micrometer adjustment. The 1 mm - diameter connecting aperture to the shock tube serves as the entrance slit. The exit slits are located in the focal plane defined by the vertically focused astigmatic image of the entrance slit, thus providing best wavelength resolution. The verticle exit slit heights were chosen to admit the entire image. Several baffles were used to reduce stray light in the spectrometer chamber. A Bausch and Lomb tripartite 600 line per mm grating masked to a 2 x 3-1/8 inch aperture was used in the final configuration. When used with 2 mm-wide exit slits, this arrangement provided bandwidths of 16 Å in first order. The grating was blazed at 1500 Å, and thus was usually used in second order, with 8 Å bandpasses for all three channels.

Mechanically, the focal plane consisted essentially of a solid plate with only the three exit slits connecting the spectrometer to the detector chamber. As shown in Fig. 15, this chamber, housing the three detectors, was separately evacuated with a liquid nitrogen trapped, 2-inch diffusion pump.

Directly behind the focal plane an externally rotatable filter wheel permitted lithium fluoride filters to be selectively inserted into any or all of the three channels. As discussed in Section IIID, this wheel was extremely useful in calibration and order-sorting tests.

3. Detectors

After separate tests to verify their applicability, the final detector configuration utilized three RCA 7075 photomultiplier tubes. These tubes are of the general RCA 1P28 dynode design except that the photocathodes are constructed of stainless steel. They are deployed without envelopes, and are hence provided with their own vacuum system. In actual test use, it was found that a fast (5 μsec) crowbar shorting system for the high voltage power supply was required to prevent damage to the tubes resulting from the small amount of gas that enters the spectrometer during each test. Pressures above 10^{-4} torr induce arcing within the dynode structure, which drastically reduces the tube gain. No attempt was made to rejuvenate the tubes that were damaged in this manner during the initial testing.

In spite of the precautions required when using these tubes, the advantages for the present experiments were invaluable. Chief among these is that the photoelectric response of the cathode peaks at about 700 Å and is practically zero at wavelengths longer than 1600 Å. Thus, discrimination is naturally achieved against the high intensity of near ultraviolet and visible light from the shock-heated gas. This aspect of the problem, which led to the rejection of the sodium salicylate detection scheme, is discussed in more detail in Section IIIE.

One such sodium salicylate channel was retained to provide a useful adjunct to calibration and monitoring functions. This channel consisted of a small target, coated with sodium calicylate, and placed on the spectrometer side of the focal plane. The fluorescent radiation resulting from ultraviolet exposure was transmitted by a light pipe to an EMI 9558 photomultiplier tube. (See Figure 15.) Its use in obtaining the relative spectral response of the bare stainless steel tubes is described in the next subsection.

III. D. WAVELENGTH AND ABSOLUTE INTENSITY CALIBRATION PROCEDURES

1. Wavelength

Wavelength calibration was readily accomplished by making use of the known resonance lines of hydrogen, argon, neon, and helium. These atomic lines were excited in a DC low pressure discharge lamp obtained from the Geophysics Corporation of America, and which is described in detail in Ref. 23. It consists primarily of a ceramic capillary at about 0.1 torr pressure, and runs at approximately 0.5 amps at 1600 volts. The lamp was attached to the spectrometer by means of a dowel-aligned adapter which essentially provided a duplicate entrance slit to the instrument. The grating angle drive-mechanism was equipped with a switch which provided pulses for the synchronization of the grating motion and oscilloscope sweeps. In this manner the spectrum could be scanned at various rates and wavelength scales. A typical scan over a large wavelength scale is shown in Fig. 16. The upper trace (a) is the lamp spectrum using a mixture of argon, neon, and hydrogen. The various resonance lines in the different orders of the grating are identified and labeled. The lower trace (b) is the resultant spectrum with a LiF window inserted into the optical path. Since LiF has its transmission cut off at about 1050 Å, only those lines at higher wavelengths were recorded. This technique, coupled with the fact the detectors do not respond to wavelengths longer than 1600 Å, permitted the unambiguous identification of the lines. Subsequent manual scanning and "peaking" of the lines was used to provide the wavelength calibration in terms of the micrometer dial reading of the grating angle.

2. Absolute Intensity Calibration

The basic difficulty in radiant energy calibration in this region of the spectrum arises from the lack of a suitable standard radiation source. Initially, with the planned use of the sodium salicylate detection system, the calibration procedure was quite involved, requiring several operations. This procedure is described in Section IIIE which discusses early developmental

problems, because of its possible relevance and use in similar shock-tube radiation problems. However, at the time that it was decided to use the bare stainless steel photomultiplier tubes, the following technique was devised for the subsequent experiments.

The absolute intensity calibration procedure that was finally employed relied on the shock-tube radiation itself as a standardizing light source. As will be shown in Section V, the high absorption coefficient for the radiating process under study permitted tests to be made in which the gas was optically very thick. Under these conditions the shock tube radiates as a blackbody at the equilibrium temperature of the gas. Thus at each wavelength of interest, a series of tests, ranging from optically thin to optically thick conditions, was used to determine the value of the absorption coefficient at that wavelength. Thus the complete system was self-calibrating, with a precision limited only by the errors associated with the temperature determination and those from possible overlapping orders of the grating. Experiments performed to evaluate the latter effect are discussed in the next subsection. The overall error analysis is presented in detail in Section V.

3. Grating Response and Overlapping Order Corrections

A series of experiments was undertaken to determine the effects of overlapping orders of the grating on the intensity data recorded during the shock-tube tests. For example, with the grating angle set to record 900 Å radiation in the second order in a given channel, the exit slit will also pass 1800 Å in first order, and 600 Å in third order. In all cases, the long wavelength cutoff of the detectors discriminated against the first order contributions. Similarly, the neon carrier gas used in these experiments provided a short-wavelength limit of 585 Å because of its high absorption edge there (see Fig. 1). Thus, the grating response requirement was limited to the remaining interval.

An overlapping-order correction requires not only a knowledge of the relative grating response, but also that of the intensity emitted at the wavelengths of the other orders. The largest correction would apply to cases in which blackbody radiation is assumed at the overlapping wavelength. However, even under such conditions, the correction may not be too large because, for example, the blackbody intensity at 13, 000 °K drops by a factor of 50 between 900 and 600 Å. The overall influence of these effects on the results is discussed in Section V.

The technique devised to evaluate these effects relied upon emission wavelength scans of the DC low pressure lamp described in Section IIID 2. By using the resonance lines of several different gases, spectra similar to those of Fig. 16 were obtained, in which the output of the system was recorded in as high as the fifth order, for the following wavelengths:

λ (Å)	Gas
584	Helium
736 743	Neon
1048 1066	Argon
1216 1608	Hydrogen

These spectra from the lamp were utilized in two ways. They first provided a direct comparison of the bare phototube output with that of the sodium salicylate detection system. For this comparison, the response of the monitoring photomultiplier (viewing the fluorescence via a light pipe) was compared with that from one of the normal recording channels. This was done at each wavelength using the first order only, to prevent overlapping order complications in the long-wavelength-sensitive detector. By taking these ratios and the well-accepted assumption that the sodium salicylate spectral response is flat, the relative spectral response of the bare stainless steel photomultiplier tubes could be derived. One such curve

is shown in Fig. 17, in which it is compared with a similarly obtained curve reported in Ref. 24, also for an RCA 7075 tube. Also shown are the photoelectric yields for nickel and iron, as reported in Ref. 25. In this figure, the ordinate scale is relative, and all curves were normalized at 1216 Å. The general agreement among the curves is good. It should be noted that the photoelectric yield curves were obtained for normal incidence, whereas the three RCA 7075 detectors were each mounted in rotatable holders and the photocathodes were angularly adjusted for maximum response. Hence, some differences in the curves may be expected. All three channels were measured in this manner and found to be the same within experimental error. Thus, the response curve shown in Fig. 17 was used in the following analysis.

The second manner in which the spectral emission scans of the lamp radiation were used resulted in a set of grating response curves for the various spectral orders. The sum of the recorded intensities diffracted into the various orders yields the total intensity diffracted by the grating for a given wavelength. Thus, the fraction formed by the intensity in a given order, divided by the total intensity, provides a measure of the relative grating efficiency for that order. This method requires that the spectral lines in the total source output are compatible with the condition of non-overlapping, and that all the radiation from a given line is recorded in each order. The results of this procedure, when used at each of the wavelengths listed above, are shown in Fig. 18a. The ordinate scale is relative, and the three scales on the abscissa correspond to the first three orders of the grating spectrum.

The overall system response to line radiation is shown in Fig. 18b, in which the curves of 18a are multiplied by the relative detector response shown in Fig. 17. From these results it is readily seen that the use of higher orders for greater overall sensitivity to line radiation is of considerable advantage.

Because the recombination spectra to be measured in the present work are continuous in wavelength, a further modification is required to predict relative grating-order efficiencies. This results from the fact that higher orders correspond to higher linear dispersion, and hence, a given

exit-slit when used in third order, for example, will subtend only one third of the wavelength interval that it would in first order. When this effect is taken into account, the final grating response curves shown in Fig. 18c are produced. It can be seen that for the detection of continuum radiation below 750 Å, there is a clear advantage to working in the second order. Similarly, the first order would be most efficient at wavelengths above 750 Å. In the present work, only the first and second orders were used, and the curves of Fig. 18c were employed in the estimation of the effect of the overlapping orders (see Section V).

III. E. EARLY DEVELOPMENTAL PROBLEMS

During the course of the development of a multichannel vacuum spectrometer applicable to the measurement of shock tube radiation in the 700 to 1400 Å region, several problems were encountered which seriously compromised the initial design of the system. The final experimental configuration has been described in Sections IIIA, B and C. The following subsections present a brief description of these problems in vacuum ultraviolet spectroscopy and point out their relevance to shock-tube applications.

1. Calibration

The use of sodium salicylate coatings in the detection of far-ultraviolet radiation is well-known. They are readily applied to light pipe or detector surfaces; when stimulated by ultraviolet radiation from 3600 Å to as low as 600 Å, they provide a fluorescent output in the more convenient 4500 Å region. Furthermore, the relative wavelength response is quite flat, and a body of knowledge on this response and the quantum yield is readily available. (See Ref. 21.)

The initial spectrometer design utilized 10 identical channels, each consisting of a sodium salicylate coating on light pipes in the vacuum chamber endwall, which then conducted the blue light to photomultipliers outside the vacuum. Calibration of the 10 channels utilized the intense H_α (1216 Å) line of the DC lamp described in Section IIID. By rotating the grating, the H_α

radiation was passed across each channel, thus relatively calibrating each channel to the 1216 Å lamp output. This procedure was planned after each shock-tube test. Because the lamp required adjustment of both gas pressure and applied voltage, its day-to-day reliability was not assured. Thus, a mercury Pen Ray lamp (Ref. 26) and filter (for the 2536 Å line) were mounted inside the spectrometer in a manner to illuminate all detector channels evenly. In this manner the output of the detectors could be monitored for changes of both photomulplier gain and sodium salicylate efficiency.

Absolute calibration at the H_α wavelength was accomplished by passing this radiation across the detectors and also into an adjacent cavity behind which was mounted a photoionization photon counter. The use of NO gas-filled ionization counters for photon counting has been documented (see Ref. 21). In our case, the NO cell was optically connected to the vacuum spectrometer by means of calibrated LiF window, and the NO pressure required for total photon absorption was determined by another detector in the back of the cell. This system operated as planned, with the measured ion current being directly proportional to the photon flux. This technique therefore calibrated each channel absolutely in terms of channel output response to the H_α photon flux input.

At this point it was planned to proceed with preliminary recombination radiation measurements, and to provide subsequently the remaining calibration factor which accounts for the grating efficiency at each channel wavelength. Not even relative efficiency data are available from grating manufacturers, nor do they provide such measurement services. Although a method was devised to measure this parameter for the grating, it was no longer required when the final system described in Sections IIIC and D was employed. The reasons for the change in overall system design are presented in the following subsection.

2. Limitations to the Use of Sodium-Salicylate Detectors

In the early shock-tube experiments it soon became apparent that extraneous radiation was seriously affecting the results. This was ascertained by comparing the radiation signals with and without the insertion of filters

(e. g., LiF, quartz) into the optical train. With the spectrometer channel set to record 900 Å radiation, for example, the insertion of such opaque filters should completely eliminate the signals. However, a sizeable signal level remained, indicating a strong long-wavelength component of unwanted radiation. Thus, a set of experiments was undertaken to establish the source of this radiation, and to check the overall spectrometer performance. For simplification, a lamp was sought which had the spectral characteristics of the shock-tube radiation, i. e., far-ultraviolet output, but much larger near-ultraviolet and visible radiation. A flash lamp of the "Garton" type[27] was subsequently used for these performance tests.* The stray-light component of the signal in each channel was measured by using this lamp together with a filter wheel which could be positioned in front of each detector channel. The filters used were lithium fluoride, calcium fluoride, sapphire, quartz and glass. In this way the contribution of radiation from various spectral regions could be measured. The flash lamp output was very intense, corresponding to a brightness temperature of 30, 000 °K in the visible part of the spectrum. Thus, the lamp provided a very stringent stray-light test, because the shock-tube intensities at wavelengths longer than 1600 Å would be much lower than those from this lamp. The quantitative aspects of these data were limited by the flash lamp irreproducibility, but showed that as much as 30-70% of the recorded signals was due to radiation from unwanted wavelengths. A separate experiment in which the grating face was covered showed that the source of the stray light was not associated with optical baffling inside the spectrometer, but was directly attributable to the grating surface itself.

These performance tests thus proved that in spite of the generally high rejection of modern gratings to radiation at wavelengths other than those to which they are adjusted, sizeable signals do reach the detectors if the radiating source under study is very intense at these unwanted wavelengths. The ultimate effect on test data depends, of course, on the relative values

*The lamp and the necessary low inductance capacitor was very kindly loaned to us by Drs. W. Parkinson and E. Reeves of the Harvard College Observatory.

of the radiation at the desired wavelengths to the values of this stray-light component. For most vacuum ultraviolet studies using nonequilibrium light sources, this is a negligible effect. In the case of the present study, the thermal nature of the shock-tube radiation provided (as did the flash lamp) very intense near-ultraviolet radiation, which produced signals of comparable intensity to the desired radiation. It should be mentioned that the same problem may exist when filters are used for wavelength isolation, considering that the reflected radiation component from optical surfaces and stops may produce large signals at intensely radiating wavelengths.

For these reasons, recourse was made to the bare stainless steel photomultiplier tubes described in Section IIIC 3. Their response becomes negligible above 1600 Å, and although the response is wavelength-dependent, it is maximum throughout the wavelength range of interest to the present problem (see Fig. 17).

The difference between these two detection systems (sodium salicylate and bare metal photoelectric) is strikingly demonstrated in Fig. 19. The hydrogen spectrum of the DC low pressure lamp is presented, taken with each of these detectors. The differences are best seen by comparing the features in each case with the Lyman H_α (1216 Å) radiation. One very obvious feature is the strong 1608 Å line shown by the sodium salicylate detector (b), and the virtual absence of this line in the bare phototube detector (a). Note also that the zero order spectrum in (a) is down by a factor of three from H_α, whereas in (b), this peak was measured to be higher by a factor of 80. Thus, the long-wavelength integrating feature of the sodium salicylate is clearly seen. The increasing relative response of the bare phototube detector to wavelengths less than 1216 Å can also be seen by the enhanced prominence of the H_β and other features down to about 900 Å. The undistorted spectrum is given by (b), since the sodium salicylate spectral response is flat.

Recalling the earlier discussion of the $\lambda > 1600$ Å stray-light problem, the advantages of the use of the bare metal photoelectric detection system are clear. Their usefulness to the present research problem was invaluable.

IV. EXPERIMENTAL RESULTS

An extensive series of shock-tube experiments was undertaken to determine the absorption coefficients of O and N in the vacuum ultraviolet region of the spectrum. During the course of these experiments a number of problems arose and were investigated as well. This section of the report will include a discussion of these problems as well as a presentation of some of the VUV measurements. However, the actual data analysis and cross-section determination will be presented in Section V.

Due to the system limitations of the experimental setup (i.e., pump-down time, detector calibration, etc.), it was found that one shock-tube experiment per day was an optimum operating schedule. The experimental procedure was as follows: after overnite pumping, the pressure level in the tube reached $1\text{-}2 \times 10^{-5}$ torr. All instrumentation and spectrometer detail would be set, the test gas loaded, and the shock-tube run completed within 3 minutes after the test gas was admitted to the shock tube. Upon completion of a test, the spectrometer was moved away from the test section, and the tube would be cleaned and new diaphragms installed. The tube was purged twice with atmospheric pressure argon, and pump down began immediately thereafter, in an effort to keep the time that the tube was exposed to the atmosphere to less than 15 minutes. During the tube pumping, the discharge lamp was attached to the spectrometer and calibration scans were obtained for the detectors. Immediately following this, the VUV spectrometer was resealed to the plunger adaptor at the test section.

Prior to actual VUV data-taking experiments, a shorter series of runs using the appropriate gas mixtures was always undertaken to determine the proper diaphragm pressure ratio for the required shock speed, the available test time and the required delay time for the explosive plunger ram. During these runs, the plunger remained sealed and the spectrometer was not used. The information obtained from these survey-type experiments served to place further limitations on the operating regime curves presented in Section II. Initial test gas pressures greater than 6 torr were not used since high driver pressures would be required. In case of plunger or high

voltage cutoff malfunction, there existed a possibility of VUV detector damage at the higher pressure levels in the shock tube. A lower test gas pressure bound was due to the shock-tube operation itself. For high shock speeds, reasonable test times could not be obtained at 1 torr operation. Thus, the lowest initial pressure used in the experiments was 2 torr.

IV. A. SYSTEM EVALUATION

1. Reflected Shock Test and Induction Times

The survey-type experiments indicated that long induction times were required to obtain final reflected-shock equilibrium conditions for very dilute neon mixtures. These long induction times reflect the fact that there is a slow initial rate of election formation from the neon carrier gas. This was determined from the visible-light-monitor time histories which showed a gradual rise in intensity to a final equilibrium plateau. A number of runs were completed, using different mixture dilutions and initial pressures to determine the optimum test gas conditions. As discussed in the previous section, the radiation from the shocked gas would be used as a calibration for the VUV detector system once blackbody conditions had been achieved. It was thus required that the test gas mixture would go from a relatively high percentage of O or N in neon (i.e., approximately 5%) for blackbody requirements, to a very dilute mixture (as low as 0.25%) to obtain optically thin gas conditions. At these very small percentages of O or N in neon, the induction time could well be of the same order as the entire reflected shock test time for low initial pressures. This can be seen in Fig. 20, which shows oscilloscope records from the visible light monitors for several 13,000°K N_2 - Ne shock-tube runs. The data are typified by a gradual rise to a plateau, which is terminated by a sudden increase in intensity, likely due to the arrival of a shock arising from the interaction of the primary reflected shock wave and the oncoming interface. The total reflected-shock test time (t) is defined as the time from shock arrival (as obtained from the wall ΔT record or the onset of visible light) to the point where this sudden intensity increase occurs. The reflected-shock arrival time is indicated by the small arrow beneath the

records. For pure neon, no radiation is observed until test time termination, indicating an extremely long induction time for the pure gas. The 0.5%N_2/99.5%Ne mixture at 2 torr initial pressure shows a gradual increase in radiation approaching a plateau, but does not obtain it in the available test time. However, increasing the initial pressure to 4 torr yields better shock tube operation (i.e. the available test time is increased by a factor of 1.6) and a 0.25% N_2/99.75% Ne mixture also obtains a radiation plateau within the available test time. Thus, very dilute test gas mixtures must be used at initial pressure greater than 2 torr to obtain meaningful data. The 3% N_2/97% Ne test gas obtains equilibrium very rapidly even at the lowest pressure of 2 torr.

A number of observations can be made concerning the data. First, the available reflected-shock test time is increased by going from 2 to 4 torr initial pressure. This is also seen in Fig. 21 where the test time (t) and induction time (τ) are plotted for the N_2 - Ne experiments. The induction time (τ) is defined here as the time from shock arrival to attainment of a level radiation plateau. Test gas mixtures that are unusable at 2 torr pressure yield valid data at a 4 torr initial pressure. Also seen on Fig. 21 are results from measurements at a reflected shock temperature of 11,000°K. Here the test time is much longer due to the slower shock speed and the increased initial pressure of 6 torr.

To obtain consistent data of the type shown in Fig. 20, the requirement of a high gas-purity level is mandatory. The slightest trace of a contaminant (nitrogen, for example) for the pure neon experiment, gave a light output similar to the other mixtures. Thus, the pure neon runs proved to be an extremely sensitive monitor on the cleanliness of the entire shock tube and loading system. Several experiments using the VUV spectrometer confirmed the importance of this visible monitor radiation. The explosive-ram time delay was purposely set to open the plunger early, during the period of this induction time. At very early times, when no visible radiation was recorded, the VUV detectors also recorded no radiation. When the plunger was synchronized to open during the gradual rise of the visible light, the VUV-detector outputs also showed a gradual rise. From the correlation of the visible and VUV radiation, it is concluded that the monitors are detecting the visible region of the ion-electron

recombination continuum arising from transitions to excited states. Consequently, for all VUV data-taking runs, the plunger was synchronized to open when a level radiation plateau had been achieved (i.e., late for the very dilute mixture and early for the higher percentage mixtures). For each shock-tube experiment, a record similar to that shown in Fig. 14 was obtained, to indicate the part of the available test time in which the VUV radiation was observed.

Similar data were also obtained for the O_2 - Ne experiments. Initial tests were attempted at a reflected-shock temperature of approximately 11,000°K, but induction times for the very dilute mixtures were extremely long. Consequently, a shock temperature of 12,500°K was used to obtain the O-atom data. However, even at this higher temperature the most dilute O_2 - Ne mixture (0.2% O_2/99.8% Ne) would not obtain equilibrium in the available test time. This can be seen in Fig. 22 which shows monitor time histories of the visible radiation. Although the 0.2% O_2/99.8% Ne mixture does not reach equilibrium, the 0.55% O_2/99.45% Ne test gas does obtain a radiation plateau at the highest temperature of 12,600°K, and very nearly reaches it at 12,100°K. Based on these measurements, the most dilute mixture used for the present O-atom experiments was 0.55% O_2/99.45% Ne.

2. Incident Shock Radiation

The red and blue incident shock radiation time-history profiles were also obtained for each nitrogen experiment. The red filter centered at 7100Å is the same one used in the nitrogen experiments discussed in Ref. 22, wherein it was shown that the radiation from the $N_2(1+)$ system was being observed behind the incident shock wave. Several radiation time histories are presented in Fig. 23 for both the blue and red wavelengths. The general character of the signals shows the radiation rising to a maximum and then decreasing. For the highest percentage mixtures, this maximum occurs near the shock front, and a level radiation plateau is obtained in later time. For the more dilute mixtures at lower temperatures, this final level value of the radiation is never reached before the driver-gas interface appears. For comparison, a thin-film wall ΔT record is shown. The appearance of the interface on this record is given by the change in character from the constant ΔT value

(indicative of a laminar boundary layer). The incident shock test time as determined from such a ΔT record would be longer than that obtained from the radiation time histories, due to the mixing of the cold driver gas with the shocked test gas mixture, and the resultant radiation quenching.

The appearance of the maximum in the red wavelength radiation is connected with the population of the $B^3\pi_g$ state of N_2, from which the (1+) system arises. An estimate of the excitation time for this state can be obtained, if this time is identified with the time to reach the maximum radiation value. These results are shown in Fig. 24, where τ is the time to reach the maximum (in μsec) and p is the post-shock pressure in atmospheres. Included in this figure are data taken from Ref. 28, where a mixture of 10% N_2 - 90% Ar was used as the test gas. The present results for a neon diluent, which cover a significantly greater temperature range, are consistent with the results of Ref. 28 for an argon carrier gas. The indication is that neon is about as effective as argon in exciting the $B^3\pi_g$ state. In calculating the gas temperature, vibrational equilibrium of the nitrogen molecules was assumed, but the chemical processes were assumed to remain frozen. This post-shock temperature is then very nearly that for pure neon, since the percentage of nitrogen is small. The largest temperature change due to vibrational relaxation was 200°K for the 10% N_2 - 90% Ne mixture.

3. Experiments with Gaseous Plunger Windows

Preceding the nitrogen and oxygen experiments, a series of tests was undertaken to investigate the gasdynamics of the windowless plunger. For a vacuum-window experiment, there will be an outflow of a small quantity of test gas through the orifice channel into the plunger itself (see Fig. 12). In turn, most of this gas will flow downward into the plunger reservoir due to the high conductance path, and a small amount will pass through the 1 mm orifice into the spectrometer. There are two possible effects of this gas outflow, both of which have been discussed briefly in Ref. 12. First, there will be an expansion wave propagating into the shocked gas from the orifice channel. This expansion wave will lower the temperature of the gas near the orifice and may affect the VUV-radiation measurements. The experiments

discussed in Ref. 12 indicate that this expansion wave had no measureable effect on the integrated intensity observed by the thin-film gauge. For the present series of experiments, no noticeable difference was observed in the reflected blue and red monitor outputs for either a VUV plunger experiment, or a test wherein the plunger remained sealed and no test gas outflow was allowed. These tests, of course, do not measure directly the possible effect of orifice outflow on the vacuum-ultraviolet radiation and further investigation of this particular problem should be pursued. However, in view of the available experimental data, it is assumed that any effect on the measured VUV radiation will be small.

There is, however, a second effect of this gas expansion which may be of greater importance. The expanded gas, both in the plunger volume and the spectrometer itself, is at a lower temperature. Thus, the possibility exists that this gas may act as an absorbing medium and diminish the VUV radiation received by the detectors. A nonequilibrium streamtube analysis was presented in Ref. 12 for the expansion plume present in those experiments. This analysis indicated that the absorption by the low temperature, low density expansion plume was negligible. The plunger configuration for the present series of experiments precluded such an analysis (i.e. the bulk of the expanded gas enters the plunger reservoir, while only a small amount forms an expansion plume within the spectrometer). A series of experiments was thus initiated to investigate this problem, using various gases to act as windows in the plunger.

A 5% Ar - 95% Ne mixture was used as the test gas at an initial pressure of 4 torr. At the reflected shock temperature for these experiments (13,300°K) calculations showed that the gas would radiate as a blackbody below the argon cutoff edge at 785Å. A spectrometer setting was used such that one channel recorded light from just inside the continuum edge (770Å), see Fig. 1, one channel was in a region of argon lines (970Å) and the third channel in a relatively clear region (1152Å). In order to assess the effect of various window gases as selective absorbing medium, argon, neon and helium were used at various pressures in the plunger. First, vacuum window experiments were performed, and VUV detector signals obtained for this

condition. Since the reflected-shock pressure was approximately 41 psia, the first window experiments used (in succession) argon, neon, and helium at 43 psia (i.e. a pressure slightly higher than the reflected shock pressure). For all three window gases at this condition, the outputs of all three detector channels were greatly reduced such that only a small fraction of the vacuum window signals were recorded. Since the neon (continuum edge at 580Å) and helium (continuum edge at 500Å), see Fig. 1, window gases are optically inactive at these wavelengths, it would be expected that the VUV radiation would not be perturbed by these gaseous windows. Thus, a gasdynamic effect appears to have caused this signal attenuation. The next experiments were performed with only a small amount of argon and neon as the window gases at a pressure of approximately 4 psia. For these runs, all three detector outputs were about the same as the vacuum window data. Finally, neon and argon windows were employed at a pressure of 17 psia (i.e. at a pressure slightly below the 19 psia value to insure choking of the window orifice for a $\gamma = 1.67$ gas). For this neon window, all three output channels recorded radiation levels similar to those obtained for the vacuum window experiments. However, for the argon window, only the channels outside of the argon continuum recorded vacuum levels. The 770Å channel was attenuated to about 1/6 of its vacuum window level, indicating that the argon window was acting as an absorbing window for this wavelength radiation.

The results of these tests are summarized in Fig. 25, where the detector output for window runs is normalized by the vacuum window output. It is seen that window gases (whether optically active or not at the wavelengths under study) at pressures near the actual test gas pressure lead to greatly attenuated output signals. This may be caused by the fact that the colder boundary layer gas in the orifice channel and at the shock tube wall is prevented from draining off. Alternatively, gaseous windows at low pressure have little or no effect on the radiation signal and are equivalent to vacuum window conditions. When the window gases are at a higher pressure, but still slightly below the maximum pressure allowable to insure choking at the orifice, the absorption characteristics seem to act in a predictable manner. That is, the colder boundary-layer-like gas is allowed to drain off, but the

window gas acts as an absorbing medium only in certain wavelength channels. It was decided on the basis of these results, to use the vacuum window configuration for all further experimental investigations.

IV. B. THE VACUUM ULTRAVIOLET EXPERIMENTS

The vacuum ultraviolet measurements were obtained in a series of tests with the spectrometer grating at a fixed setting. As noted in a previous section of the report, the radiation from the shocked gas would act as a calibration of a particular grating-detector setting, when blackbody conditions had been reached (i.e. the detector output would remain constant as the atom concentration was further increased). Thus, a number of experiments were needed to obtain a value for the absorption coefficient at any selected wavelength. The program, then, consisted of a set of these experimental series wherein the radiating gas ranged from optically thin to the blackbody limit.

For the N_2 - Ne experiments, data were obtained at two nominal reflected shock temperatures, 11,000°K and 13,000°K. The following table shows the neon-diluted gas mixtures and initial pressures used for the nitrogen series (the mixtures and pressures used were based on the calculations discussed in Section II):

T_R = 13,000°K	T_R = 11,000°K
0.25% N_2 at 4 torr	0.53% N_2 at 6 torr
0.5% N_2 at 4 torr	3% N_2 at 6 torr
0.53% N_2 at 4 torr	7% N_2 at 4 torr
3% N_2 at 2 torr	
3% N_2 at 4 torr	

It may be noted that except for the 0.53% N_2/99.47% Ne mixture (purchased as a premixed gas), all other test gases were mixed in the loading manifold for the nitrogen experiments (see Section III). A number of experiments were undertaken at several values of grating micrometer setting to obtain preliminary

data and thus establish signal output levels for the VUV detectors. The two primary grating settings finally used in the run series allowed each of the three detectors to view radiation from the three plateau regions of the continuum as shown, for example, in Fig. 4. Thus, one detector viewed radiation arising in the 1020Å - 1130Å interval, another was positioned in the 852Å - 1020Å interval, and the third was located below 852Å. In addition, wavelength intervals were selected to be relatively free of line radiation, see Ref. 19. The wavelengths under investigation are given in the following table:

Grating Micrometer Setting = 496

	PMT #1	PMT #2	PMT #3
1st Order	1534Å	1944Å	2310Å
2nd Order	767	972	1155
3rd Order	511	648	770

Grating Micrometer Setting = 486

	PMT #1	PMT #2	PMT #3
1st Order	1440Å	1840Å	2210Å
2nd Order	720	920	1105
3rd Order	480	613	737

The wavelength settings were chosen so that the radiation under study would be viewed in 2nd order giving an 8Å spectral bandpass per channel. Contributions to the detected radiation signals from overlapping orders are a function of detector sensitivity and grating efficiency, and have been discussed in Section III. Possible first order contributions from the line radiation in the longer wavelength region will, in most cases, be negligible, due primarily to the large decrease in photomultiplier sensitivity at these wavelengths (i.e. the detectors are essentially blind to radiation at wavelengths longer than 1800Å). A possibility of a 1st order contribution arises in the PMT #1 signal, which records the lowest wavelength radiation. Several experiments were undertaken with lithium-fluoride filters placed in front of the detectors, using

the filter wheel mounted in the spectrometer. Since these filters have a low wavelength cutoff of approximately 1050Å, only radiation at wavelengths longer than this would be recorded. The results of these experiments will be presented in the next section.

For the O_2 - Ne experiments, data were obtained at one reflected shock temperature of 12,500°K. The neon-diluted gas mixtures and initial pressures used in the oxygen series are given in the following table:

T_R = 12,500°K
0.55% O_2 at 5 torr
1.1% O_2 at 4 torr
1.88% O_2 at 4 torr
4.14% O_2 at 4 torr

All of the test gases used in these tests were purchased as pre-mixed test gases based on the calculations presented in Section II. Nominal mixtures of 0.5, 1, 2, and 4% of O_2 in neon were requested, and the final gas analysis sent with the mixtures showed the actual percentage of O_2 as indicated in the table. The wavelength range of the O continuum is considerably less than that for N (see Fig. 6) with the cutoff edge at 911Å. Consequently, a grating micrometer setting was chosen so that at least two of the detectors viewed radiation arising from the prominent plateaus in this region (666Å - 732Å and 732Å - 911Å), at wavelength intervals free from line radiation, see Ref. 19. The wavelengths under investigation are given in the table:

Grating Micrometer Setting = 451

	PMT #1	PMT #2	PMT #3
1st Order	1040	1450	1815
2nd Order	520	725	907
3rd Order	347	483	605

Again, the radiation was monitored in 2nd order with PMT #2 and PMT #3

giving the primary data.

With the bare photomultipliers operating at 2000 volts, the output signals were quite substantial, ranging from about 10-200 millivolts, depending upon the detector wavelength location and gas mixture.

V. ANALYSIS OF DATA AND DISCUSSION

V. A. DATA ANALYSIS

The values of the photoionization cross-sections, (σ), for N and O were obtained from the vacuum-ultraviolet radiation data, wherein the shocked gas ranged from optically thin to blackbody conditions. From the recombination reactions under study

$$N^+ + e \longrightarrow N + h\nu$$
$$O^+ + e \longrightarrow O + h\nu \quad , \tag{7}$$

it is seen that the rate of emission is proportional to the ion-electron product,

$$\frac{d(h\nu)_N}{dt} \propto (N^+)(e)$$
$$\frac{d(h\nu)_O}{dt} \propto (O^+)(e) \quad . \tag{8}$$

The results obtained from the normal-shock computer program gave the concentration of species behind the reflected shock wave. It can be seen from Figs. 7 and 8 that the contribution of the positive neon ion (Ne^+) to the formation of electrons may be of importance for the shock speeds used in the experimental series. This is especially true for very dilute mixtures, where the Ne^+ ion is present in larger concentration than the atomic ions N^+ or O^+. Since the cross-sections under study are for reactions involving electrons and only N^+ or O^+, the contribution of the neon ion must be taken into consideration. That is, the observed radiation signals may be significantly affected by the presence of the excess electrons $\left(\text{i.e. } [e^-] > [N^+] \text{ or } [O^+]\right)$ in the dilute mixtures. From the measured shock speed and computer results, the factor R was determined as

$$R = \frac{(N^+)(e)}{(N^+)^2} \quad \text{or} \quad \frac{(O^+)(e)}{(O^+)^2} \quad . \tag{9}$$

When the Ne^+ concentration is very small, the number of atomic ions equals the number of electrons, i.e. $(N^+)(e^-) = (N^+)^2$ and $R=1$. For very dilute mixtures, however, $R > 1$. The data were normalized by this factor, R,

during the data reduction procedure. Typical values of this R factor, obtained from measured shock velocities and computer program results were:

N_2 - Ne Experiments				O_2 - Ne Experiments	
T_R = 13,000°K		T_R = 11,000°K		T_R = 12,500°K	
Test Gas	R	Test Gas	R	Test Gas	R
3% N_2 at 4 torr	1.15	7% N_2 at 4 torr	1	4.14% O_2 at 4 torr	1.1
3% N_2 at 2 torr	1.18	3% N_2 at 6 torr	1	1.88% O_2 at 4 torr	1.23
0.5% N_2 at 4 torr	2.45	0.5% N_2 at 6 torr	1.3	1.1% O_2 at 4 torr	1.57
0.25% N_2 at 4 torr	4.2			0.55% O_2 at 5 torr	2.4

The double diaphragm technique used in the experiments insured close control over the diaphragm burst pressure. However, there was a small scatter in the shock velocity measured near the observation section for a number of shock-tube tests. This, in turn, gave rise to a scatter in the reflected-shock temperatures. Figure 26 presents typical shock speed attenuation as obtained from the megacycle timing counters. The reflected-shock temperature was obtained from the computer-program results, using the measured incident-shock velocity near the endwall. This is consistent with wave-diagram analysis that indicated the fluid particles under observation originated within the last three feet of the shock tube. Since the blackbody distribution is a strong function of temperature in the VUV region, it is necessary to maintain close repeatability in a given experimental series. For the nitrogen experiments, at a nominal temperature of 13,000°K, the maximum temperature spread was 300°K (i.e., 12,900 - 13,200°K). It should be noted that for the shock wave velocities employed in the experiments, a difference of 1 μsec in the final timing interval gave rise to approximately a 100°K temperature difference between tests. The observed detector outputs were then normalized to the nominal temperature (say 13,000°K) using a linear blackbody relationship for the small temperature intervals involved. This approach was used for all data in a given test series. The temperature spread for the oxygen series (nominal temperature of 12,500°K) was 250°K, ranging

from 12,300°K to 12,550°K.

The normalized output for a given detector at a selected wavelength was then divided by the maximum output of that detector for mixtures having a high percentage of nitrogen, forming the ratio referred to as I/I_{BB}. These results are shown in Fig. 27 for two wavelengths, 720Å and 767Å, in the 13,000°K nitrogen test series, plotted as a function of N atom concentration behind the reflected shock $(\rho/\rho_o)_N$. The solid curves are taken from the emissivity calculations given in Section II and are not drawn through the experimental points. Since the output signal at these wavelengths did not increase when the $(\rho/\rho_o)_N$ concentration was increased from 1.2×10^{-3} to 2.6×10^{-3} (i.e., initial 3% N_2/97% Ne test gas pressure increased from 2 to 4 torr), it was assumed blackbody conditions had been reached. The data shown in Fig. 27 indicate that in this wavelength region, the experimentally determined emissivity, or I/I_{BB} ratio, agrees quite well with the theoretical calculations. However, data obtained in the middle plateau region for the N continuum gives an emissivity somewhat higher than the calculated value at 920Å. Figure 28 indicates the experimentally determined emissivity to be midway between the calculated values for the two plateau regions. The I/I_{BB} ratios obtained from the oxygen experiments are shown in Fig. 29 and compared with the calculated emissivities for 905Å (just inside the photoionization cutoff edge) and 725Å in the second oxygen plateau.

Referring to the equations discussed in Section II, and using the experimentally determined values of I/I_{BB}, it is possible to write the following relation

$$I/I_{BB} = 1 - e^{-\alpha \ell} \tag{10}$$

Using Eq. 10, the absorption coefficient, α was then obtained at the selected wavelength. The diameter of the shock tube, 7.62 cm, was used as the optical path length, ℓ. From the absorption coefficient, the effective photoionization cross-section, σ, was obtained using

$$\sigma = \frac{\alpha}{L_o (\rho/\rho_o)_{ATOMS}} \tag{11}$$

The values of $(\rho/\rho_o)_{atoms}$ were obtained from the shock calculations for the given test gas mixture, pressure and observed shock velocity (see Figs. 27-29, for example). These final σ values are given in Figs. 30-31 for both the N and O atoms at the wavelengths under study. The calculated effective cross-sections are also given (i.e., from Section II).

A number of observations may be made concerning these two figures. For the nitrogen atom, no σ results were obtained in the longest wavelength plateau region (i.e., the 1020Å - 1130Å interval) although radiation measurements were obtained. The experimental results indicated that the emissivity of this region did not approach blackbody conditions. The data, when plotted as a function of $(\rho/\rho_o)_N$, as in Fig. 27, continued to show an increase. Thus, a blackbody calibration for the detector wavelength setting could not be obtained. On the basis of the 13,000°K calculations discussed in Section II, the highest value of ϵ_λ was about 0.2 for this region, the majority of the measurements being made in an optically thin gas. For the middle plateau in nitrogen (852Å - 1020Å) all of the run series did not reach the blackbody limit. The measurements indicated this to be accomplished for the 920Å data, while the 970Å results approached, but did not quite reach, a level value. Since these data very nearly obtained the blackbody calibration point, an attempt was made to determine the absorption coefficient from the available results. Since the experimental points at a selected wavelength lie on an I/I_{BB} curve tending to reach a common calibration point of $I/I_{BB} = 1$, the following relations were used:

$$I_1 = I_{BB}\left(1 - e^{-\alpha^*(\rho/\rho_o)_{n_1}\ell}\right)$$
$$I_2 = I_{BB}\left(1 - e^{-\alpha^*(\rho/\rho_o)_{n_2}\ell}\right) \quad , \tag{12}$$

where

$$\alpha = \alpha^*\left(\frac{\rho}{\rho_o}\right) \quad . \tag{13}$$

Thus, the ratio of intensities for two different atom concentrations (n_1 and n_2) is

$$\frac{I_1}{I_2} = \frac{1 - e^{-\alpha^*(\rho/\rho_o)_{n_1}\ell}}{1 - e^{-\alpha^*(\rho/\rho_o)_{n_2}\ell}} \quad . \tag{14}$$

Equation (14) can be rewritten as

$$\frac{I_1}{I_2} = \frac{1 - e^{-\frac{(\rho/\rho_o)_{n_1}}{(\rho/\rho_o)_{n_2}} t}}{1 - e^{-t}} \quad , \tag{15}$$

where $t = \alpha^* \ell (\rho/\rho_o)_{n_2}$. This equation was solved for the parameter t, using as inputs the ratios I_1/I_2 and $(\rho/\rho_o)_{n_1}/(\rho/\rho_o)_{n_2}$. The values of σ obtained from this calculation are also shown in Fig. 30 for the nitrogen atom. By using this successive ratio technique, the data, as expected, show a somewhat larger scatter than that obtained when a blackbody calibration was reached. Under those conditions, the scatter shown in Fig. 30 was due to typical radiation measurements and data reduction procedure. As can be seen from Fig. 27, for example, the experimentally determined I/I_{BB} ratios scatter above and below the theoretical curve. As a check on this iterative procedure, values of σ obtained from Eq. 15 were checked with those obtained at the blackbody calibration wavelengths (for N : 720Å, 767Å and 920Å). These data agreed with the original cross-section values, with a somewhat greater scatter.

The experimentally determined effective photoionization cross-sections for N agree quite well with the calculated values at 13,000°K for recombination to the ground state ($\lambda < 852$Å). However, the σ values are larger than the calculations in the middle plateau, i.e., a factor of 3 greater at 920Å and a factor of 2 greater at 970Å for a temperature of 13,000°K.

The 11,000°K nitrogen shock-tube series were subject to a considerably greater temperature scatter due to less control over the diaphragm break pressure. A temperature spread of approximately 700°K (i.e., 10,700°K to 11,400°K) was obtained and the resulting σ data are not considered as precise as the 13,000°K results. In addition, blackbody calibration limits were not achieved for the middle nitrogen plateau and the successive ratio technique was used to obtain cross-sections from the radiation measurements. This gave rise to considerable scatter in the results, as shown in Fig. 30, which still indicate, however, a higher value of σ than the calculations would predict.

V. B. EXPERIMENTAL UNCERTAINTY

1. Radiation Contribution From Other Spectral Orders

A possible factor in the experimentally determined higher cross-section values could be the contribution of radiation from other orders falling on the detector, i.e., first order radiation at wavelengths greater than 1400Å, and third order radiation at the lower wavelengths. The grating settings were chosen to minimize the possibility of first order line radiation contributions by choosing a suitable spectral bandpass. Various N-atom line positions were obtained from Ref.19, with subsequent reference to the spectral scans presented in the later work discussed in Ref.29. In addition, based on the grating efficiency and detector sensitivity measurements discussed in Section III, estimates of different order contributions were made for the various second order measurements. It was assumed that all radiation below 580Å (the neon photoionization edge) does not contribute, and that radiation above 1800Å would be very small due to the extreme loss of detector sensitivity. The spectral purity of each channel viewing radiation in second order was examined, and the following conclusions were obtained (refer to previous tables of grating settings).

A. The nitrogen #1 channels at 720Å and 767Å were clear since there is no line radiation from first order (i.e., N lines are located at 1412Å, 1493Å and 1743Å) and a third order contribution is below the neon cutoff.

B. The nitrogen #2 channels at 920Å and 972Å were clear in first order (since this contribution is above 1800Å where the detectors are blind). The relative contribution from the low wavelength third order was a function of the optical thickness of the gas:

Thick Gas (High Percentage Mixture)	
648Å Contribution	.04 at 13,000°K
972Å Contribution	.017 at 11,000°K
613Å Contribution	.05 at 13,000°K
920Å Contribution	.01 at 11,000°K

Thin Gas (Dilute Mixture)	
648Å Contribution	.14 at 13,000°K
972Å Contribution	.06 at 11,000°K
613Å Contribution	.09 at 13,000°K
972Å Contribution	.033 at 11,000°K

It can be seen that, in general, the third order contribution is less than 5%. The maximum contribution of about 10% to the measurements occurs in the dilute mixtures from the low wavelength first order. This is due to the fact that although the middle plateau region is optically thin, the lower wavelength regime is still optically thick. These calculated contributions were not subtracted when reducing the measured radiation data, and, therefore, a possible uncertainty of less than 10% exists in the final cross-section values.

C. The nitrogen #3 channels at 1105Å and 1155Å indicated the possibility of a much greater contribution from third order, as:

Thick Gas	
770Å Contribution	0.65 at 13,000°K
1155Å Contribution	0.28 at 11,000°K
737Å Contribution	0.43 at 13,000°K
1105Å Contribution	0.18 at 11,000°K

Thin Gas	
770Å Contribution	2.7 at 13,000°K
1155Å Contribution	1.15 at 11,000°K
737Å Contribution	1.7 at 13,000°K
1105Å Contribution	0.73 at 11,000°K

The calculations for this channel indicate that for the dilute mixtures especially, the detected radiation is coming from third order. This is due to the high emissivity at the lower wavelengths and the greater photomultiplier sensitivity there. These calculations provided another reason why this #3 channel information was not used to obtain cross-section data in the third nitrogen plateau. It is of interest to consider a possible means of eliminating this unwanted lower-wavelength contribution. On the basis of the gaseous-window experiments discussed in Section IV, it may be possible in future experiments to eliminate this radiation with the proper window gas. Argon, for example,

would absorb all wavelengths below about 800Å and act as a filter for the second order wavelengths.

Similar spectral purity analyses were undertaken for the oxygen measurements, with the following conclusions;

D. The #1 channel for oxygen will record only 1st order 1040Å radiation, since the 2nd and 3rd order contributions are below the neon cutoff. In the experimental series, substantial signals were obtained from this detector, likely from the atom lines at 1027Å and 1046Å.

E. The #2 oxygen channel will receive no third order contribution (this lies below the neon cutoff), while the first order wavelength at 1450Å is in a relatively clear spectral band with no lines present.

F. The third channel for oxygen has no first order contribution, $\lambda >$ 1800Å, and the third order contribution was calculated as

$$\frac{605\text{Å Contribution}}{907\text{Å Contribution}} = .013 \text{ or a } 1.3\% \text{ contribution.}$$

Experimental verification of these conclusions was undertaken, and several experiments were performed with lithium-fluoride filters placed in front of the detectors to check possible first order (longer wavelength) contributions for both the nitrogen and oxygen test gases. The nitrogen experiments used the 13,000°K 3% N_2/97% Ne and 0.53% N_2/99.47% Ne mixtures and indicated about a 0.3% 1st order contribution for the #2 channel and a possible 5% 1st order contribution for channel #1. In addition, experiments were performed at a different grating angle, close to the original setting used in the run series. In this case, channel #1 viewed 1494Å in 1st order (747Å in 2nd order) and the unfiltered signal was approximately double that of the 767Å signal observed in the run series. Placing a LiF filter in front of this channel lowered the signal to about 1/2 of its original value. This first order contribution arises from the strong nitrogen line at 1492Å (see Ref.19, and the spectral scan shown in Ref.29). The other channels, #2 and

#3, gave unfiltered signals to within about 10% of the original run series values, and again, channel #2 showed only a fraction of a percent contribution from 1st order.

For oxygen, the experiments were performed with the 1.1% O_2/98.9% Ne mixture and the results indicated that for channel #3 (907Å) a contribution of 0.25% of the unfiltered signal was detected through the filter. For the 725Å channel a contribution of about 8% was detected from the 1450Å region. The source of this radiation is as yet unresolved. For channel #1 (at 1040Å in 1st order), the actual filtered signal was only 0.5% of the unfiltered signal. However, the transmission of the LiF at this wavelength is almost zero, and it would be expected to absorb essentially all radiation at that wavelength.

The conclusion that can be reached from both the calculations and the lithium-fluoride filter experiments is that there is very little order overlap in the wavelength channels which were used to obtain the final cross-section data. At most, uncertainties of the order 10-15% in σ may arise from unwanted contributions from either 1st or 3rd order.

2. Detector Stability

The response stability of the bare photomultiplier detectors is an important part of meaningful radiation measurements. As discussed in Section III, the discharge lamp was used to check possible relative degradation or changes in detector sensitivity using line radiation. In addition, the 3% N_2/97% Ne experiment at 13,000°K was often repeated at various intervals to check the detector outputs under actual experimental conditions. The results of these runs showed excellent photomultiplier stability. Experiments repeated at two-month intervals, for example, gave repeatable detector outputs to within 2%. This dependability is attributed to the cleanliness of the system, the separately pumped photomultiplier chamber, and the high-voltage cutoff system to insure against possible detector damage.

3. Free-Free Radiation

Possible contribution from other radiation was also considered, in

particular from the free-free radiation from N^+ in the nitrogen experiments. The expression given in Ref. 1 was used to compute the magnitude of this effect;

$$\frac{dI}{dV\,d\tilde{\nu}\,d\Omega} = 1.63\times 10^{-35} T^{-1/2} N_e N_i z^2 e^{-\frac{hc\tilde{\nu}}{kT}} \qquad \frac{watts}{cm^2\ ster}, \quad (16)$$

with an effective $z^2 = 1.5$. If Eq. 16 is divided by the atom concentration N_A, it can be rewritten as

$$\frac{dI}{dV\,d\tilde{\nu}\,d\Omega}\ \frac{1}{N_A} = M K_1 T^{-1/2} e^{-\frac{hc\tilde{\nu}}{kT}} \qquad \frac{watts}{atom-cm^{-1}-ster}, \quad (17)$$

where K_1 is the equilibrium constant for the recombination reaction, and M is a constant. Multiplying the calculated results of Eq. 17 by $\frac{10^{-4}}{\lambda^2\,(cm^2)}$ yields the free-free radiation in units of $\frac{\text{watts}}{\text{atom-ster-}\mu}$, which can be directly compared with the calculated recombination continuum radiation given in Ref. 17. At a temperature of 13,000°K, this calculated free-free radiation is approximately 5 orders of magnitude below the recombination continuum at wavelengths below 1130Å.

4. Thermal Layer Growth

The visible-radiation monitors for the reflected shock region, given in Fig. 20 for example, showed, in general, a gradual rise in radiation towards a level plateau. However, for some of the higher percentage mixtures for both oxygen and nitrogen, these detectors recorded a drooping of this plateau. For these experiments, the windowless plunger was synchronized to open at the beginning of this region, to insure that the vacuum-ultraviolet measurements were obtained at the initial plateau level. The cause of this intensity decrease as a function of time could be possible radiation cooling of the gas, the lowering of the gas temperature due to the growth of the thermal layer from the endwall, etc. As discussed in Section IV, the observed radiation was unaffected by the windowless plunger open time, and thus the possibility of cooling due to expansion waves originating at the orifice passage was discounted. Figure 32 gives oscilloscope records of such visible-radiation time histories and VUV detector signals, indicating the plunger synchronization.

When the VUV data were obtained at the initial radiation level, the results were internally consistent for a given test series; that is, the I/I_{BB} ratios showed proper agreement.

The problem of thermal layer growth from the reflecting wall was considered in detail, since this could be a contributing factor to this radiation decay through cooling of the shocked gas. Referring to the analysis presented in Ref. 30, the temperature profiles of the gas and endwall are pictured as

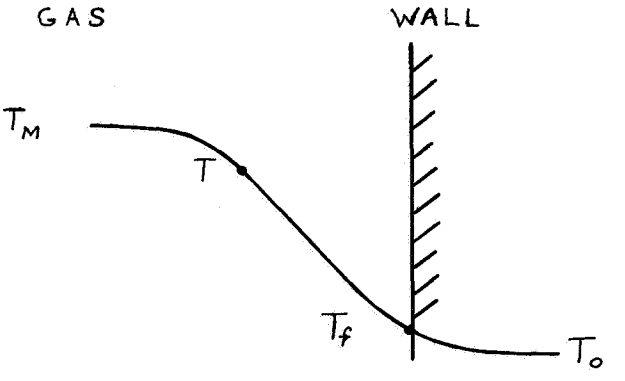

where T_M is the gas temperature behind the reflected shock, T_f is the temperature approached by the wall surface and T_o is the initial gas and wall temperature. The solution for the temperature T is given by an error function solution. Following Ref. 30, it is possible to calculate the distance (X) from the wall surface where the gas temperature (T) has dropped 1/2 percent of its maximum value (T_M). This is given as

$$\frac{T - T_f}{T_M - T_f} \geq 0.995 \qquad \text{for} \quad X \geq 4 \frac{T_M}{T_f} \sqrt{k_f T} \tag{18}$$

where k_f is the gas thermal diffusivity at temperature T_f and density ρ_f. The thermal diffusivity is defined as

$$k_f = \frac{K(T_f)}{\rho_f c_p} \tag{19}$$

where K(T) is the thermal conductivity of the gas and c_p is the gas specific heat at constant pressure. The distance X was computed for the nitrogen

run series at both 11,000°K and 13,000°K, but approximated by pure neon, since this is the bulk of the test gas. In addition, since the endwall surface temperature (T_f) will be only a small increment above the initial temperature (T_o), it was assumed that $T_f = T_o = 300°K$. Thus, the values used to calculate k_f for neon were:

$$c_{p_f} = 0.24 \text{ Btu/lb °R}$$

$$K_f = 7.4 \times 10^{-6} \text{ Btu/ft-sec-°R},$$

and the ρ_f values for neon were taken from the ρ_M values obtained from the shock computer program multiplied by the temperature ratio; i.e.,

$$\rho_f = \rho_M \frac{T_M}{T_f} .$$

The calculated results for pure neon are given in the following table:

T = 13,000°K

t μsec	X, (P_1 = 4 torr)	X, (P_1 = 2 torr)
1	0.7 mm	0.92 mm
10	2.22	2.92
60	5.4	7.1
100	7.	9.2

T = 11,000°K

t μsec	X, (P_1 = 6 torr)
1	0.6 mm
10	1.9
60	4.65
100	6.
200	8.5

The plunger orifice is located 1/2-inch or approximately 12 mm from the shock-tube endwall. The thin film gauge wall ΔT record indicated a transit time of 10-15 μsec for the reflected shock to travel from the endwall to the plunger orifice. On the basis of the above approximate calculations, it appears that during the time scale for the experimental observations, the endwall thermal layer growth will not affect the results.

5. Nonequilibrium Chemistry Effects

The results of the incident-shock radiation measurements presented in Section IV showed that for certain experimental conditions, the flow behind

the incident-shock wave may not attain full equilibrium. As a result of this, there arises the possibility of uncertainty in the determination of reflected-shock conditions for a measured incident-shock speed. An attempt was made to determine this uncertainty in the state of the gas, and also, the uncertainty in the photoionization cross-sections obtained from the VUV radiation measurements for a given test series. Calculations indicated a possible 30% uncertainty in the experimentally determined cross-sections at the shorter wave lengths.

In order to obtain estimates of the effect of nonequilibrium chemistry on the results, the shock computer program discussed in Section II was utilized. This program has a number of options available for computing the state of the gas behind the shock waves. For the calculations under discussion here, the option of

Incident Shock	Reflected Shock
Equilibrium Vibration Frozen Chemistry	Full Equilibrium

was used to compare the reflected-shock results with the previous calculations employing the option

Incident Shock	Reflected Shock
Full Equilibrium	Full Equilibrium

The test cases were the 13,000°K nitrogen experimental series, for both a thick (3% N_2/97% Ne mixture at 4 torr) and a dilute mixture (0.5% N_2/99.5% Ne at 4 torr).

The calculations were completed at several intervals of incident-shock velocity, and some of the results are tabulated below:

Option E = full equilibrium incident and reflected

Option F = frozen chemistry incident (with vibrational equilibrium) and full equilibrium reflected

Case A. 0.5% N_2 - 99.5% Ne at 4 torr

V_s - ft/sec	T_{REFL} °K		$(\rho/\rho_o)_{N\ REFL}$		$(\rho/\rho_o)_{e\ REFL}$		$(\rho/\rho_o)_{N^+\ REFL}$		$R = \frac{(N^+)(e)}{(N^+)^2}$	
9843	9484	9467	4.3-4	4.3-4	5.5-5	5.4-5	5.2-5	5.09-5	1.06	1.06
11,483	12,158	12,037	2.7-4	2.6-4	4.6-4	4.1-4	2.62-4	2.45-4	1.75	1.67
13,123	13,826	13,723	2.0-4	1.9-4	1.4-3	1.28-3	3.87-4	3.68-4	3.62	3.48
	E	F	E	F	E	F	E	F	E	F

Case B. 3% N_2 - 97% Ne at 4 torr

V_s - ft/sec	T_{REFL} °K		$(\rho/\rho_o)_{N\ REFL}$		$(\rho/\rho_o)_{e\ REFL}$		$(\rho/\rho_o)_{N^+\ REFL}$		R	
9843	7857	7823	3.3-3	3.2-3	2.1-5	1.96-5	2.06-5	1.95-5	1.02	1.00
11,483	10,818	10,516	3.3-3	3.1-3	4.8-4	3.7-5	4.71-4	3.6-4	1.02	1.02
13,123	13,109	12,571	2.7-3	2.4-3	2.1-3	1.4-3	1.74-3	1.25-3	1.14	1.14
	E	F	E	F	E	F	E	F	E	F

Note: -4 indicates 10^{-4}, etc.

The calculations indicate that for the very dilute mixtures, which experimentally exhibited the greatest degree of nonequilibrium incident shock flow based on the monitor radiation, the effect on the final reflected-shock results is very small. The electron concentrations are within 10%, the N atom concentration within 4% and the computed temperature differs by about 100°K (which corresponds to about a 12% change in blackbody radiation at 770Å). Thus, during the actual data reduction procedure, possible uncertainties include a 4% in the R factor and about 4% in the N atom concentration, both of which would tend to increase the final value of σ. The calculated decrease in the blackbody function would tend to lower the cross-section values obtained experimentally. For the dilute mixtures then, the calculated uncertainties are small, and lie within the data scatter of the measurements.

For the 3% N_2/97% Ne mixture, the calculations indicate a larger uncertainty corresponding to 20% in electron concentration, 10% in N atom concentration, and about 500°K in the reflected-shock temperature, although the R factor is essentially the same. The calculation for this mixture should be considered very conservative, since the approach to equilibrium is

accomplished much faster behind the incident shock than for the dilute case. A more realistic assessment would be to consider some fraction of this calculated temperature uncertainty. Arbitrarily choosing, for example, one half of this difference, or 250°K, allows estimates of possible uncertainties to be undertaken. A 250°K temperature difference corresponds to a 30% change in the blackbody radiation at 770Å and about 23% at 970Å. Since the temperature uncertainty is in the negative direction, the detected VUV radiation may also be decreased due to the change in the blackbody function. The net effect in a test series would be to indicate a higher value for σ . On the basis of these calculations, the final cross-section data shown in Figs. 30 and 31 may be high due to this uncertainty, but no more than about 30% for the short wavelength N data and about 20% for the middle plateau region. Thus, the 720Å and 767Å data for N are still in reasonable agreement with the theoretical calculations, while the 920Å and 970Å data still indicate a higher cross-section than that calculated. For the O-atom measurements, the shock temperature is lower, and these results may indicate a 20% uncertainty in the value of σ . These oxygen results should be considered as somewhat preliminary since the test series were not as extensive as those for nitrogen.

V. C. DISCUSSION

The photoionization cross-sections obtained from the shock-tube experiments are compared with those obtained in other types of experiments in Figs. 33 and 34. There are few spectrally resolved photoionization cross-section measurements for O and N in the windowless regime ($\lambda < 1100$Å). This is pointed out in Ref. 31, for example, where available data are discussed, and absorption measurements were attempted using a microwave afterglow as the atom source. For the nitrogen atom, no data were obtained, but the results of a previous attempt to measure N-atom photoionization cross-sections are discussed. In this experiment, also using a discharge technique, data were obtained for recombination to the ground state only in the wavelength range 400Å - 700Å (Ref. 32). Since the nitrogen atom concentration was not measured, the absolute accuracy of the data is uncertain. However, the cross-

section obtained at 700Å, for example, is approximately 8×10^{-18}-1.5×10^{-17} cm^2, in fair agreement with the 720Å results obtained in the present study.

Additional measurements of photoionization cross-sections for the ground state N atom ($\lambda < 852$Å) have been reported in Ref. 33. Again, the nitrogen atoms were produced in a discharge. A pulsed light source was used to obtain absorption measurements. These data are in close agreement with the calculated cross-section values for wavelengths below 850Å.

Recently, a comprehensive series of spectrally resolved measurements using a constricted arc has been reported in Ref. 29, which is an extension of the work published earlier in Ref. 15. Using argon as the principal operating gas within the arc, with the addition of a small amount of nitrogen, cross-section values down to 900Å were obtained. Using neon as the carrier gas, measurements were made between 700Å and 800Å. The N-atom absorption coefficient was determined from both emission and absorption measurements in the temperature range from 10,800°K to 13,600°K. In general, the experimentally observed photoionization cross-sections at wavelengths greater than 900Å, confirm the results of Ref. 15. For the middle and last plateau for nitrogen ($\lambda > 900$Å), the measurements lie somewhat below the calculated values, ranging from about 0.4 to 0.9 of the theoretical value with an estimated accuracy of ± 40%. The results of the present shock-tube runs at 920Å and 970Å, however, indicate σ values approximately a factor of 2 greater than the calculations. This difference in the results for two types of experimental facilities is unresolved at the present time. Using neon as the carrier gas, arc measurements in the 700Å - 800Å region were obtained for σ, giving results greater than theory by approximately a factor of 3. As noted in Ref. 29, however, the reliability of these low-wavelength data is not high, due to the large uncertainties in the temperature and thermodynamic state of the gas. In this wavelength region, the present shock-tube results agree quite well with the theoretical calculations and other measurements. Figure 33 summarizes the results of nitrogen atom photoionization cross-section measurements, using the discharge, the constricted arc and the reflected-shock technique.

The results of microwave discharge measurements for the O-atom

cross-sections are also discussed in Ref. 31. Near the photoionization cutoff edge (911Å), the data are in fair agreement with the theoretical calculations. However, between about 650Å and 800Å, the discharge results lie considerably above the theory. A possible reason for this conclusion is that there could be appreciable absorption by discrete transitions in atomic oxygen. As indicated in Ref. 31, the high absorption coefficients obtained at 685Å and 725Å occur near the series limits for certain oxygen lines. The present shock tube data for the oxygen atom should be considered somewhat preliminary, since an extensive series of runs were not completed. However, the data thus far obtained agree quite well with the theoretical calculations. Figure 34 summarizes the oxygen atom data.

In summary, the present experimental program has demonstrated the usefulness of this shock-tube technique for absolute spectral radiation measurements in the windowless region of the vacuum ultraviolet. The complex plunger-spectrometer-detector system has been shown to operate reliably in microsecond time intervals. In addition, the repeatability of the explosively driven plunger and the stability of the detector system have been demonstrated. One of the major sources of potential problems lies in the absolute purity level of the gas-handling system and shock tube itself, and a high level of effort was devoted to this aspect of the experiment. The major uncertainty in such an experiment arises in defining the state of the gas behind the reflected-shock wave. This was considered in some detail, and uncertainties of the order of 30% in final cross-section data may arise at the shorter wavelengths.

Two other problem areas encountered in the experiments should be pursued. First, obtaining a blackbody calibration point at wavelengths where this was not achieved for the nitrogen tests may be accomplished using the recombination radiation from the carbon ion. Calculations have indicated (Ref. 19) the cross-section for carbon to be larger than that for the nitrogen atom and cover a more extensive wavelength range. Thus, once a calibration point at a selected wavelength has been obtained, further nitrogen measurements should yield cross-section data at these wavelengths. Secondly, the problem of grating order overlap in the radiation signals may be reduced with the use of gaseous windows acting as filters to absorb lower wavelength radiation.

ACKNOWLEDGEMENT

The authors wish to acknowledge helpful discussions with Dr. Charles E. Treanor and Dr. William J. Rae, and the assistance of Miss Marcia J. Williams in obtaining the shock-computer program results. They also acknowledge the assistance of Mr. Robert Phibbs in the experimental phase of the work and Mr. Richard Hiemenz for the development of the complex electronic control and protective systems.

REFERENCES

1. Allen, R. A., Air Radiation Graphs: Spectrally Integrated Fluxes Including Line Contributions and Self Absorption. AVCO Everett Research Laboratory Report No. 230. September 1965.

2. Allen, H. Julien, Some Problems of Planetary Atmosphere Entry. J. Royal Aero. Soc. Vol. 71, pp. 813-820. December 1967.

3. Hoshizaki, H. and Wilson, K. H., Convective and Radiative Heat Transfer During Superorbital Entry. AIAA Jour., Vol. 5, No. 1, pp. 25-36. January 1967.

4. Biberman, L. M., Vorob'ev, V. S., Norman, G. E. and Yakubov, I. T., Radiation Heating in Hypersonic Flow. Cosmic Research, Vol. 2, pp. 376-387, 1964. Also Foreign Technology Division Translation FTD-TT-64-770/1+2.

5. Dirling, R. B. Jr., Rigdon, W. S. and Thomas, M., Stagnation-Point Heating Including Spectral Radiative Transfer. Paper presented at Heat Transfer and Fluid Mechanics Institute, Univ. of Calif., La Jolla. June 1967. Also Douglas Paper No. 2019.

6. Wilson, K. H. and Grief, R., Radiation Transport in Atomic Plasmas. J. Quant. Spect. and Radiat. Transfer. Vol. 8, No. 4 (April 1968). pp. 1061-1087. Lockheed Palo Alto Research Lab. Report No. 6-77-67-31. November 1967.

7. Syvertson, C. A., Entry and Landing Requirements for Manned Planetary Missions. Presented at AIAA Technology for Manned Planetary Missions Meeting, New Orleans, March 1968.

8. Page, W. A., Compton, D. L., Borucki, W. J., Ciffone, D. L. and Cooper, D. M., Radiative Transport in Inviscid Nonadiabatic Stagnation-Region Shock Layers. Paper presented at AIAA 3rd Thermophysics Conference, Los Angeles, June 1968.

9. Nerem, R. M. and Stickford, G. H., Shock-Tube Studies of Equilibrium Air Radiation. AIAA Jour. Vol. 3, No. 6, pp. 1011-1019, June 1965.

10. Nerem, R. M. and Golobic, R. A., Shock Tube Measurements of End-Wall Radiative Heat Transfer in Air. AIAA Paper No. 67-695. Presented at AIAA Electric Propulsion and Plasmadynamics Conference, Colorado Springs, September 1967.

11. Gruszczynski, J. S. and Warren, W. R. Jr., Study of Equilibrium Total Air Radiation. AIAA Jour. Vol. 5, No. 3, pp. 517-526, March 1967.

12. Wood, A. D., Hoshizaki, H., Andrews, J. C. and Wilson, K. H., Measurements of the Total Radiant Intensity of Air. AIAA Paper No. 67-311. Presented at AIAA Thermophysics Specialist Conference, April 1967. Also NASA CR-585, September 1966.

13. Compton, D. L., Measurements of Ultraviolet (575Å - 1800Å) Radiation From Nitrogen at Temperatures From 13,000°K to 16,000°K. Paper presented at AIAA 4th Aerospace Sciences Meeting, Los Angeles, June 1966.

14. Appleton, J. P. and Steinberg, M., Vacuum-Ultra-Violet Absorption of Shock-Heated Vibrationally Excited Nitrogen. J. Chem. Phys., Vol. 46, No. 4, pp. 1521-1529, 15 February 1967.

15. Morris, J. C. and Garrison, R. L., Nitrogen Recombination Continuum in the Vacuum Ultraviolet. J. Quant. Spect. and Radiat. Transfer, Vol. 6, pp. 899-902, 1966.

16. Samson, J. A. R. and Kelley, F. L., Planetary Physics, III. Photoionization Cross Sections of the Rare Gases. Geophysics Corporation of America. NASA CR-68, July 1964.

17. Hahne, G. E., The Vacuum Ultraviolet Radiation From N^+ and O^+ Electron Recombination in High-Temperature Air. NASA TN D-2794, June 1965.

18. Gilmore, F. R., Basic Energy-Level and Equilibrium Data for Atmospheric Atoms and Molecules. The RAND Corporation Report RM-5201-ARPA, March 1967.

19. Wilson, K. H. and Nicolet, W. E., Spectral Absorption Coefficients of Carbon, Nitrogen and Oxygen Atoms. J. Quant. Spect. and Radiat. Transfer, Vol. 7, No. 6, pp. 891-943. Nov./Dec. 1967.

20. Williams, M. J. and Garr, L. J., A Description of the CAL Equilibrium Normal Shock Program. Cornell Aeronautical Lab. Internal Memorandum, September 1966.

21. Samson, J. A. R., Techniques of Vacuum Ultraviolet Spectroscopy. John Wiley and Sons, Inc., New York (1967).

22. Wurster, W. H. and Marrone, P. V., Nitric-Oxide Radiation in the Near IR Spectrum of Shock-Heated Air. J. Quant. Spect. and Radiat. Transfer, Vol. 7, pp. 591-604, July/August 1967.

23. Samson, J. A. R., Planetary Aeronomy, V: Vacuum Ultraviolet Light Sources. Geophysics Corporation of America. NASA CR-17, September 1963.

24. Michels, D. J. and Hunter, W. R., Detectors for the Extreme Ultraviolet. I. Photomultipliers used in the DC Output Current Mode. Appl. Optics, Vol. 6, No. 3, pp. 385-390, March 1967.

25. Cairns, R. B. and Samson, J. A. R., Metal Photocathodes as Secondary Standards for Absolute Intensity Measurements in the Vacuum Ultraviolet. J. Opt. Soc. of America, Vol. 56, No. 11, pp. 1568-1573, November 1966.

26. Childs, C. B., Low-Pressure Mercury Arc for Ultraviolet Calibration. Appl. Optics, Vol. 1, p. 711 (1962).

27. Wheaton, J. E. G., Improvements in Design and Performance of the Large Aperture Lyman Flash Tube. Appl. Optics, Vol. 3, p. 1247 (1964).

28. Losev, S. A. and Smekhov, G. D., Excitation Time of the $B^3\pi_g$ State of N_2 at High Temperatures. Optics and Spectroscopy, Vol. 27, No. 6, pp. 484-486, June 1967.

29. Morris, J. C., Krey, R. U. and Garrison, R. L., Radiation Studies of Arc Heated Nitrogen, Oxygen and Argon Plasmas. AVCO Space Systems Division Report AVSSD-0049-68-RR, March 1968.

30. Smiley, E. F., The Measurement of the Thermal Conductivity of Gases at High Temperatures With a Shock Tube. Experimental Results in Argon at Temperatures Between 1000°K and 3000°K. Ph. D. Thesis, Catholic Univ. of America, Washington, 1957.

31. Cairns, R. B. and Samson, J. A. R., Studies of Photoabsorption by Atomic Hydrogen, Oxygen and Nitrogen. Geophysics Corporation of America. NASA CR-998, March 1968.

32. Ehler, A. W. and Weissler, G. L., Ultraviolet Absorption of Atomic Nitrogen in its Ionization Continuum. J. Opt. Soc. of America, Vol. 45, No. 12, pp. 1035-1043, December 1955.

33. Comes, F. J. and Elzer, A., Photoionization of Atomic Nitrogen, Phys. Letters, Vol. 25A, No. 4, pp. 334-335, 28 August 1967. Also Z. Naturforsch, Vol. 23-A, p. 133, 1968.

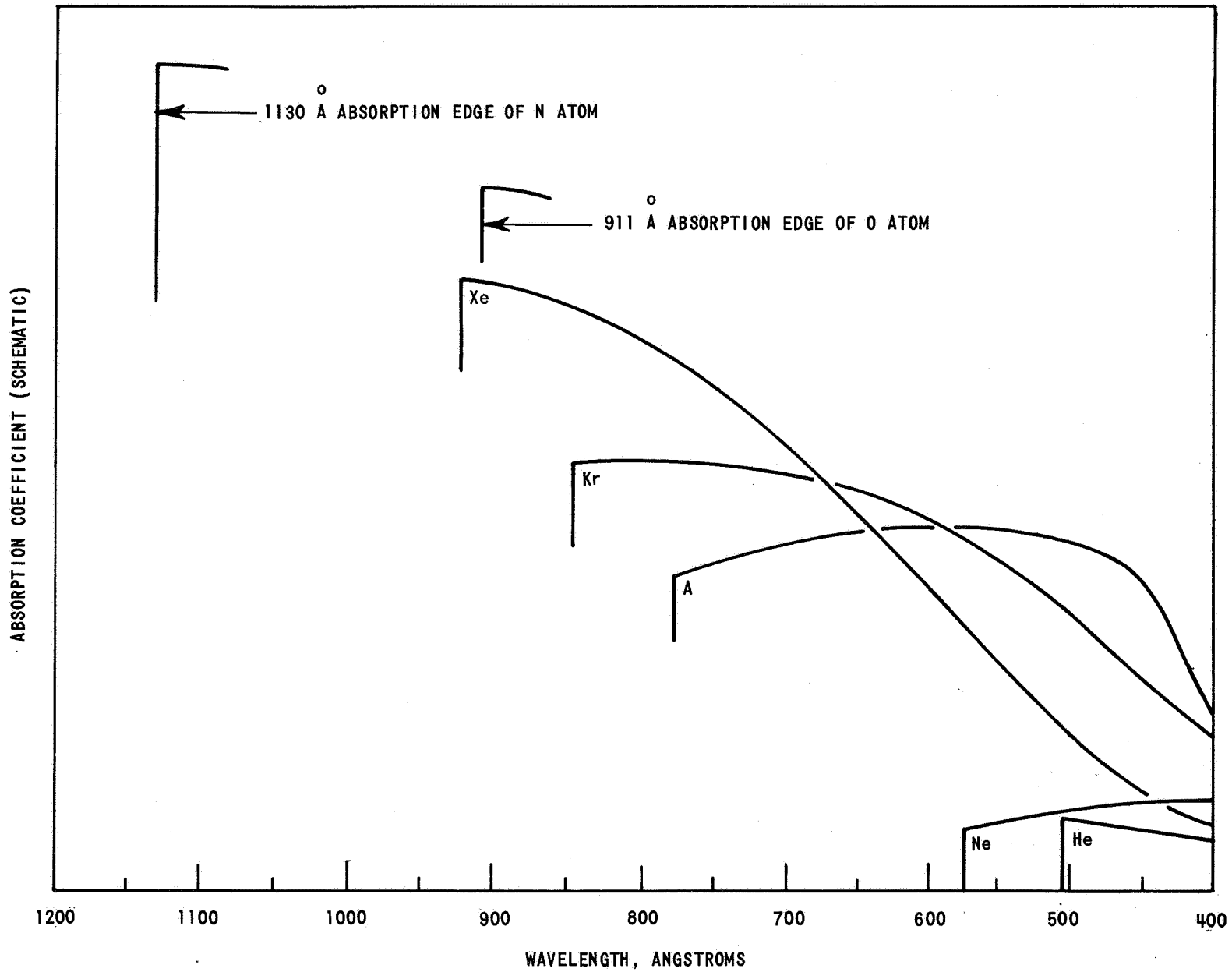

Figure 1 ABSORPTION COEFFICIENTS IN THE VACUUM ULTRAVIOLET

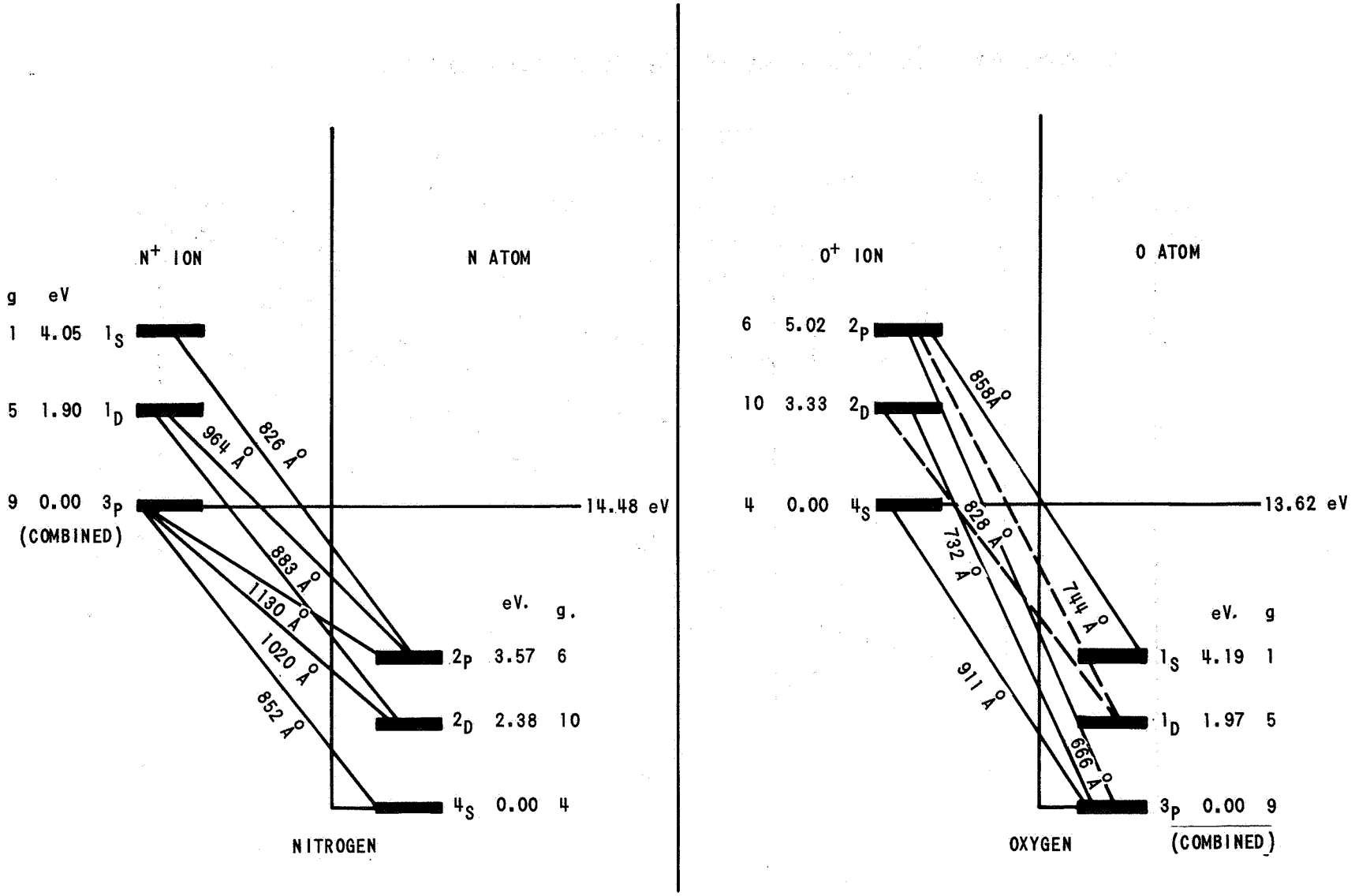

Figure 2 TRANSITIONS IN THE VACUUM ULTRAVIOLET

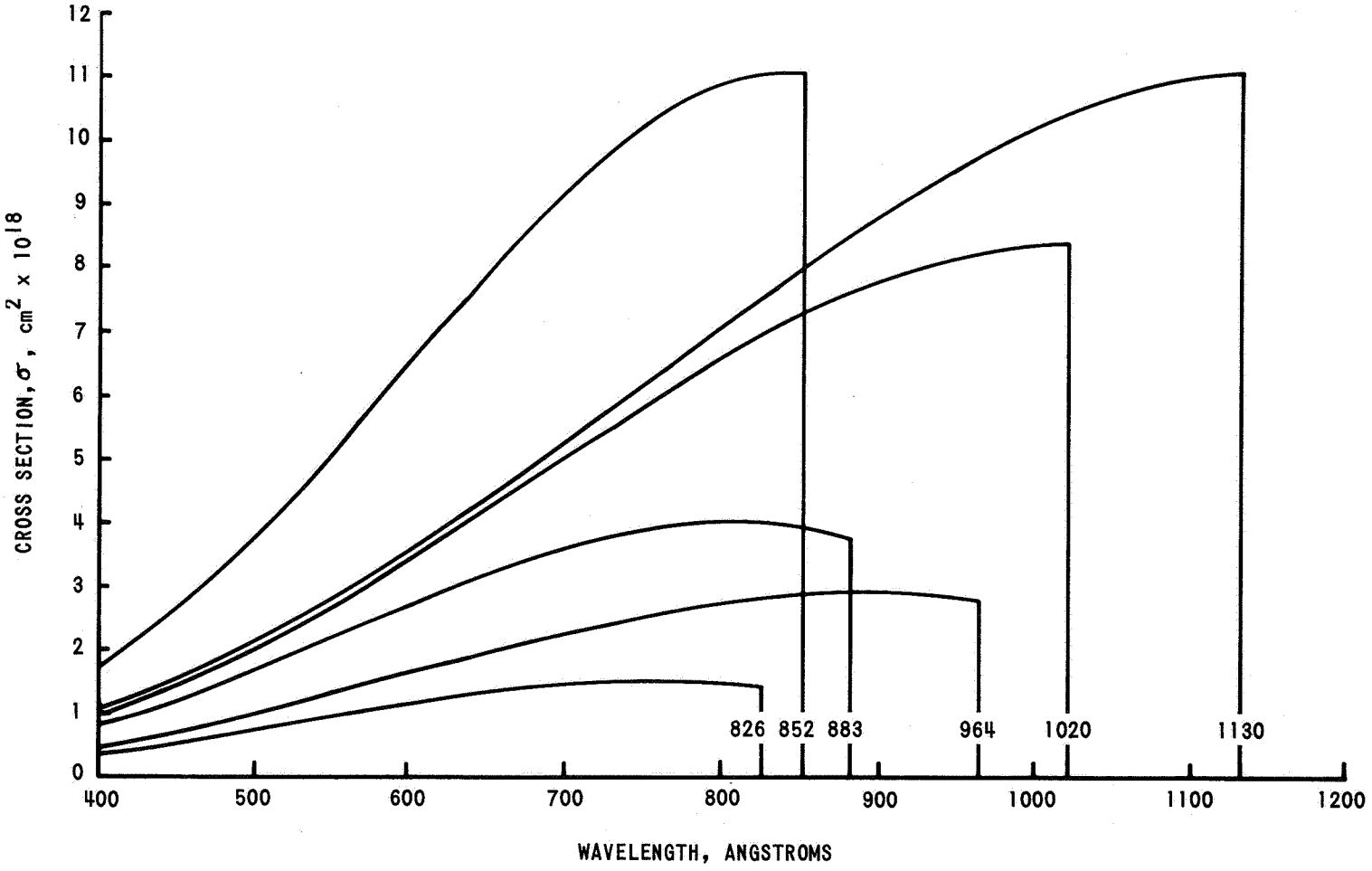

Figure 3 PHOTOIONIZATION CROSS SECTIONS FOR NITROGEN (N). TAKEN FROM REF. 17

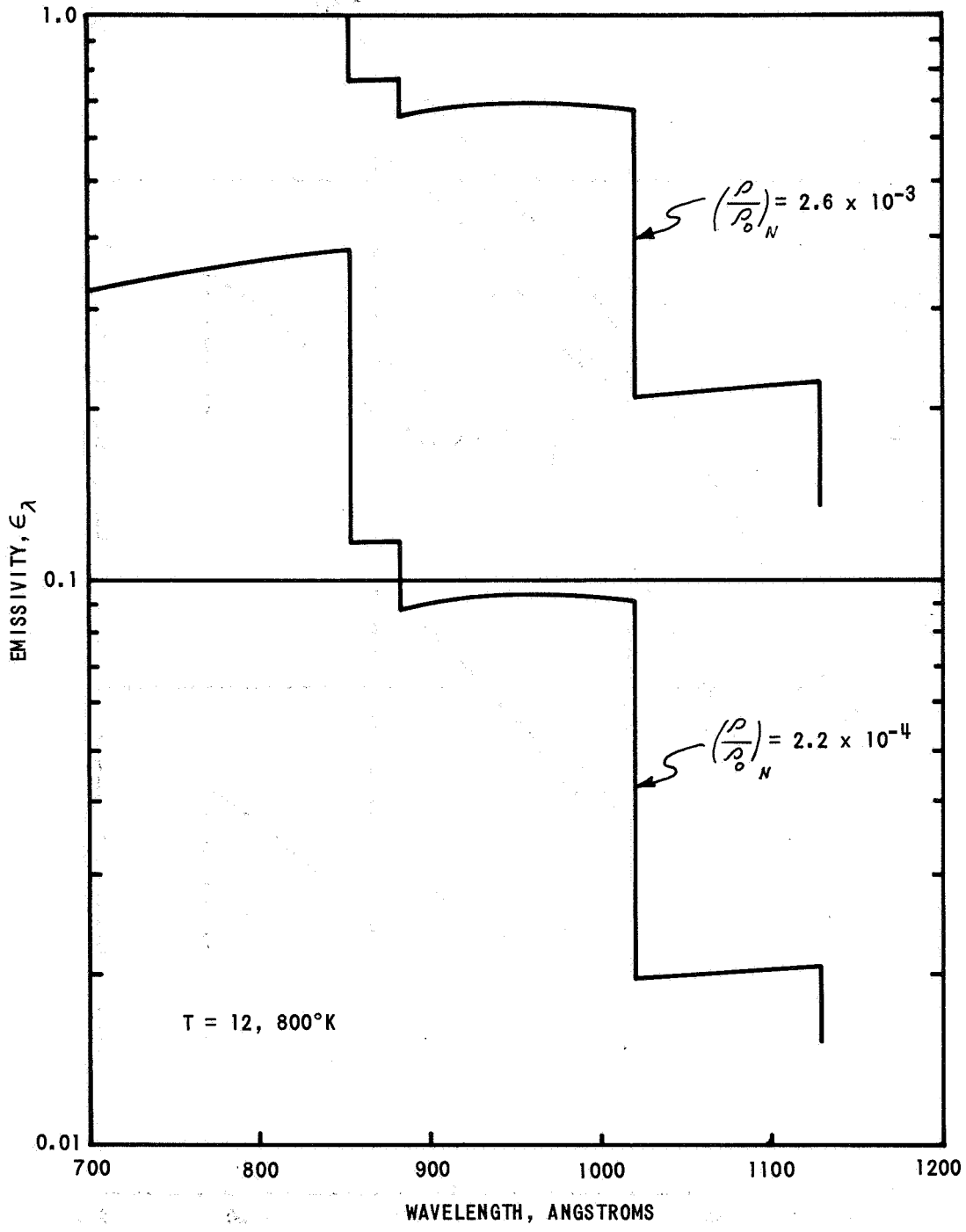

Figure 4a CALCULATED EMISSIVITY FOR NITROGEN RECOMBINATION CONTINUUM

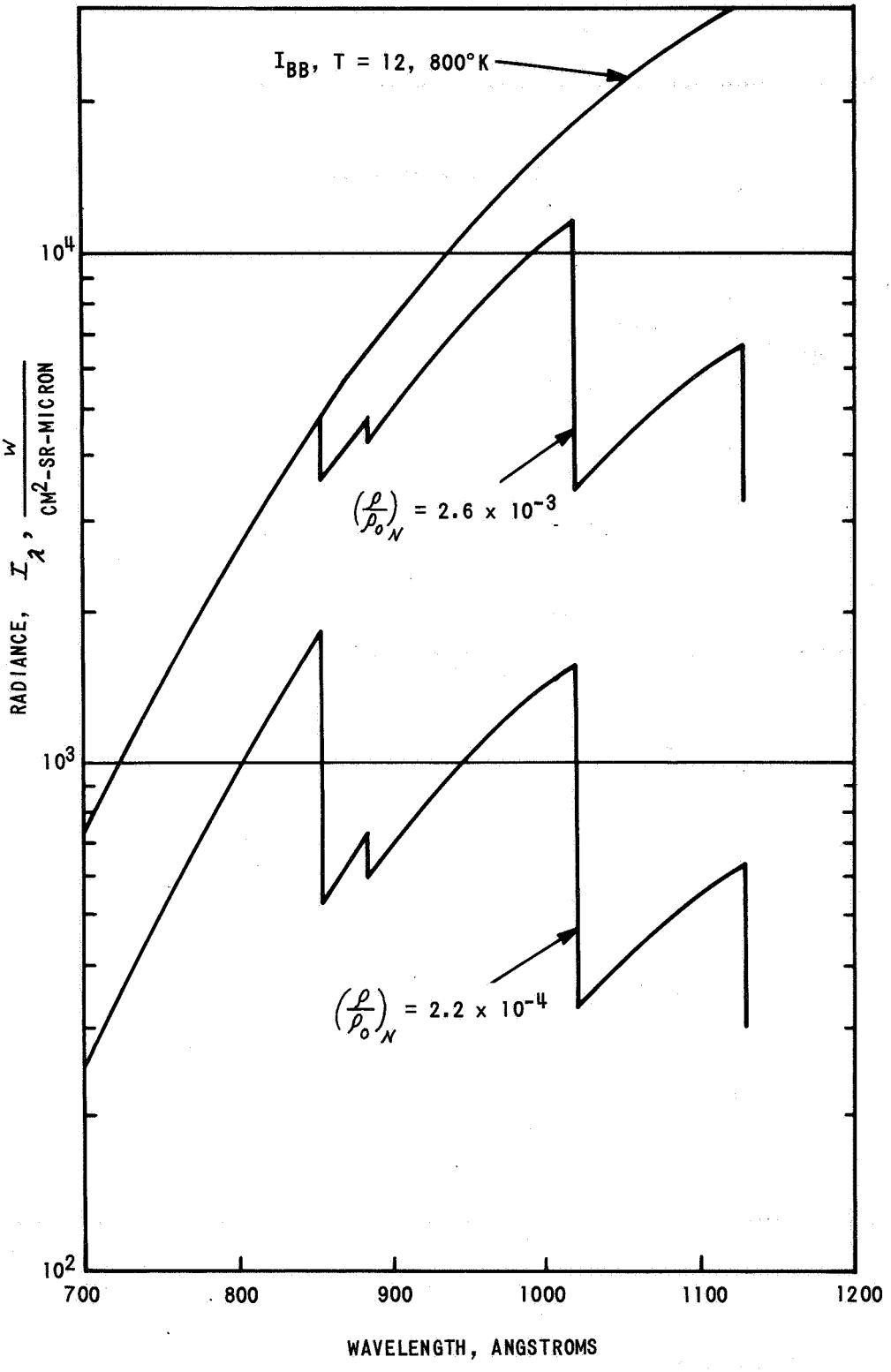

Figure 4b CALCULATED RADIANCE FOR NITROGEN RECOMBINATION CONTINUUM

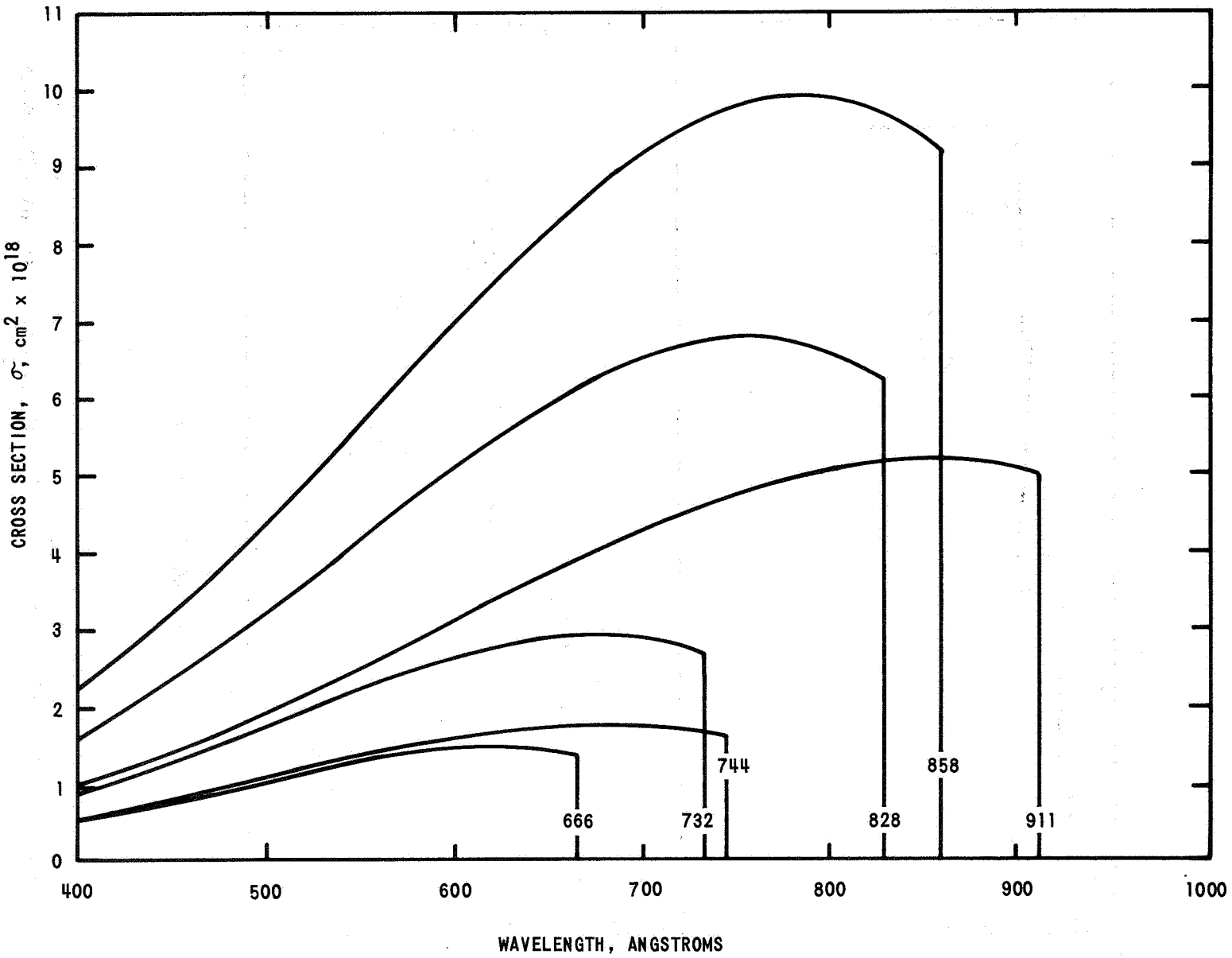

Figure 5 PHOTOIONIZATION CROSS SECTIONS FOR OXYGEN (O)
TAKEN FROM REF. 17

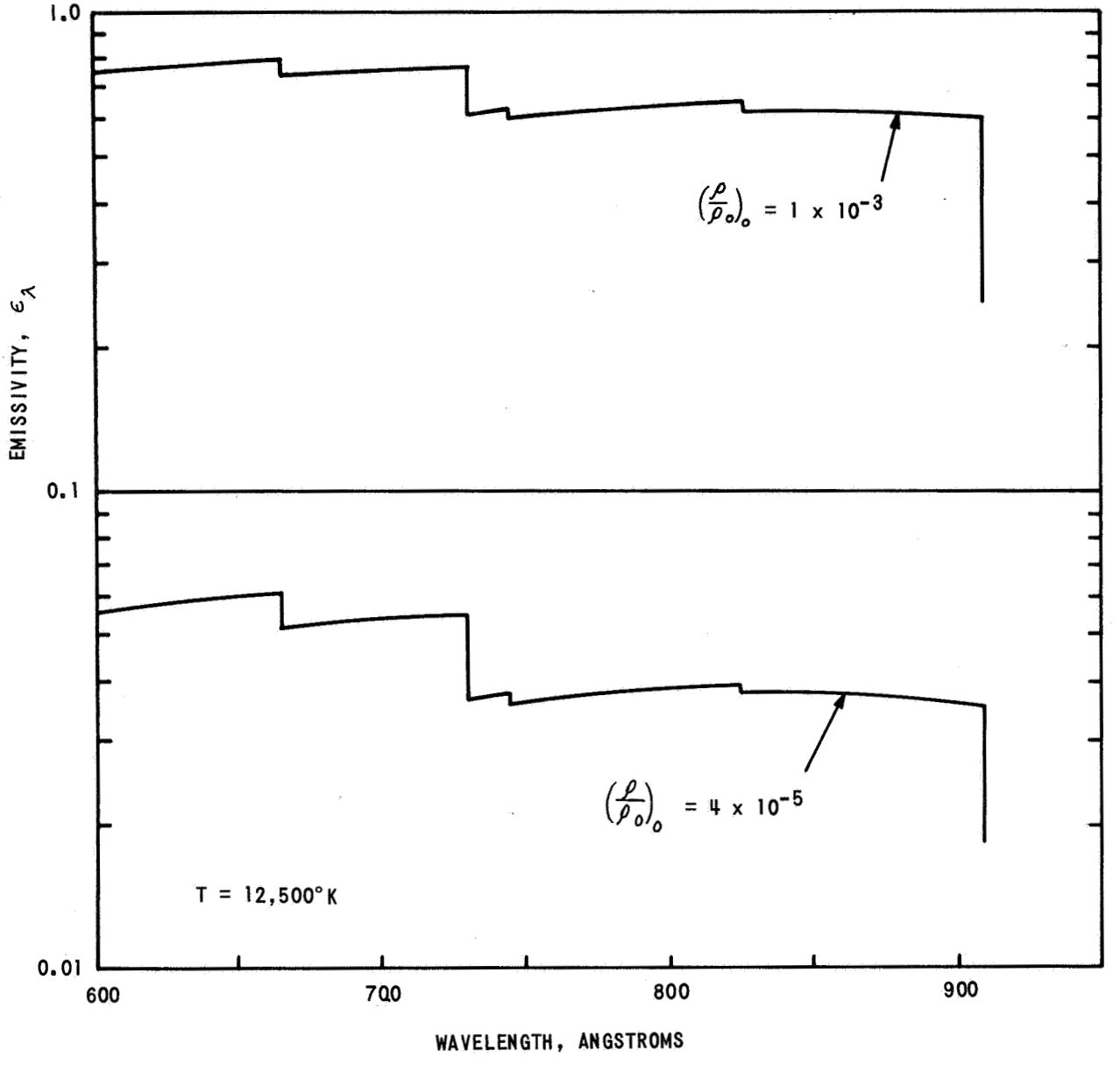

Figure 6 CALCULATED EMISSIVITY FOR OXYGEN RECOMBINATION CONTINUUM

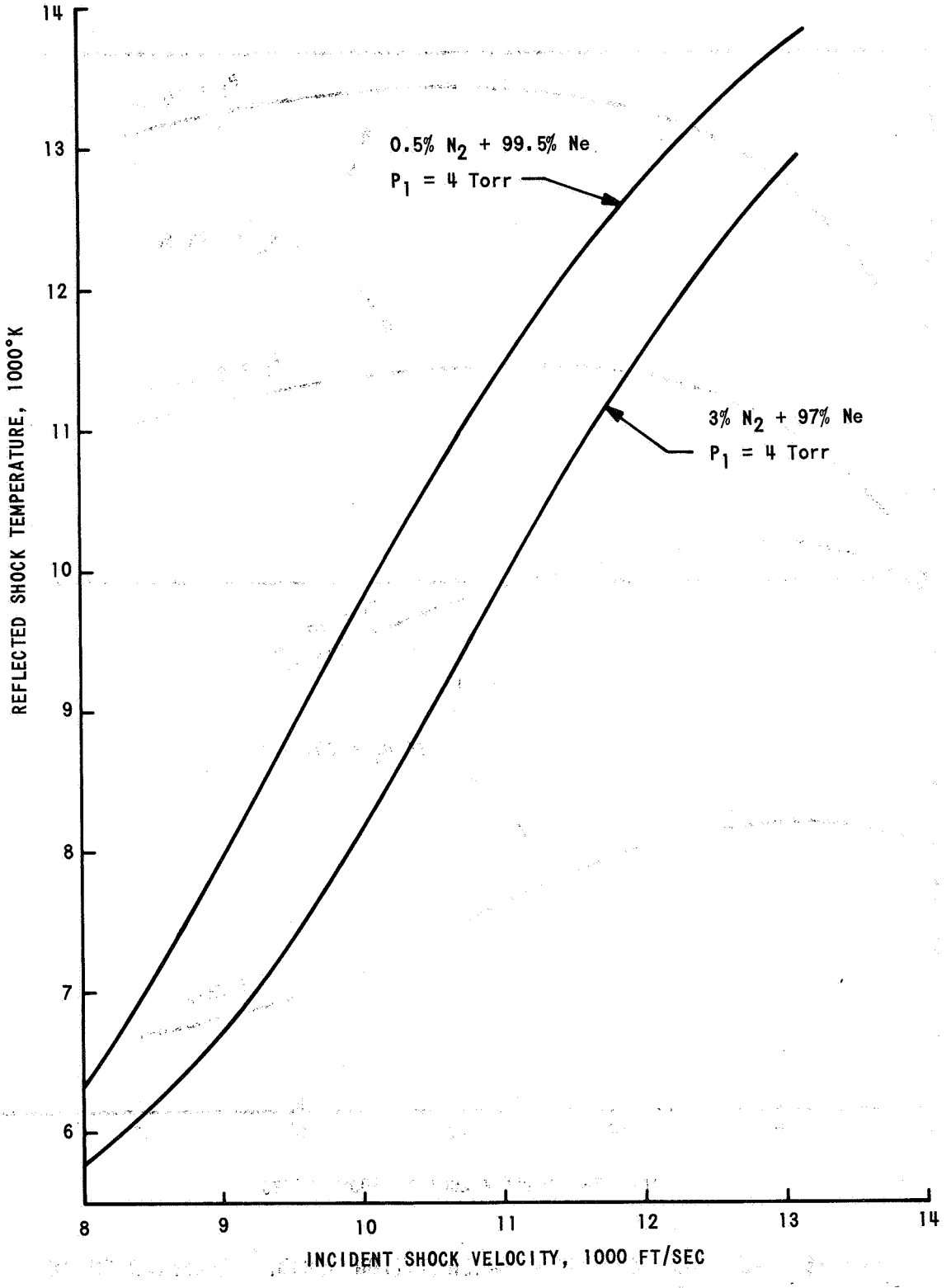

Figure 7a EQUILIBRIUM TEMPERATURE BEHIND REFLECTED SHOCK WAVE FOR NITROGEN - NEON MIXTURES

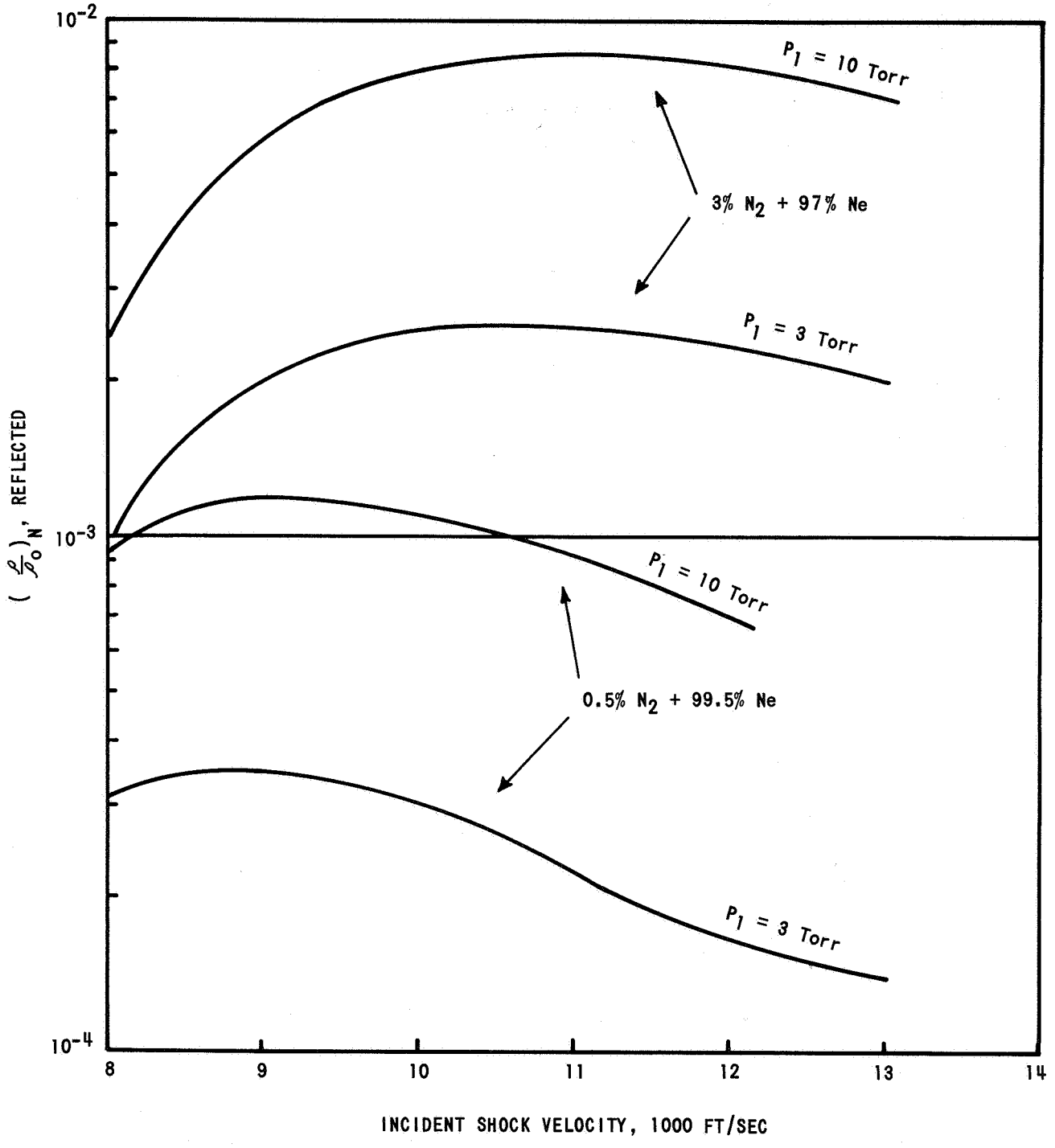

Figure 7b EQUILIBRIUM N ATOM CONCENTRATION BEHIND REFLECTED SHOCK FOR NITROGEN - NEON MIXTURES

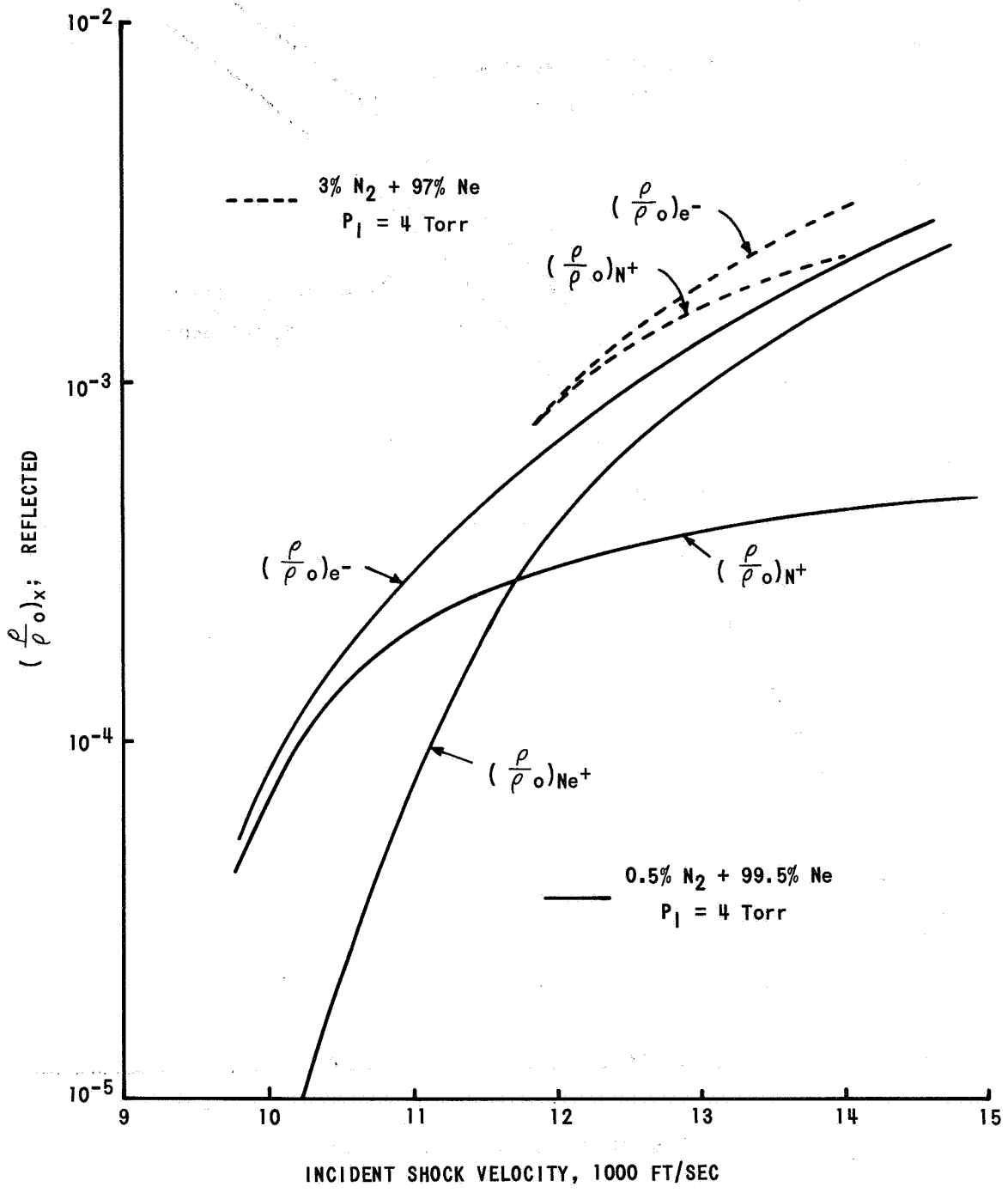

Figure 7c EQUILIBRIUM REFLECTED SHOCK CONDITIONS FOR NITROGEN - NEON MIXTURES

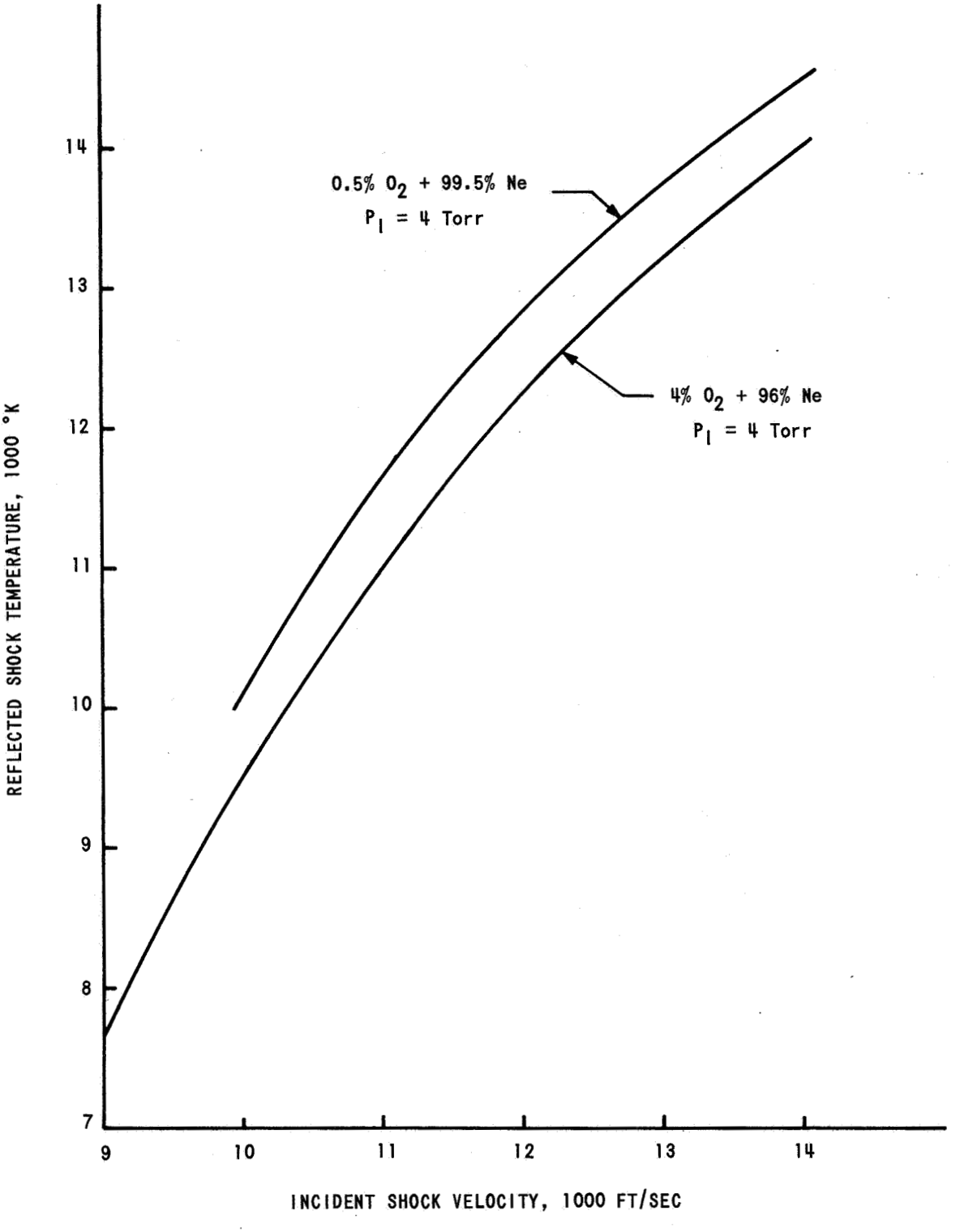

Figure 8a EQUILIBRIUM TEMPERATURE BEHIND REFLECTED SHOCK WAVE FOR OXYGEN-NEON MIXTURE

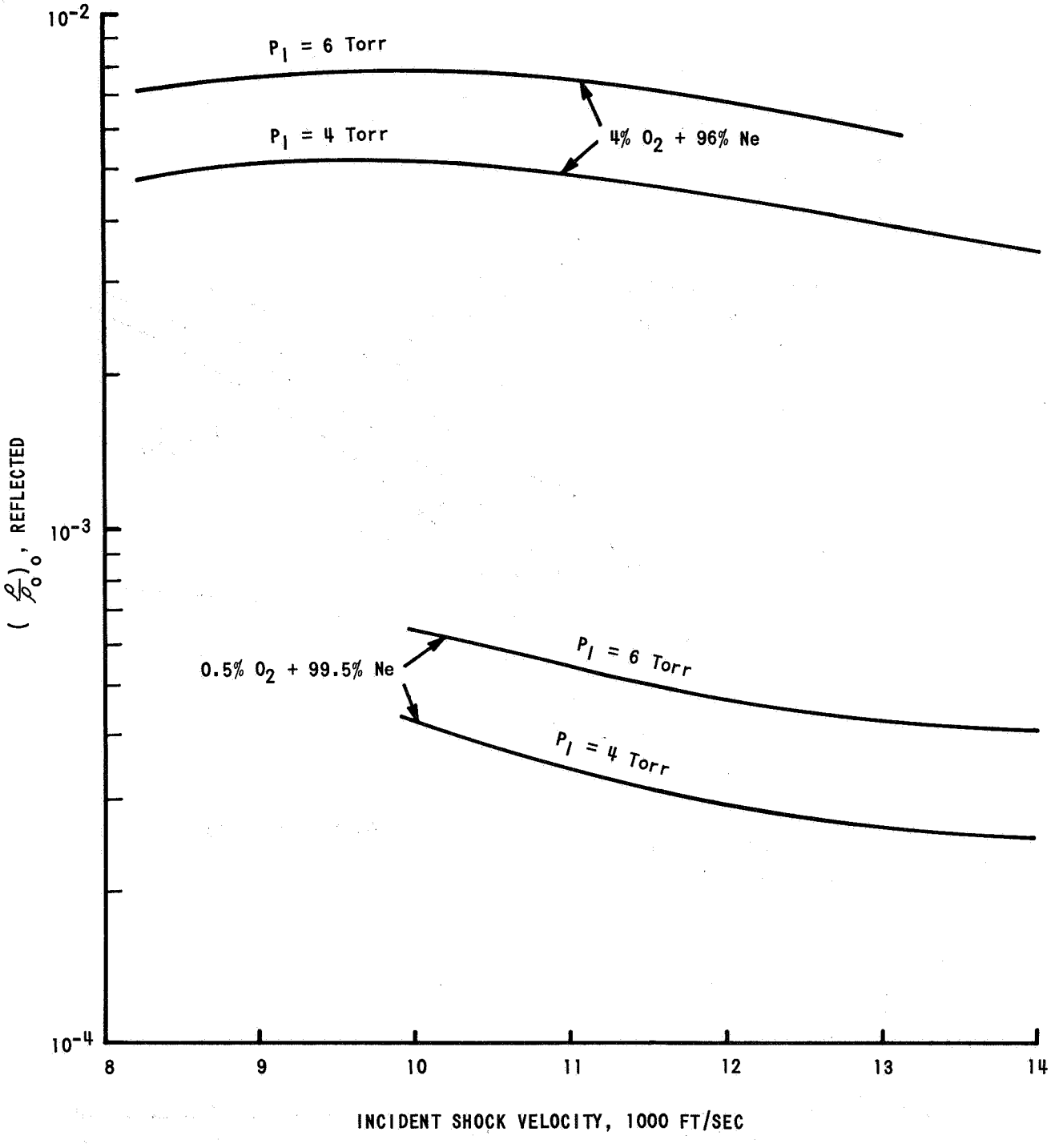

Figure 8b EQUILIBRIUM O ATOM CONCENTRATION BEHIND REFLECTED SHOCK FOR OXYGEN - NEON MIXTURES

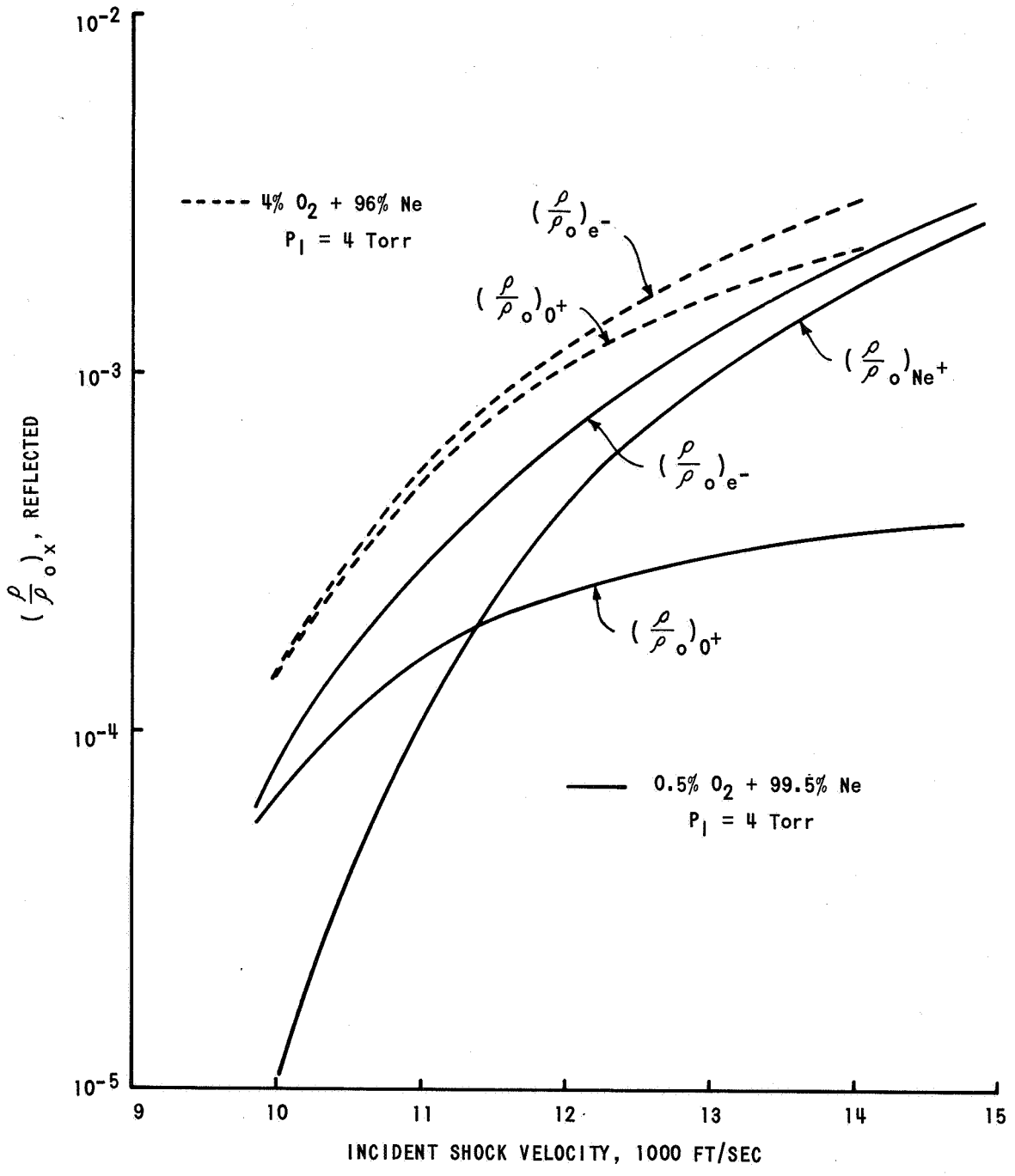

Figure 8c EQUILIBRIUM REFLECTED SHOCK CONDITIONS FOR OXYGEN - NEON MIXTURES

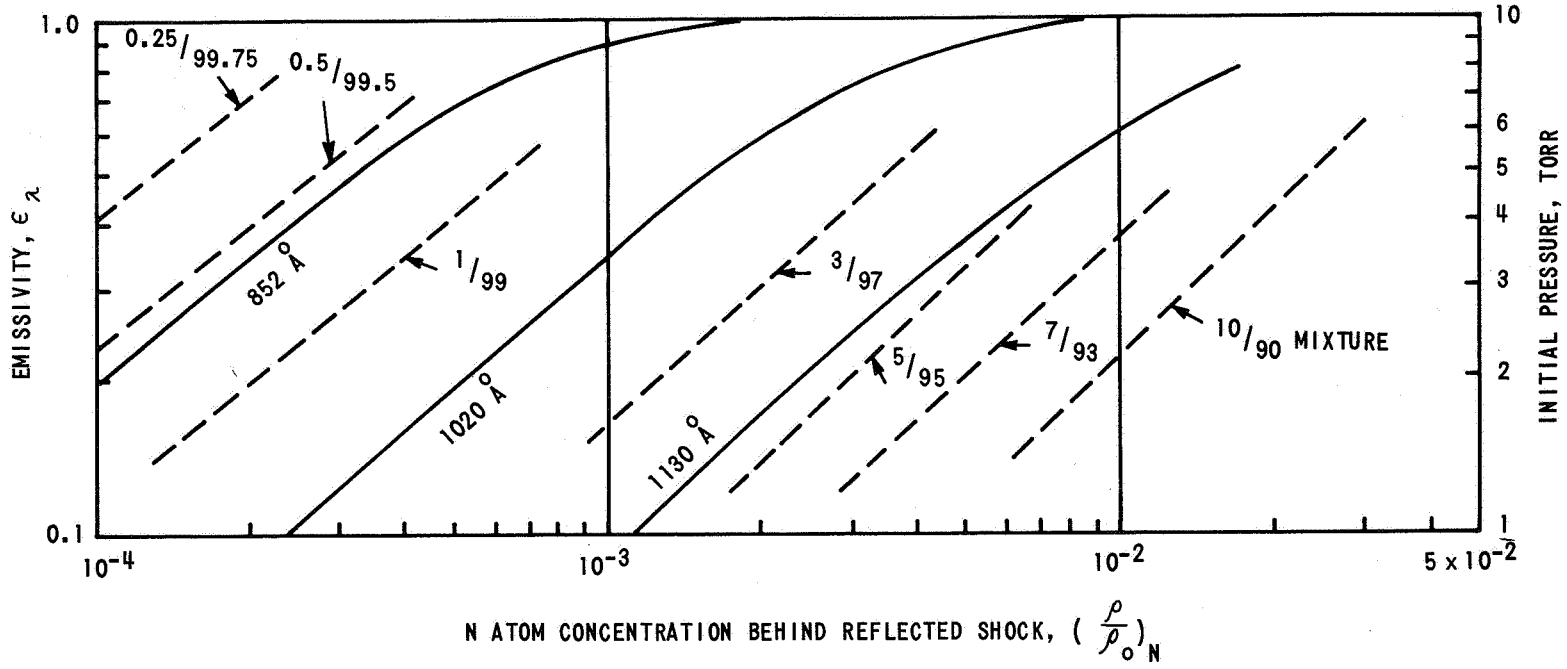

NOTE:

T = 12,800°K

—— = EMISSIVITY

– – = INITIAL PRESSURE

$^3/_{97}$ = DENOTES 3% N_2 + 97% NEON MIXTURE, etc.

Figure 9 SHOCK TUBE OPERATING REGION FOR $N_2 - N_e$ EXPERIMENTS

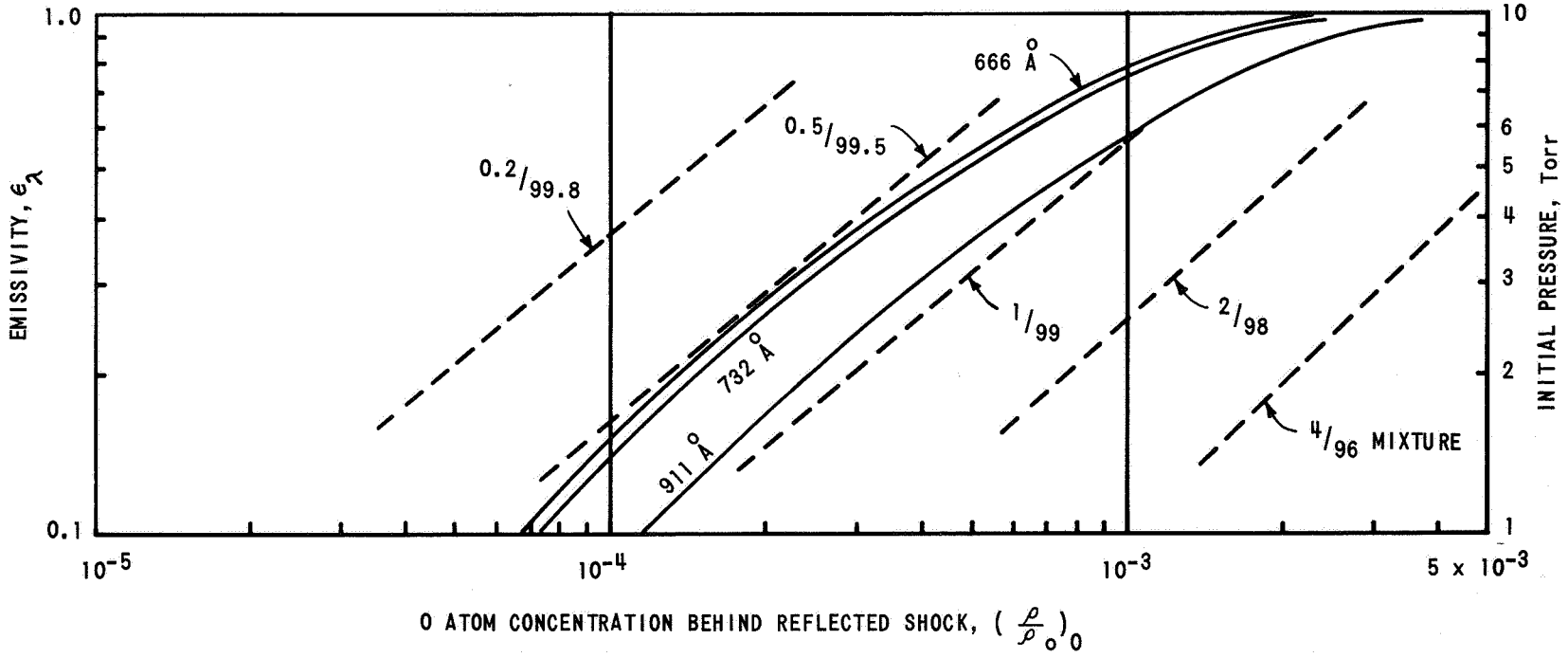

NOTE:

T = 12,500 °K

—— = EMISSIVITY

— — = INITIAL PRESSURE

$^2/_{98}$ = DENOTES 2% O_2 + 98% NEON MIXTURE, etc,

Figure 10 SHOCK TUBE OPERATING REGION FOR O_2-Ne EXPERIMENTS

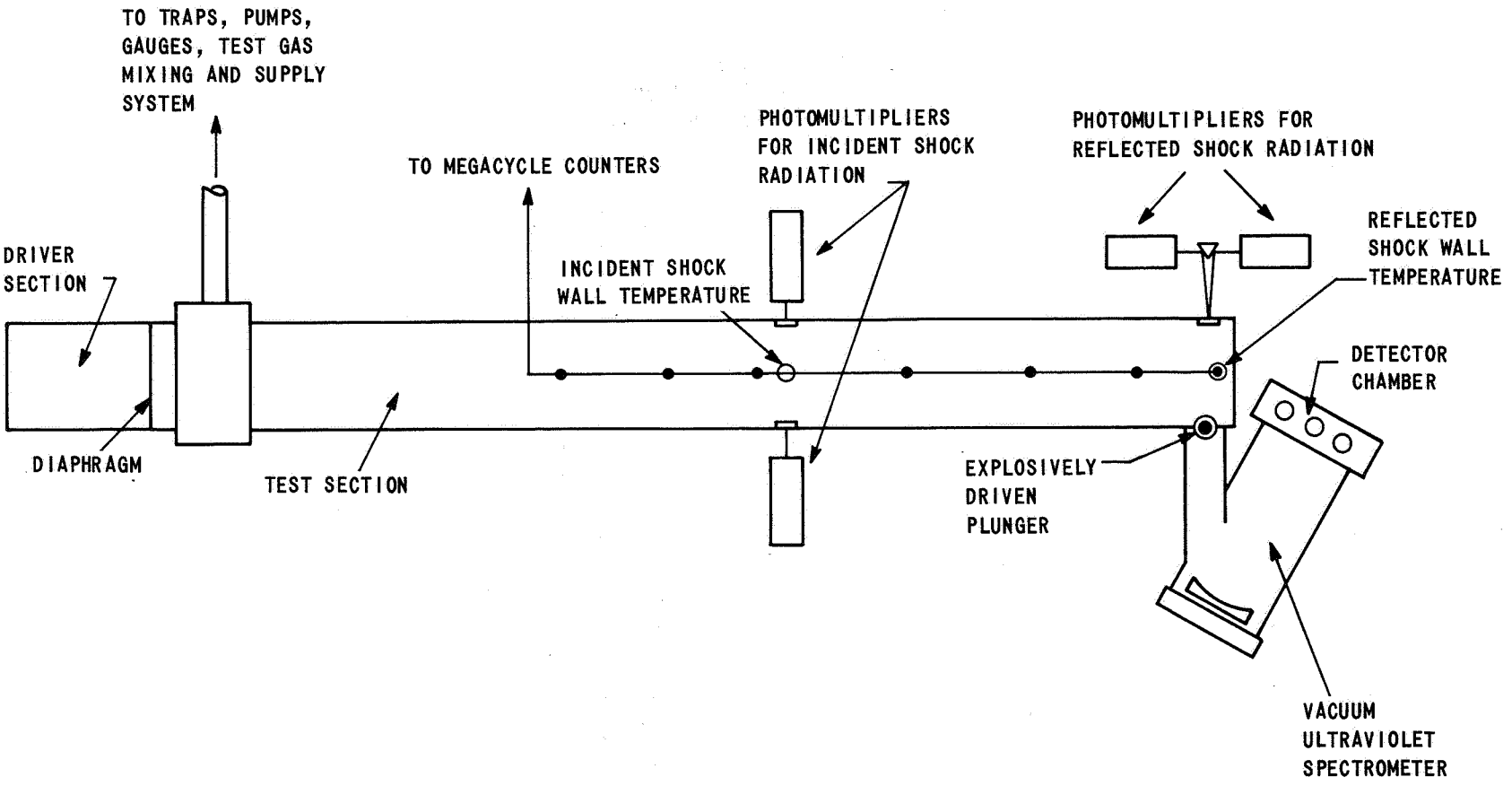

Figure 11 SCHEMATIC OF EXPERIMENTAL APPARATUS

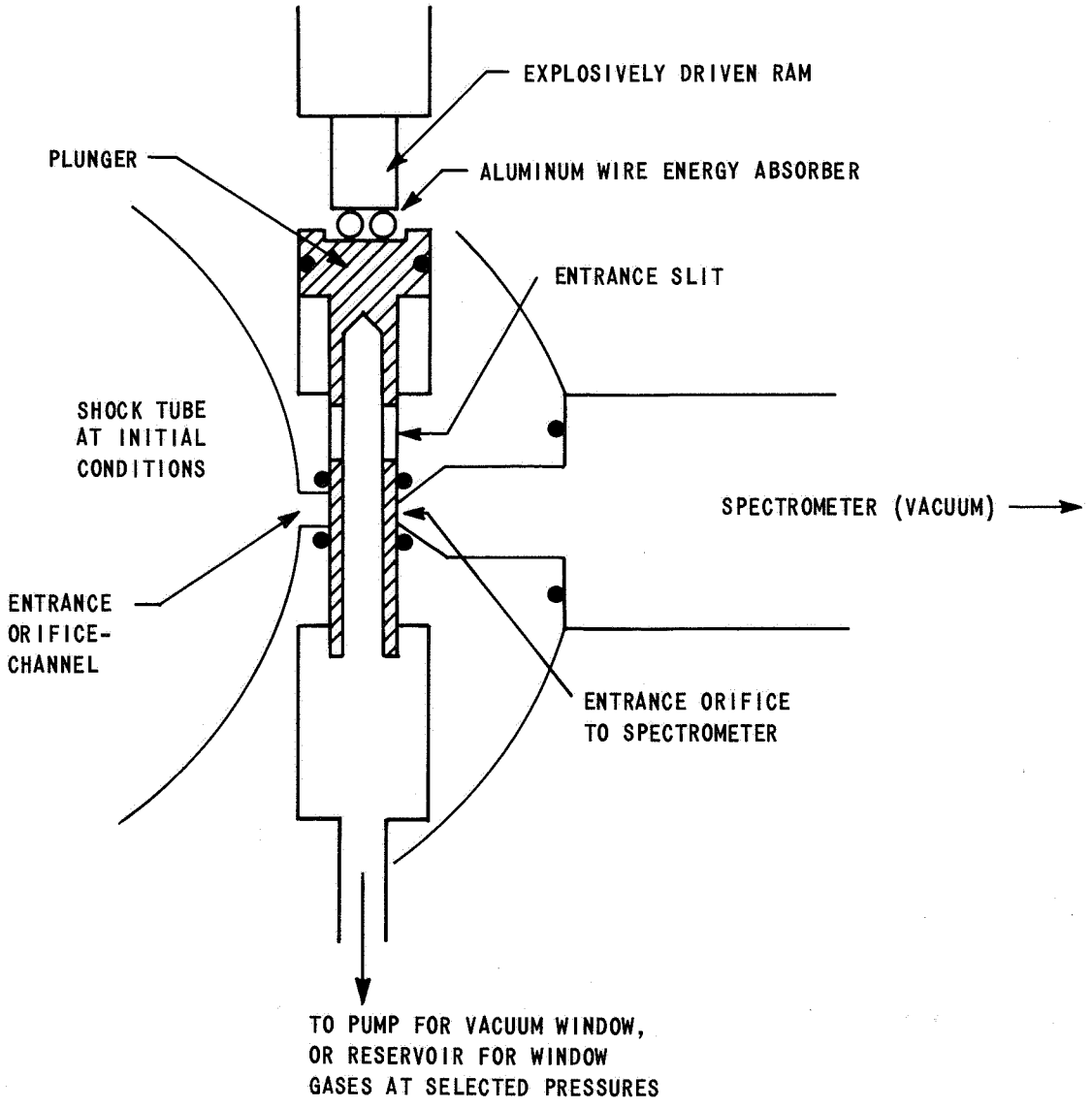

Figure 12 SCHEMATIC OF WINDOWLESS PLUNGER ASSEMBLY

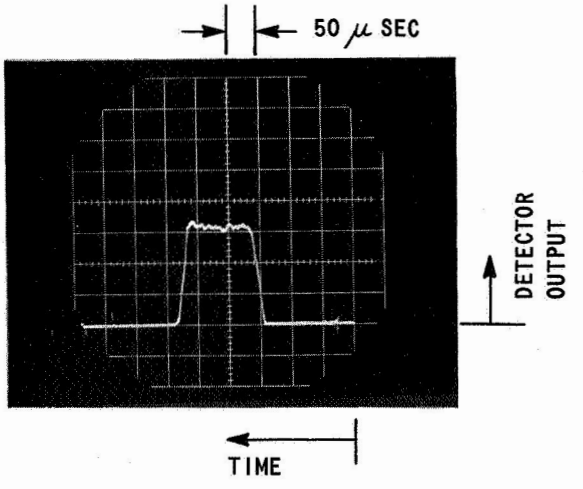

Figure 13 WINDOWLESS PLUNGER OPEN TIME WITH ALUMINUM WIRE ENERGY ABSORBER

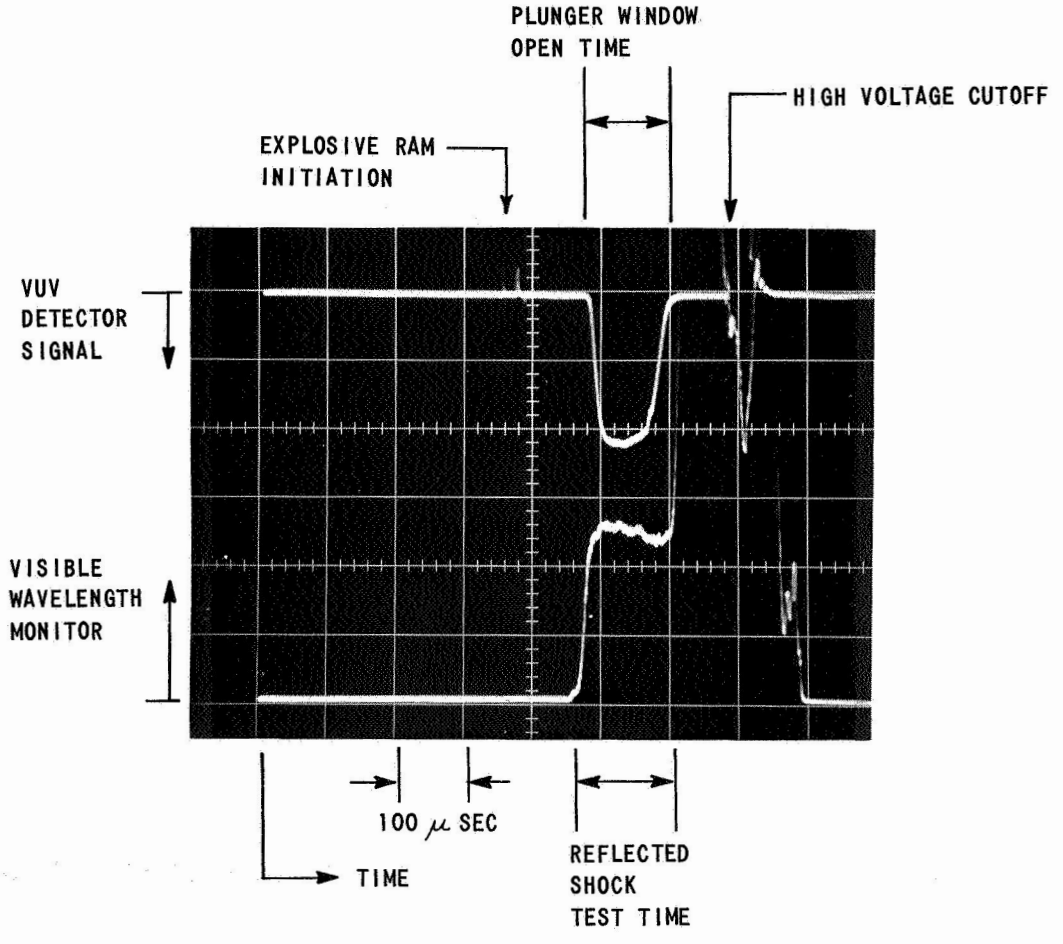

Figure 14 REFLECTED SHOCK RADIATION DATA SHOWING SYNCHRONIZATION OF WINDOWLESS PLUNGER

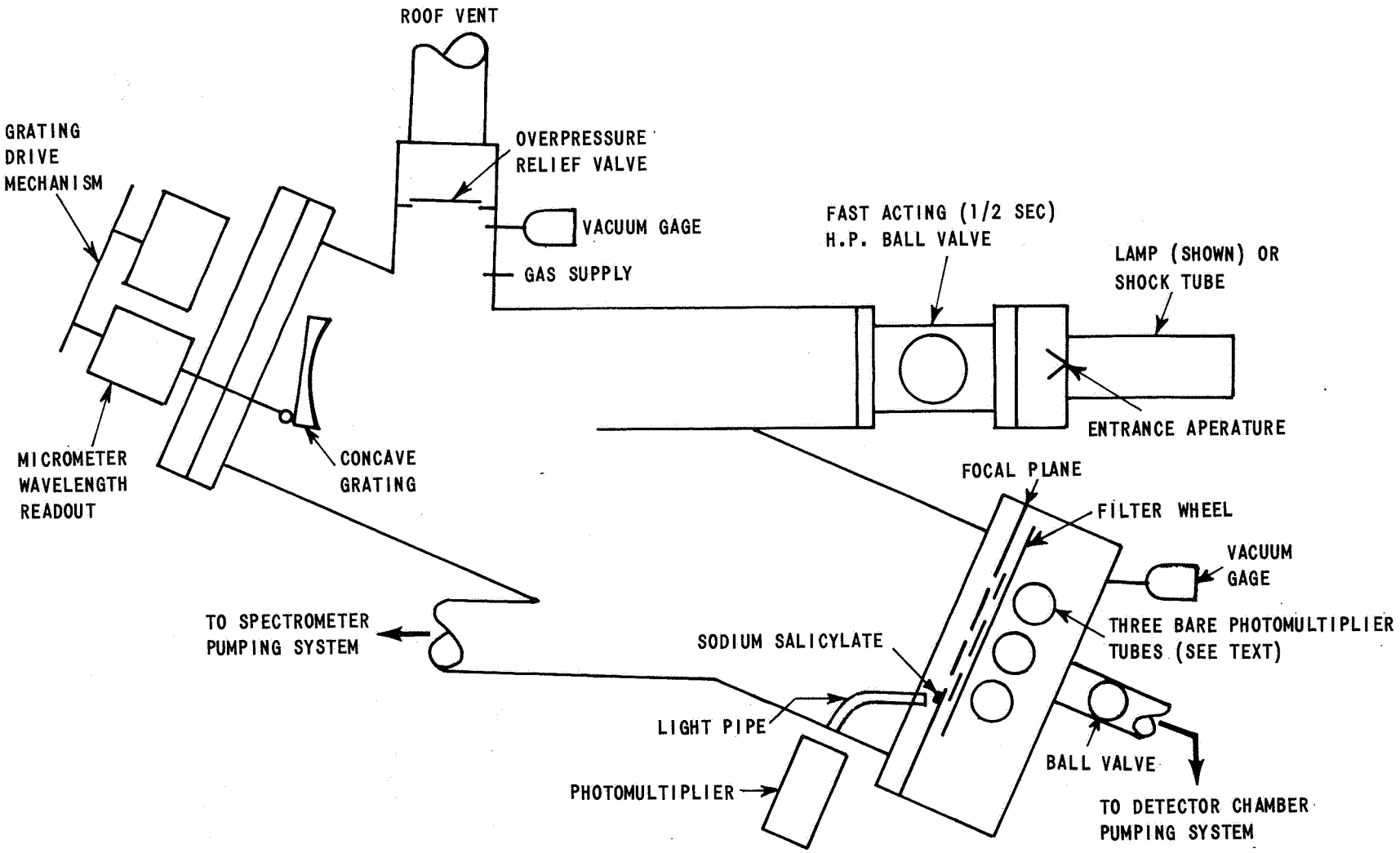

Figure 15 SCHEMATIC OF VACUUM ULTRAVIOLET SPECTROMETER

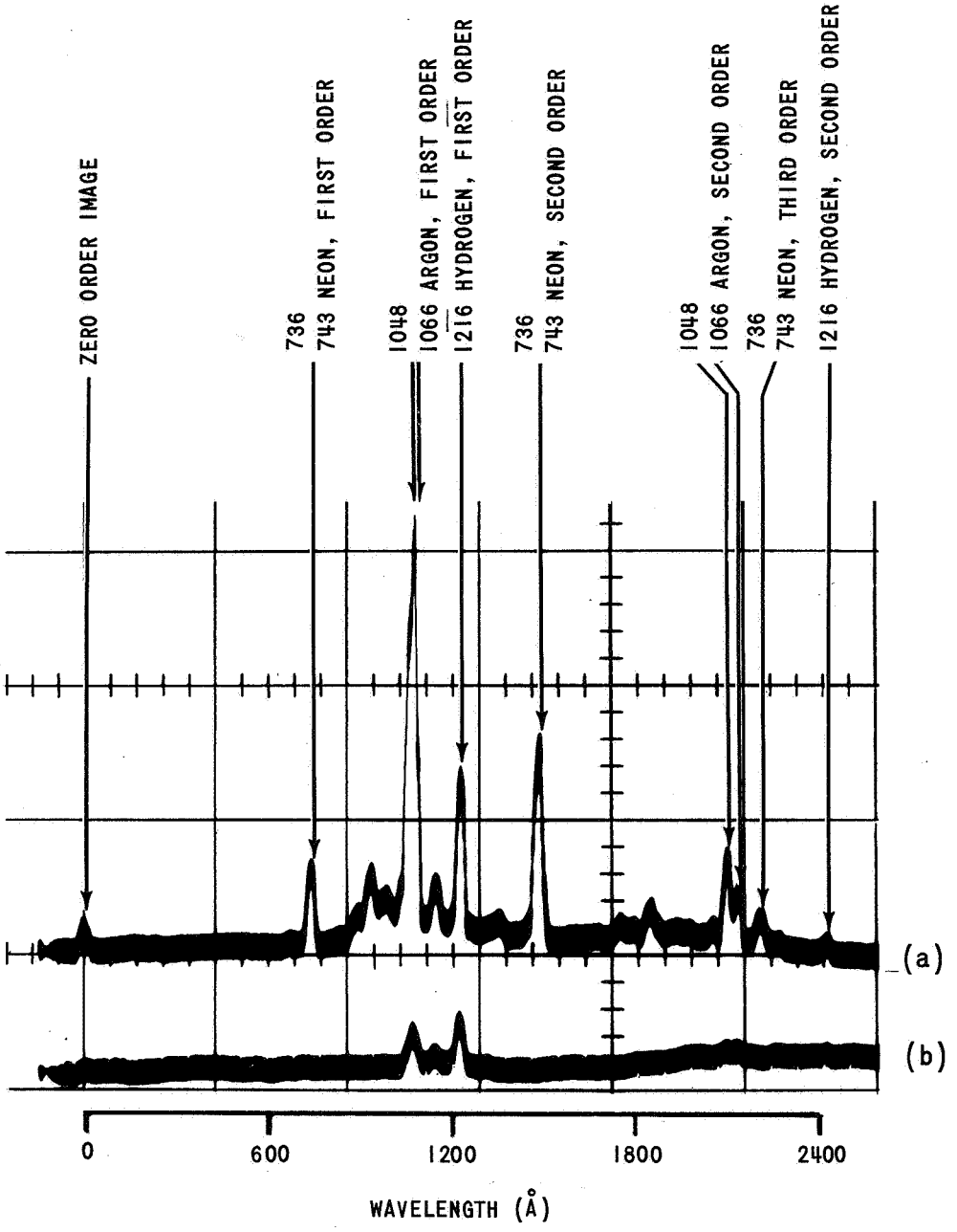

Figure 16 (a) EMISSION SPECTRUM OF AN AR/NE/H_2 MIXTURE RECORDED WITH THE RCA 7075 BARE PHOTOMULTIPLIER TUBES.

(b) SAME SPECTRUM WITH 0.5mm LITHIUM FLUORIDE PLACED INTO OPTICAL BEAM.

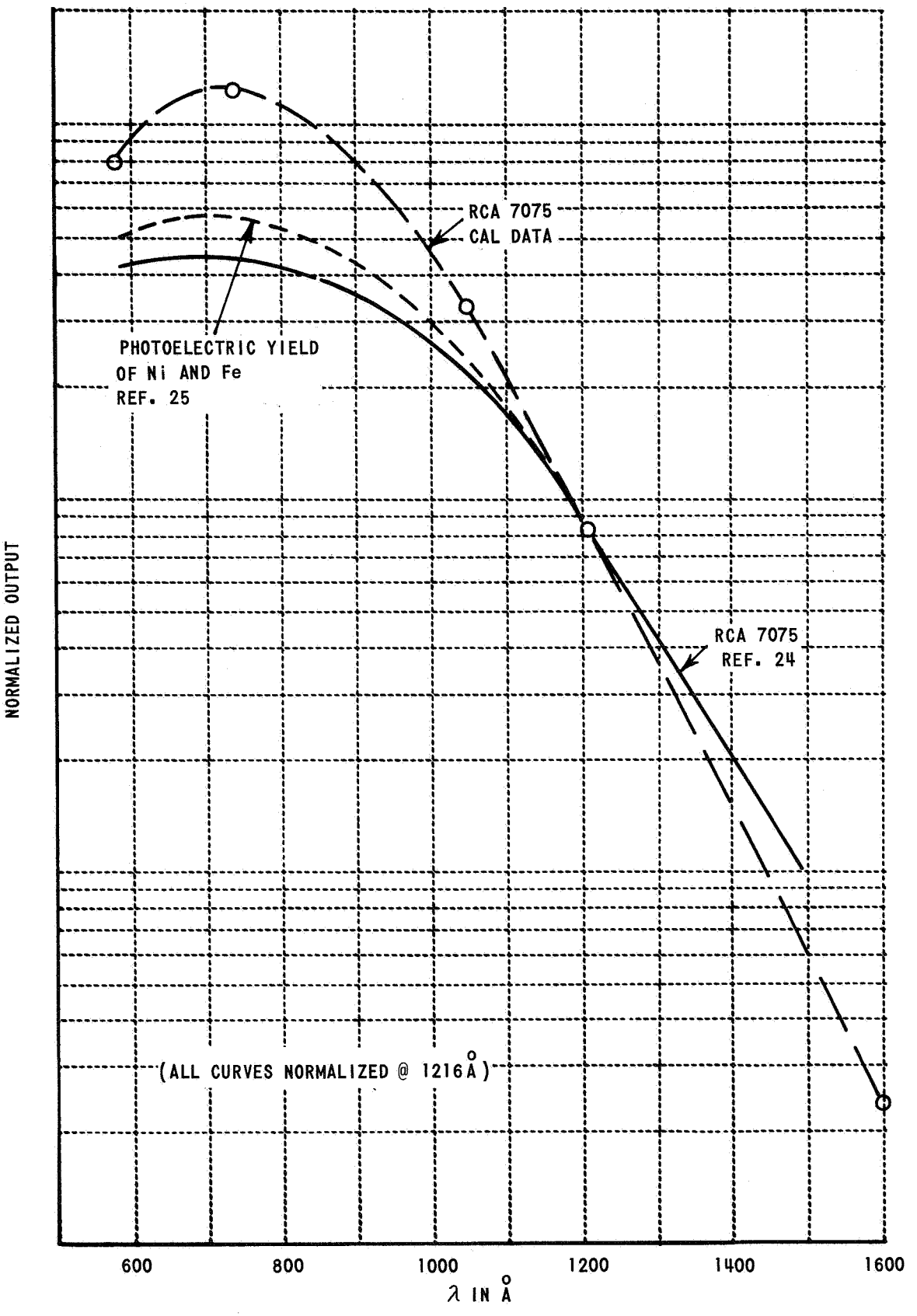

Figure 17 RELATIVE WAVELENGTH SENSITIVITY

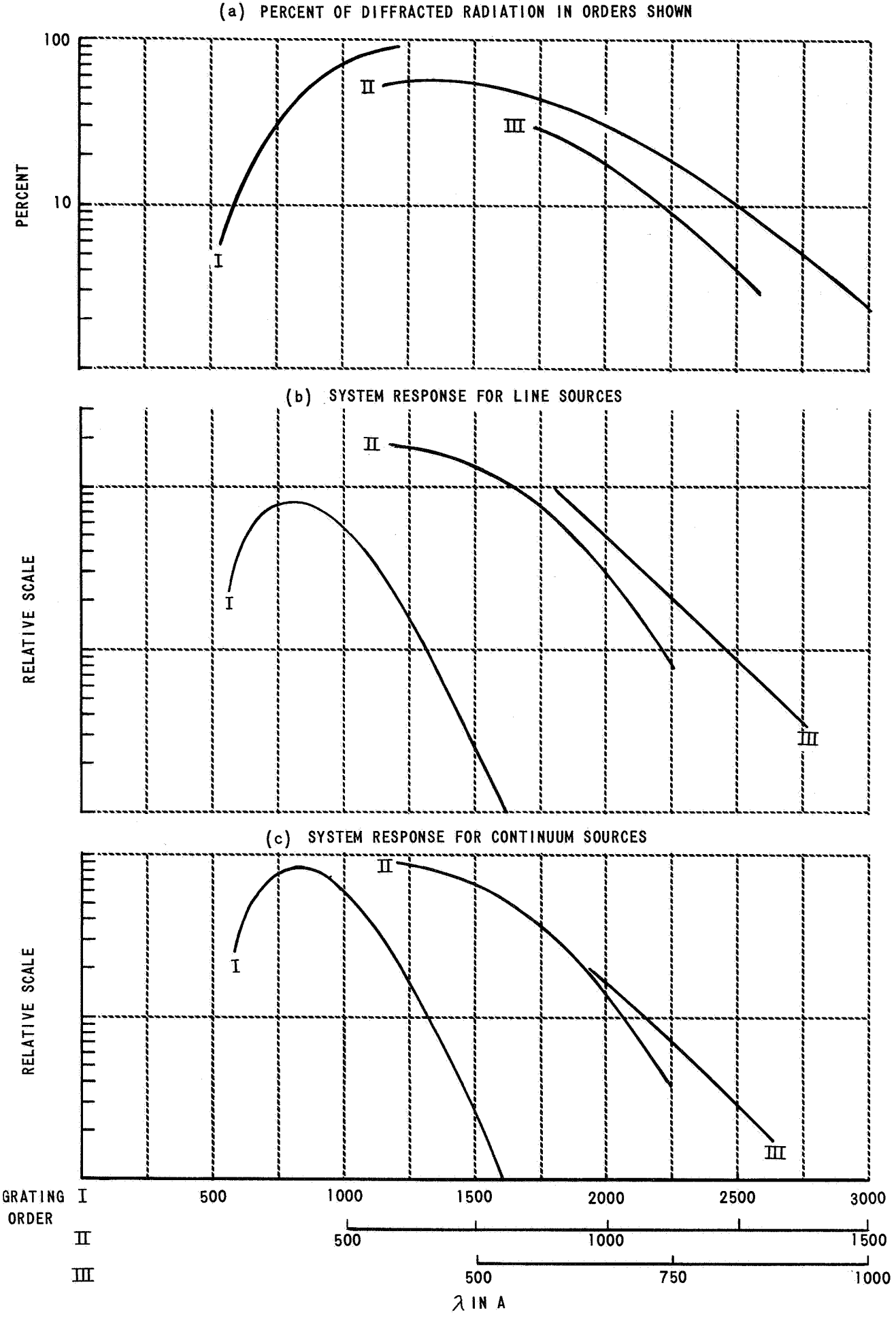

Figure 18 SPECTROMETER PERFORMANCE

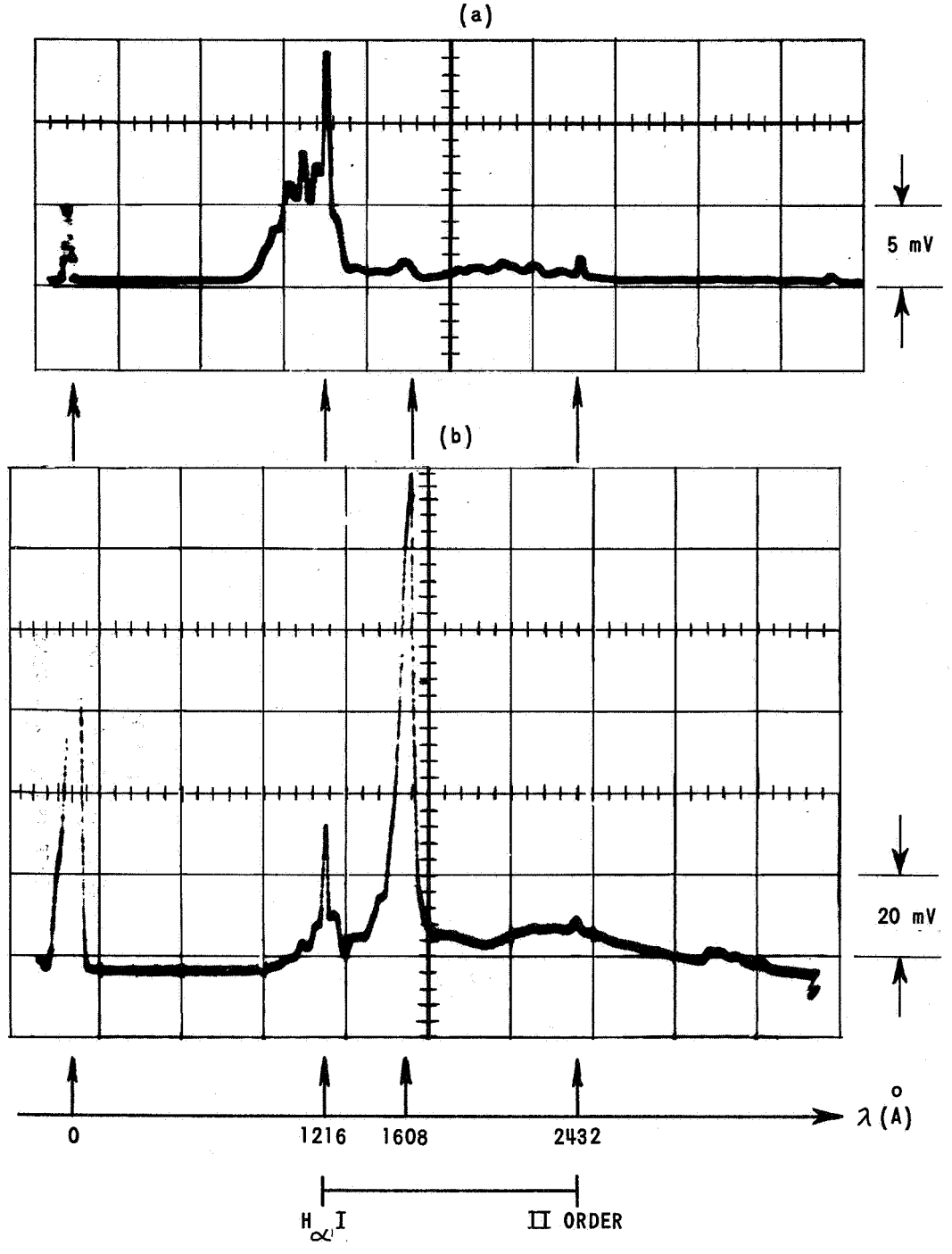

Figure 19 COMPARISON OF HYDROGEN DISCHARGE SPECTRUM USING
(a) RCA 7075 BARE STAINLESS STEEL PHOTOMULTIPLIER,
(b) SODIUM SALICYLATE AND CONVENTIONAL PHOTOMULTIPLIER

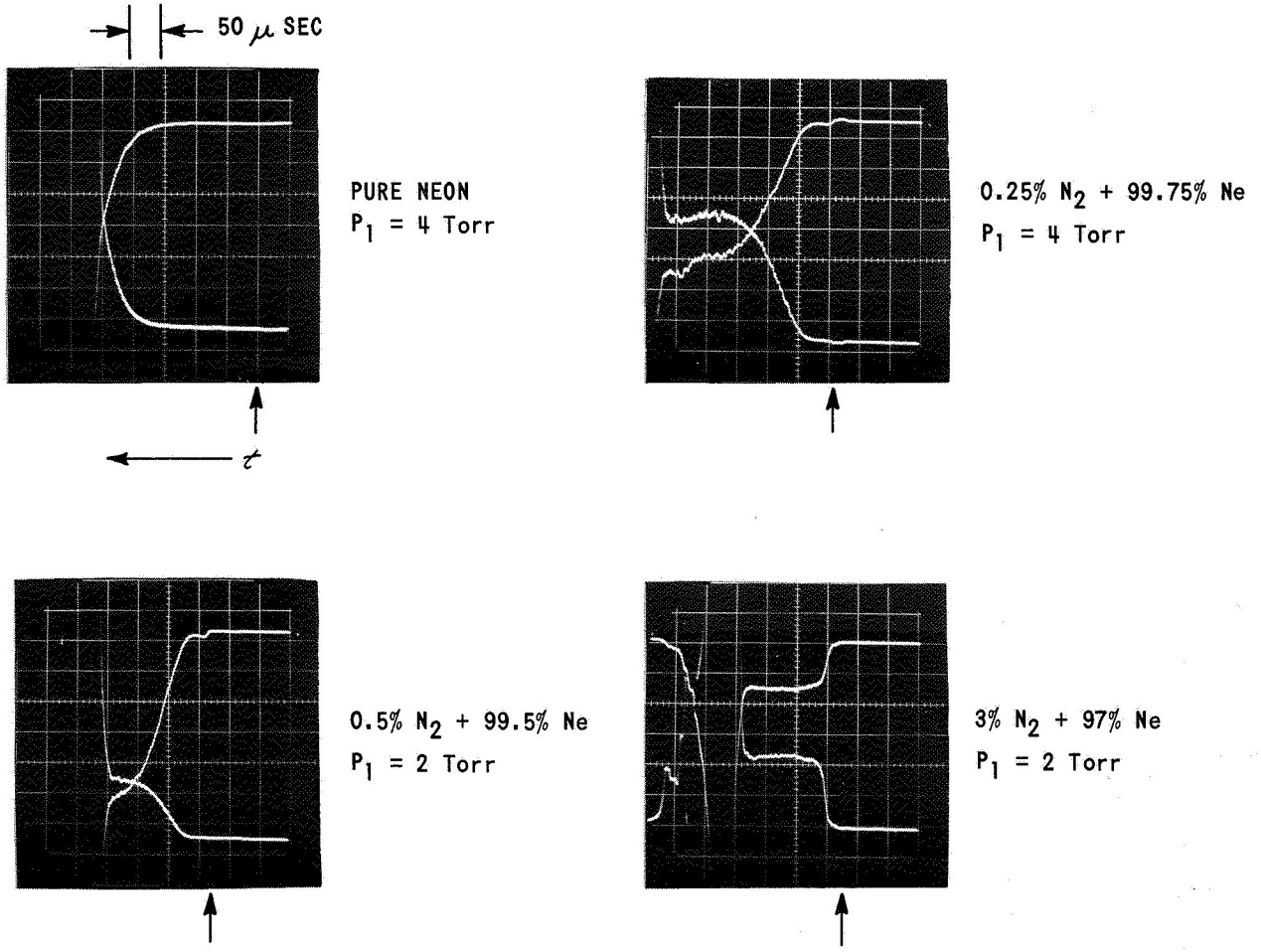

Figure 20 RADIATION PROFILES BEHIND REFLECTED SHOCK IN NITROGEN-NEON MIXTURES

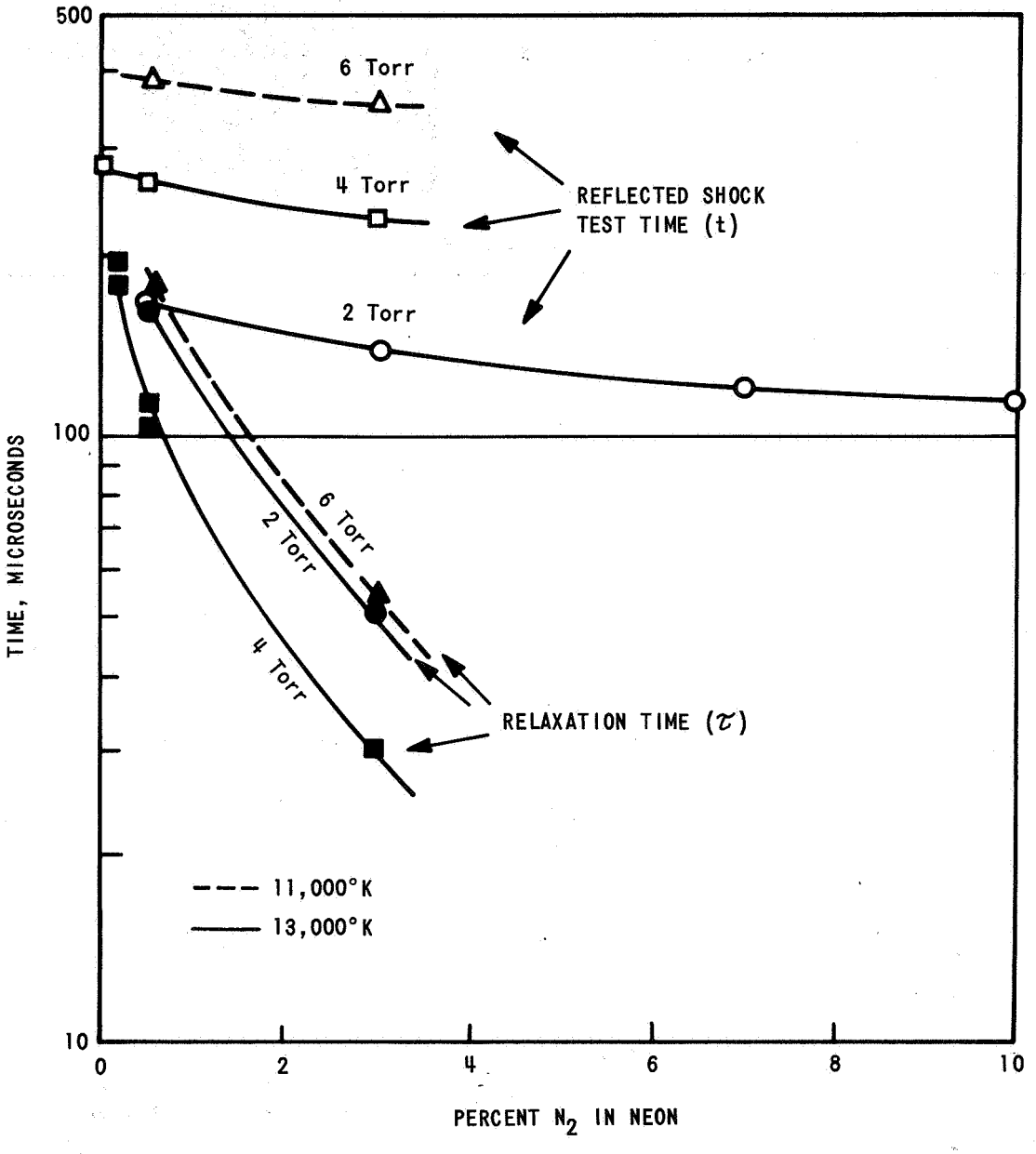

Figure 21 REFLECTED SHOCK TEST AND RELAXATION TIMES

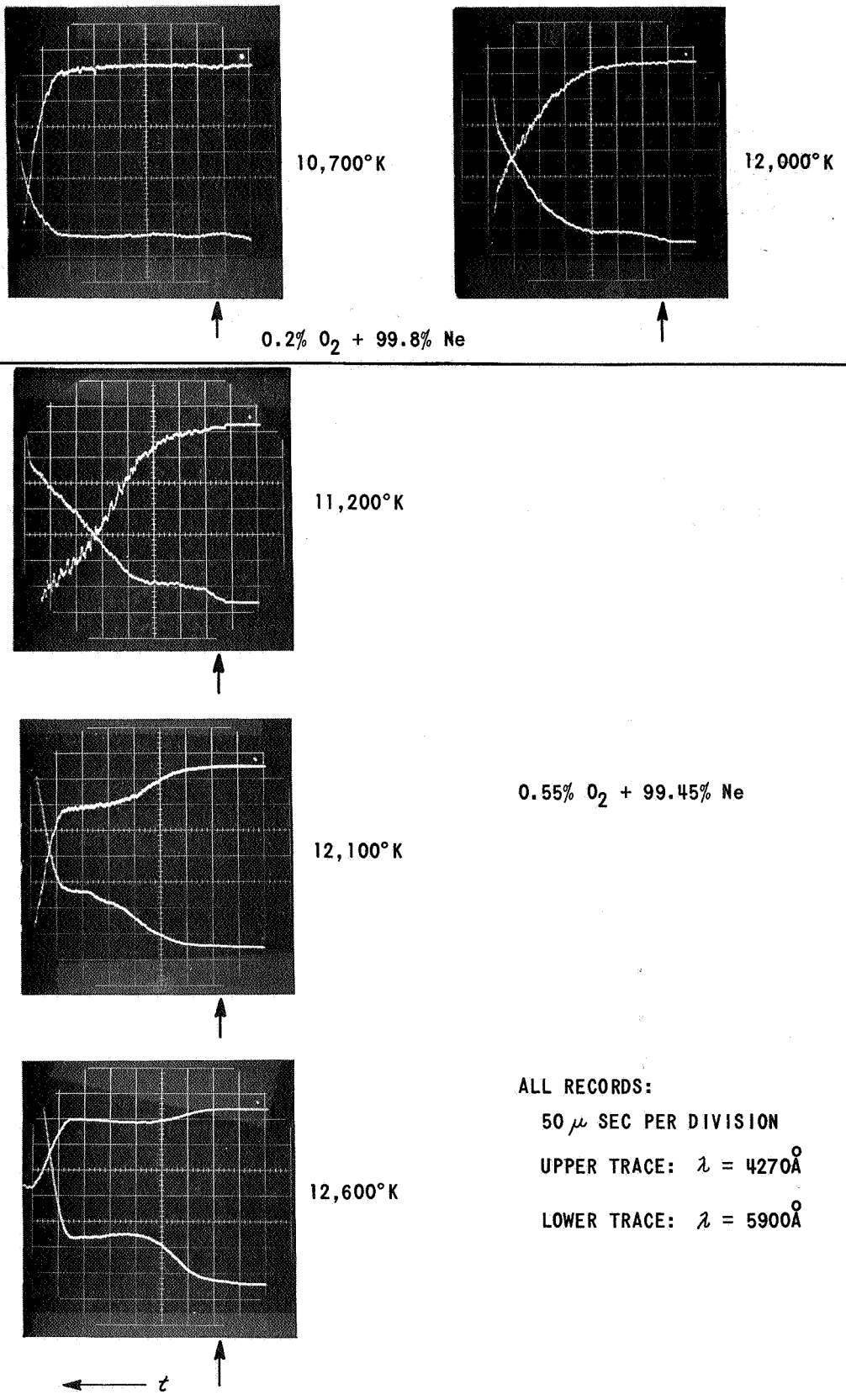

Figure 22 RADIATION PROFILES BEHIND REFLECTED SHOCK IN OXYGEN-NEON MIXTURES

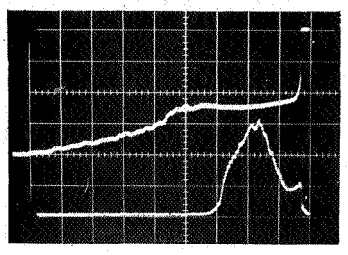

WALL TEMPERATURE

4270Å RADIATION

3% N_2 + 97% Ne
P_1 = 2 Torr
50 μ SEC PER DIV.

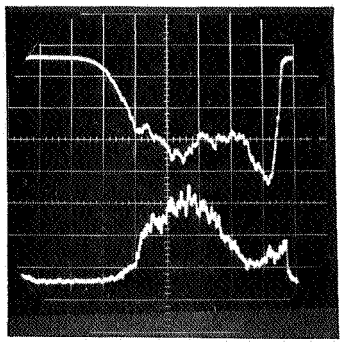

7100Å RADIATION

4270Å RADIATION

0.5% N_2 + 99.5%
P_1 = 4 Torr
50 μ SEC PER DIV.

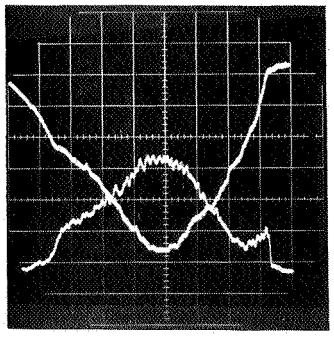

7100Å RADIATION

4270Å RADIATION

3% N_2 + 97% Ne
P_1 = 2 Torr
20 μ SEC PER DIV.

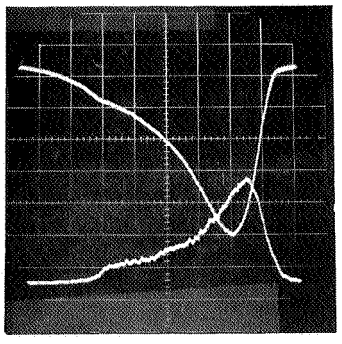

7100Å RADIATION

4270Å RADIATION

10% N_2 + 90% Ne
P_1 = 2 Torr
20 μ SEC PER DIV.

t

Figure 23 INCIDENT SHOCK RADIATION PROFILES FOR NITROGEN-NEON MIXTURES

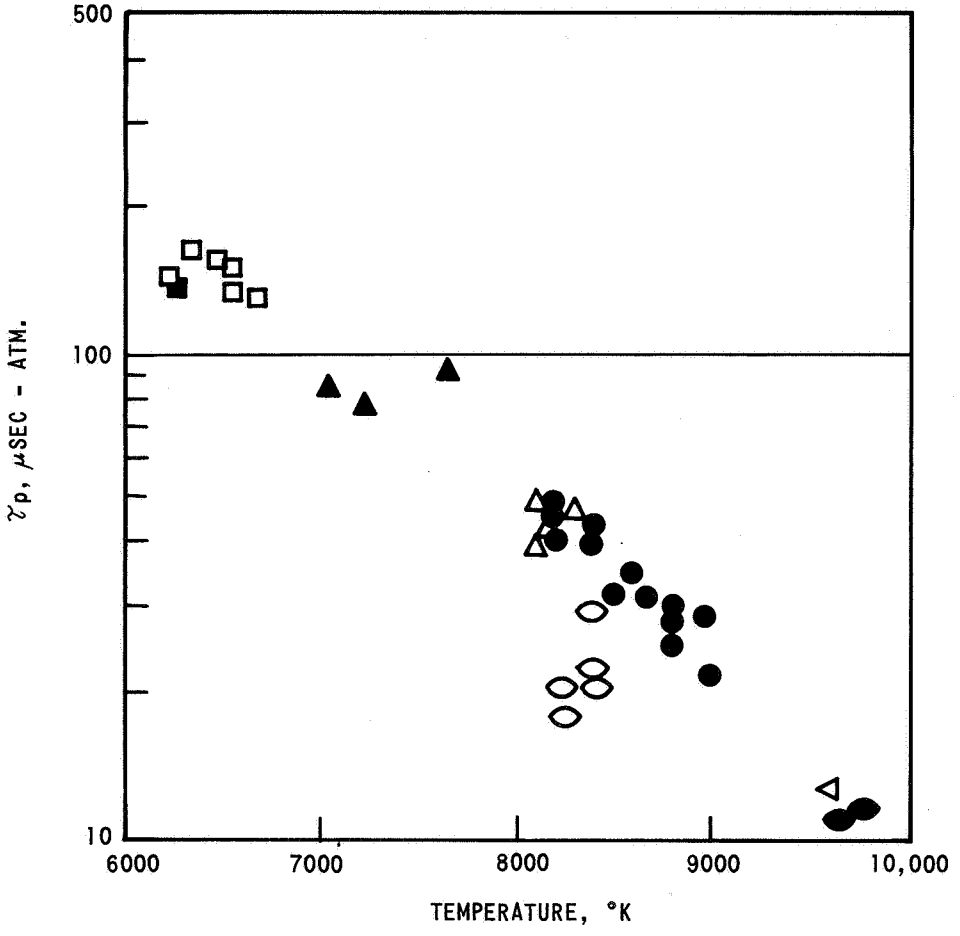

KEY:

- ● 10% N_2 + 90% ARGON AT 6 Torr REF. 28.
- ■ 0.5% N_2 + 99.5% NEON AT 6 Torr
- □ 3% N_2 + 97% NEON AT 6 Torr
- ▲ 0.5% N_2 + 99.5% NEON AT 4 Torr
- △ 3% N_2 + 97% NEON AT 4 Torr
- ○ 3% N_2 + 97% NEON AT 2 Torr
- ⬬ 10% N_2 + 90% NEON AT 2 Torr
- ◁ 7% N_2 + 93% NEON AT 2 Torr

Figure 24 TIME TO REACH PEAK RADIATION (7100 Å) BEHIND INCIDENT SHOCK WAVE.

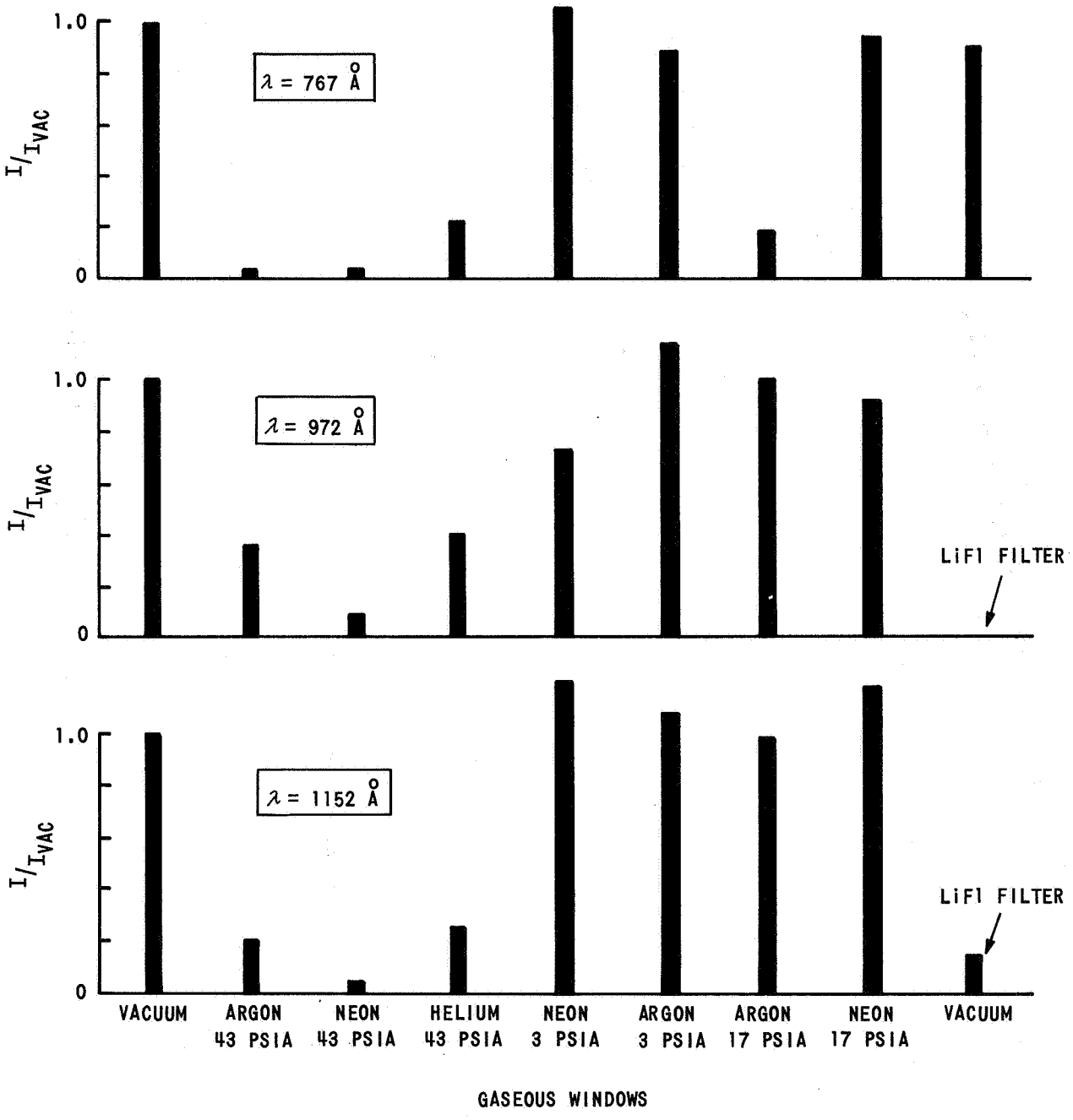

Figure 25 GASEOUS WINDOW PLUNGER EXPERIMENTS 5% ARGON + 95% NEON; T = 13,300 °K

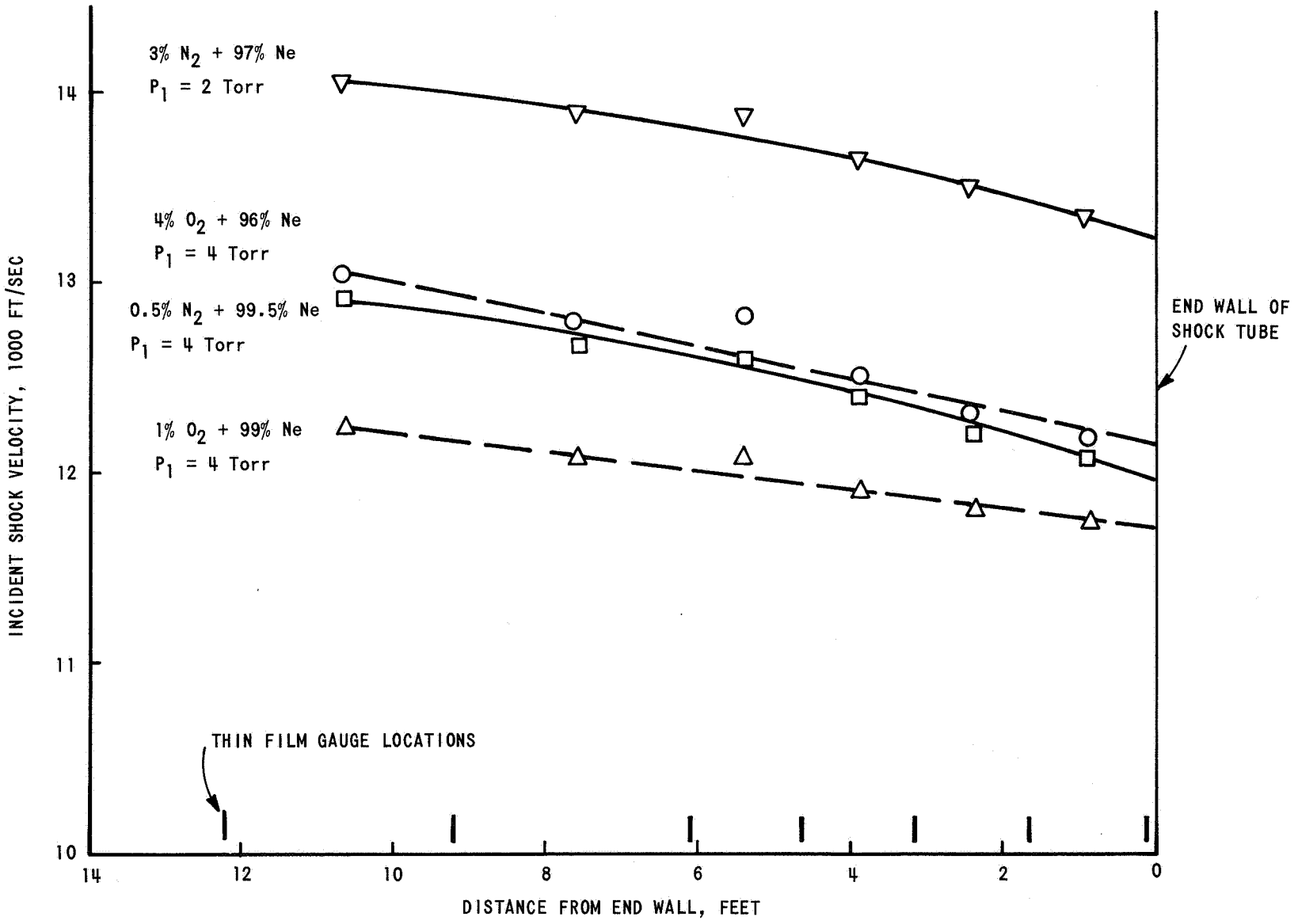

Figure 26 INCIDENT SHOCK VELOCITY

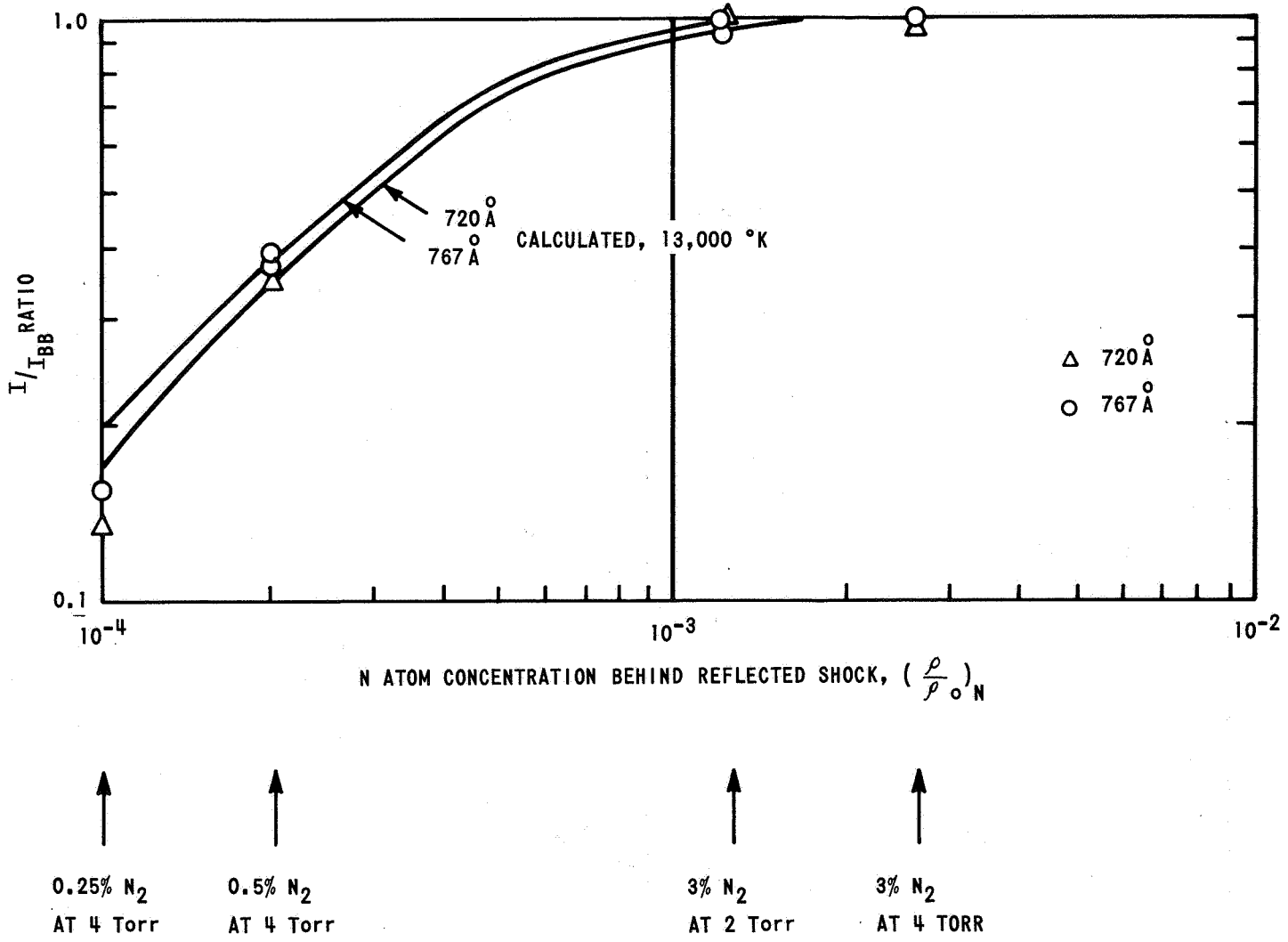

Figure 27 EXPERIMENTAL N ATOM EMISSION RATIO

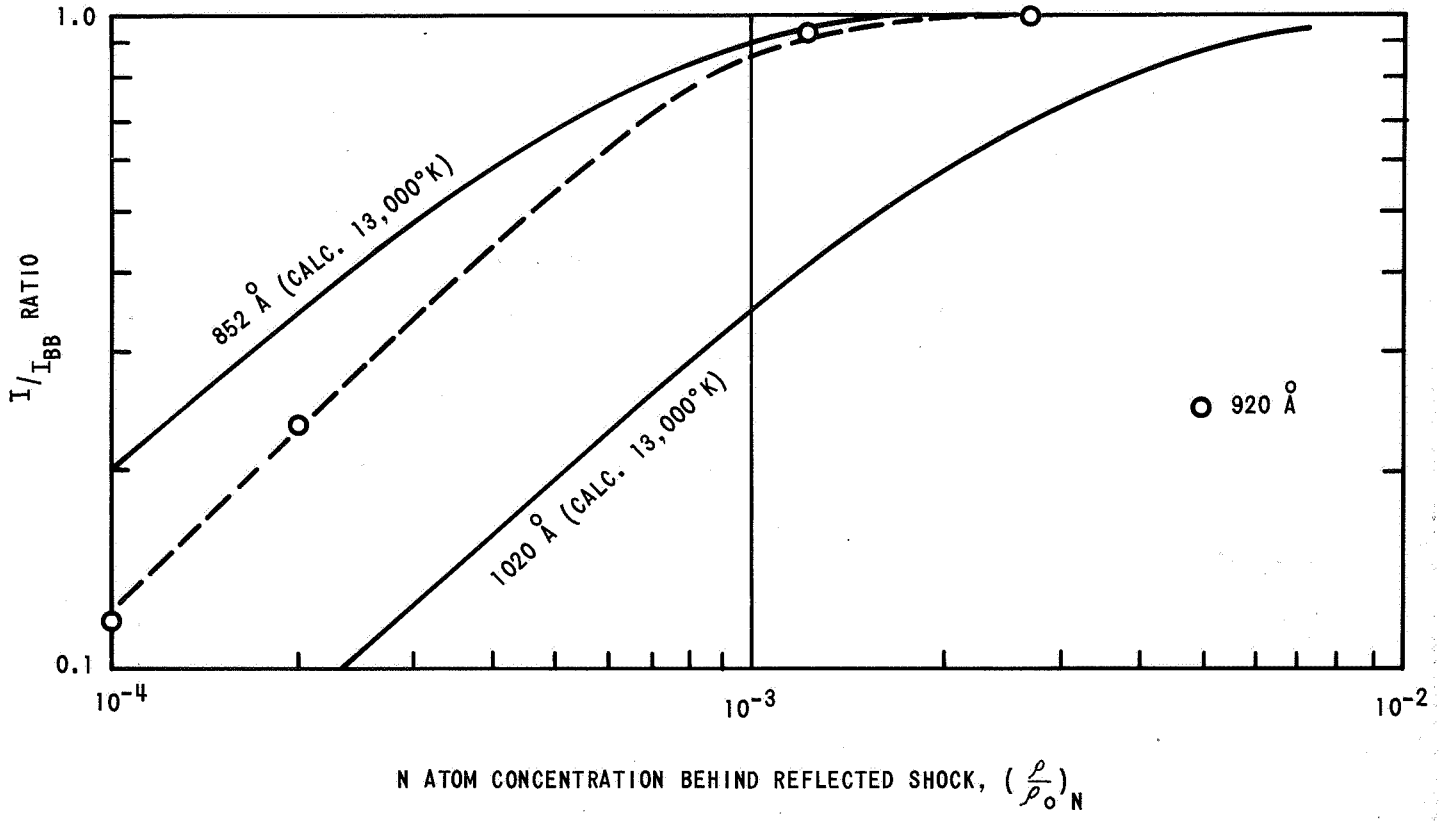

Figure 28 EXPERIMENTAL N ATOM EMISSION RATIO

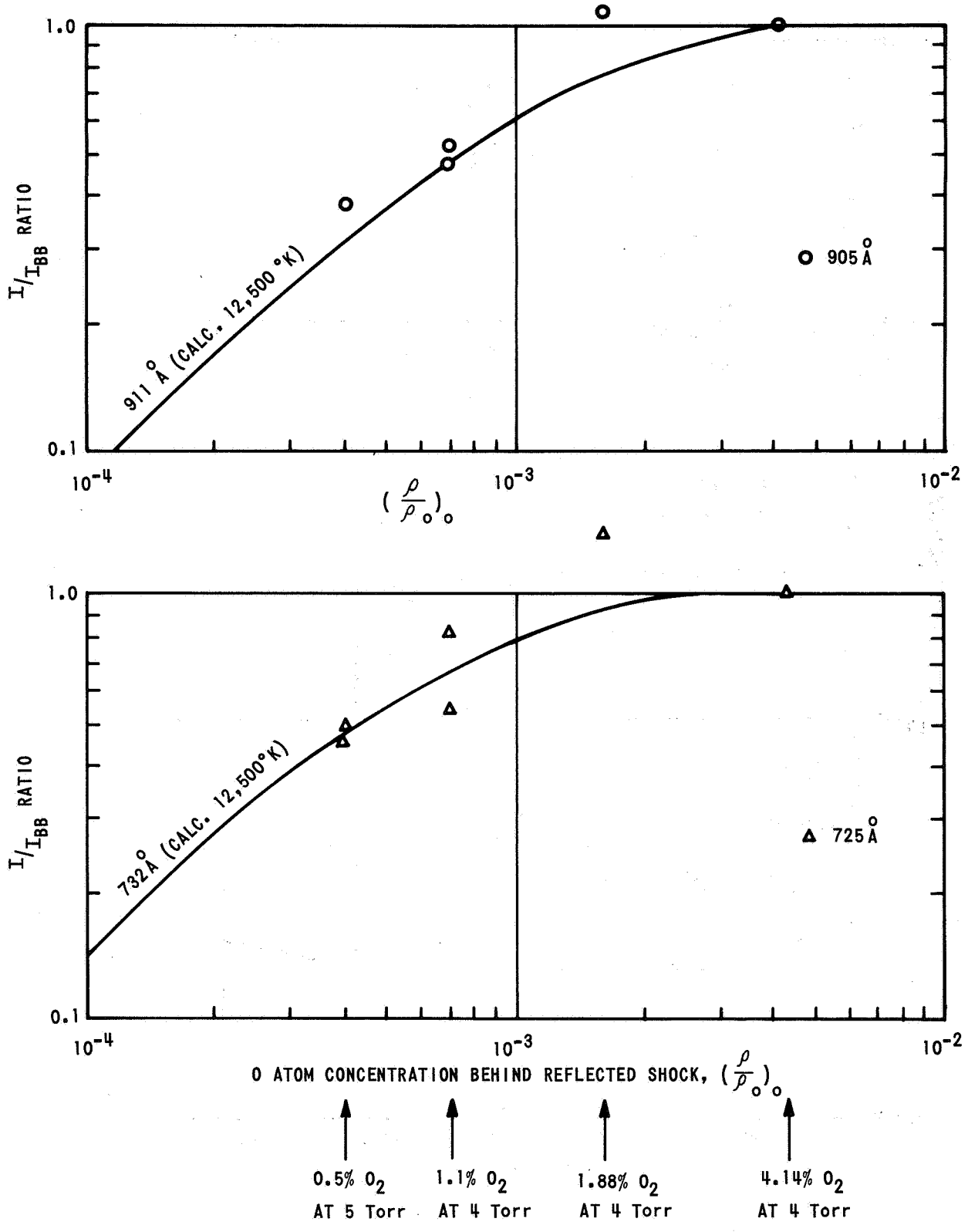

Figure 29 EXPERIMENTAL O ATOM EMISSION RATIO

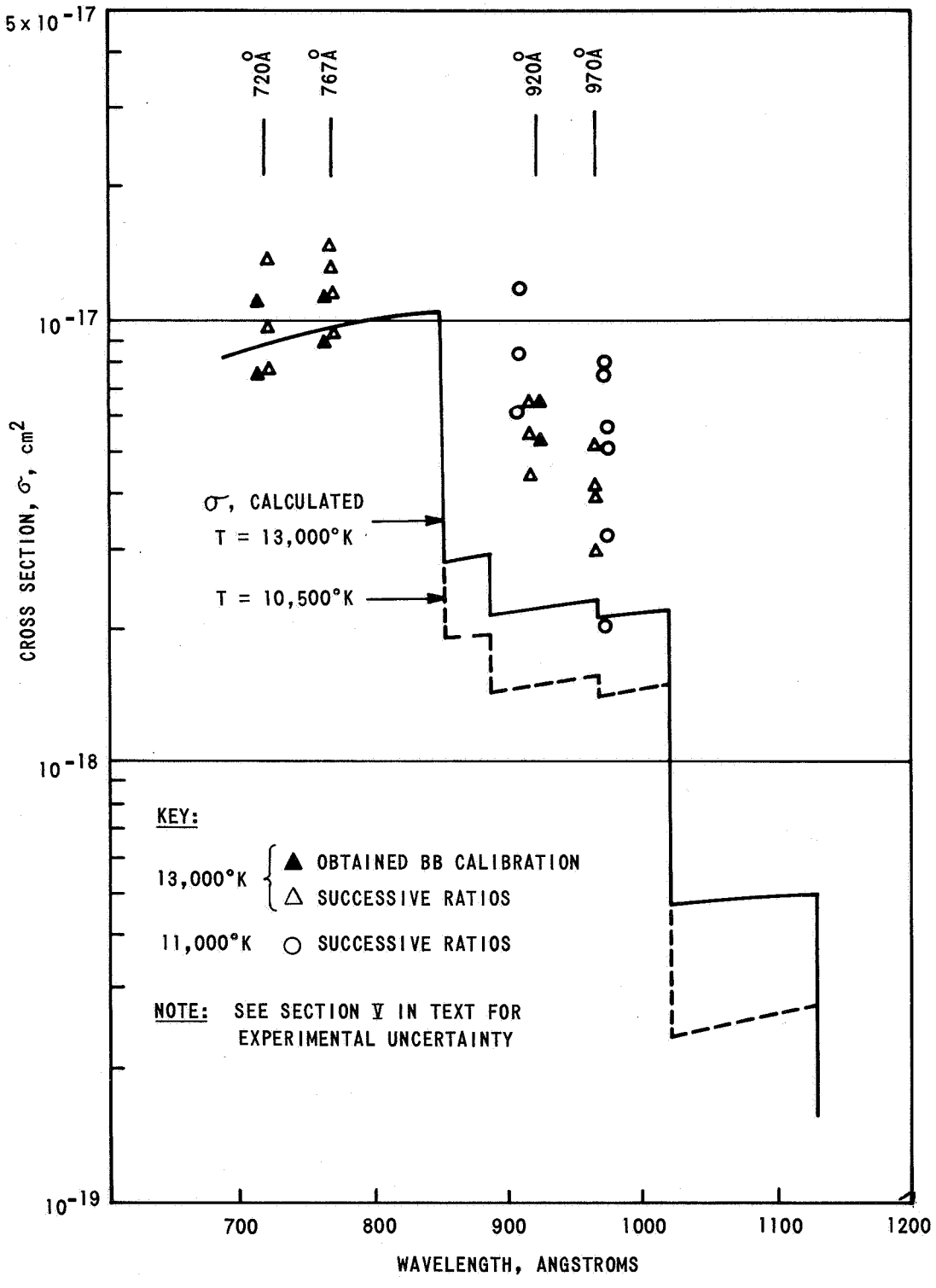

Figure 30 NITROGEN ATOM PHOTOIONIZATION CROSS SECTION

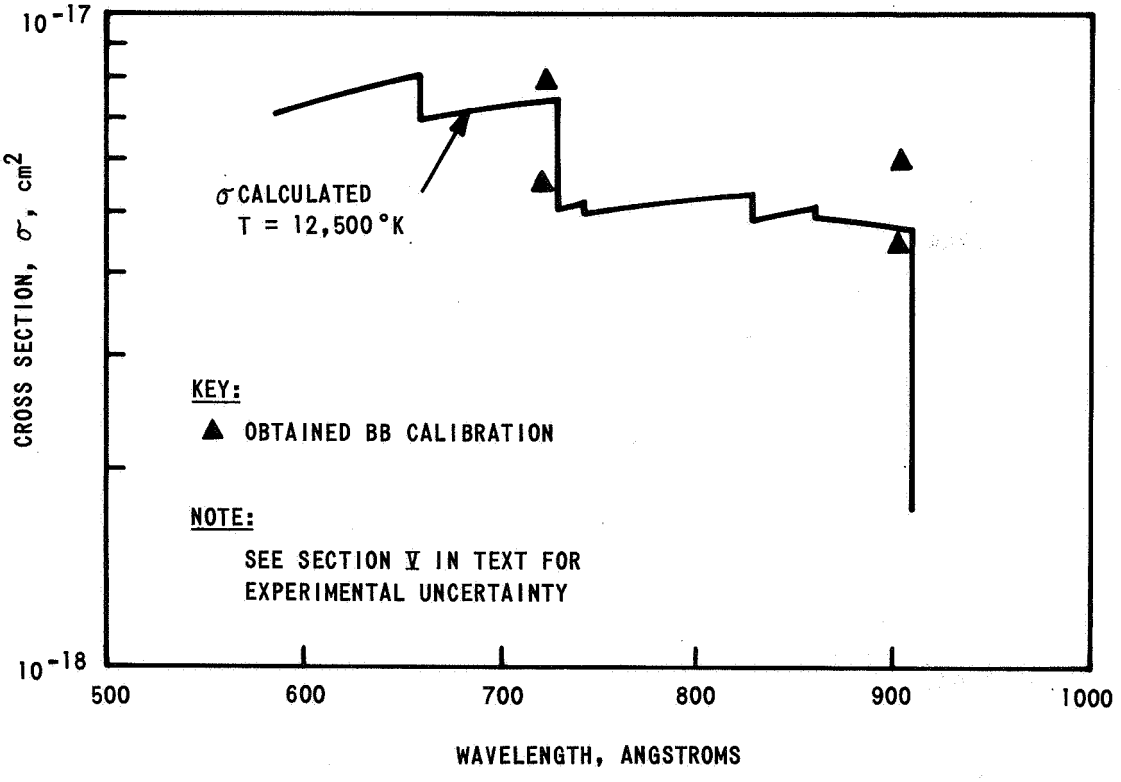

Figure 31 OXYGEN ATOM PHOTOIONIZATION CROSS SECTION

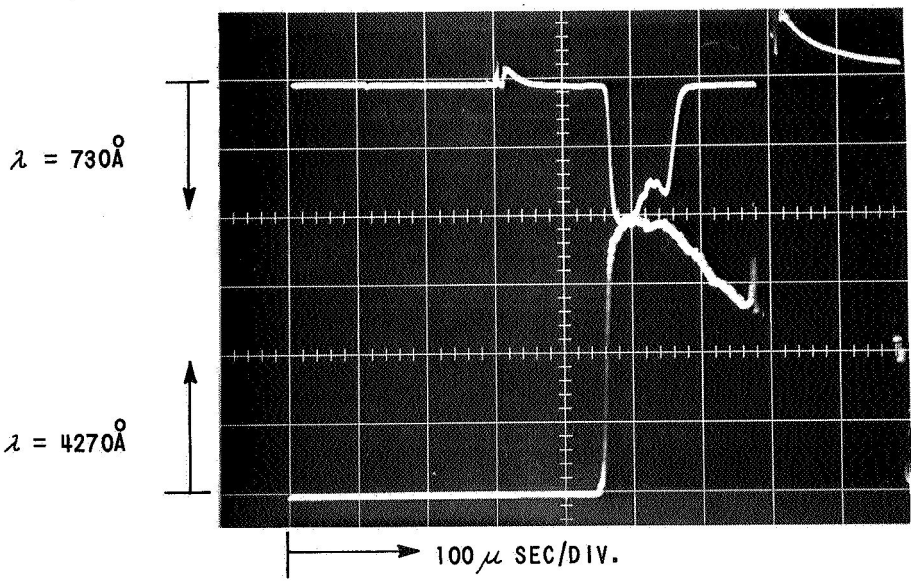

3% N_2 + 97% Ne

P_1 = 4 Torr

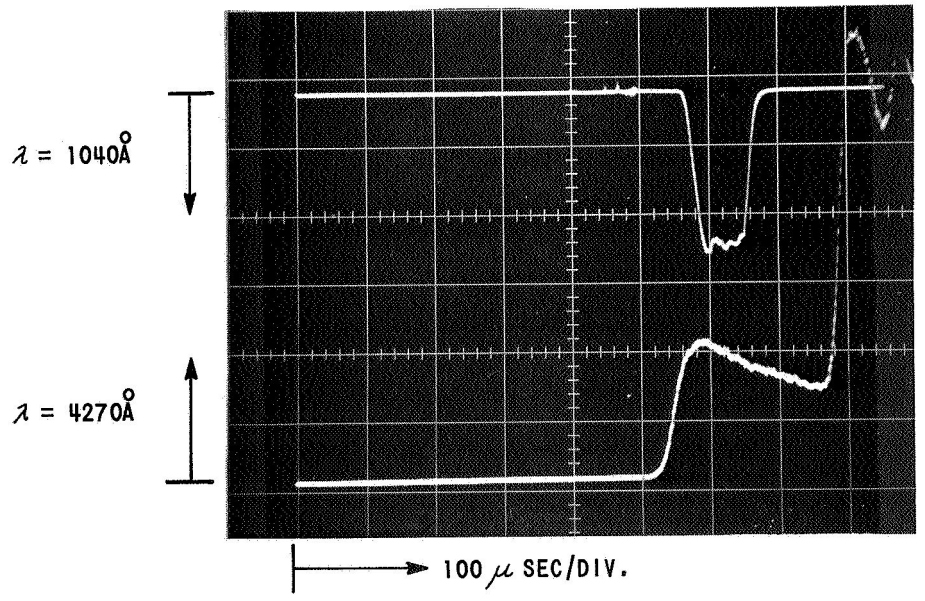

2% O_2 + 98% Ne

P_1 = 4 Torr

Figure 32 REFLECTED SHOCK RADIATION FOR NITROGEN AND OXYGEN

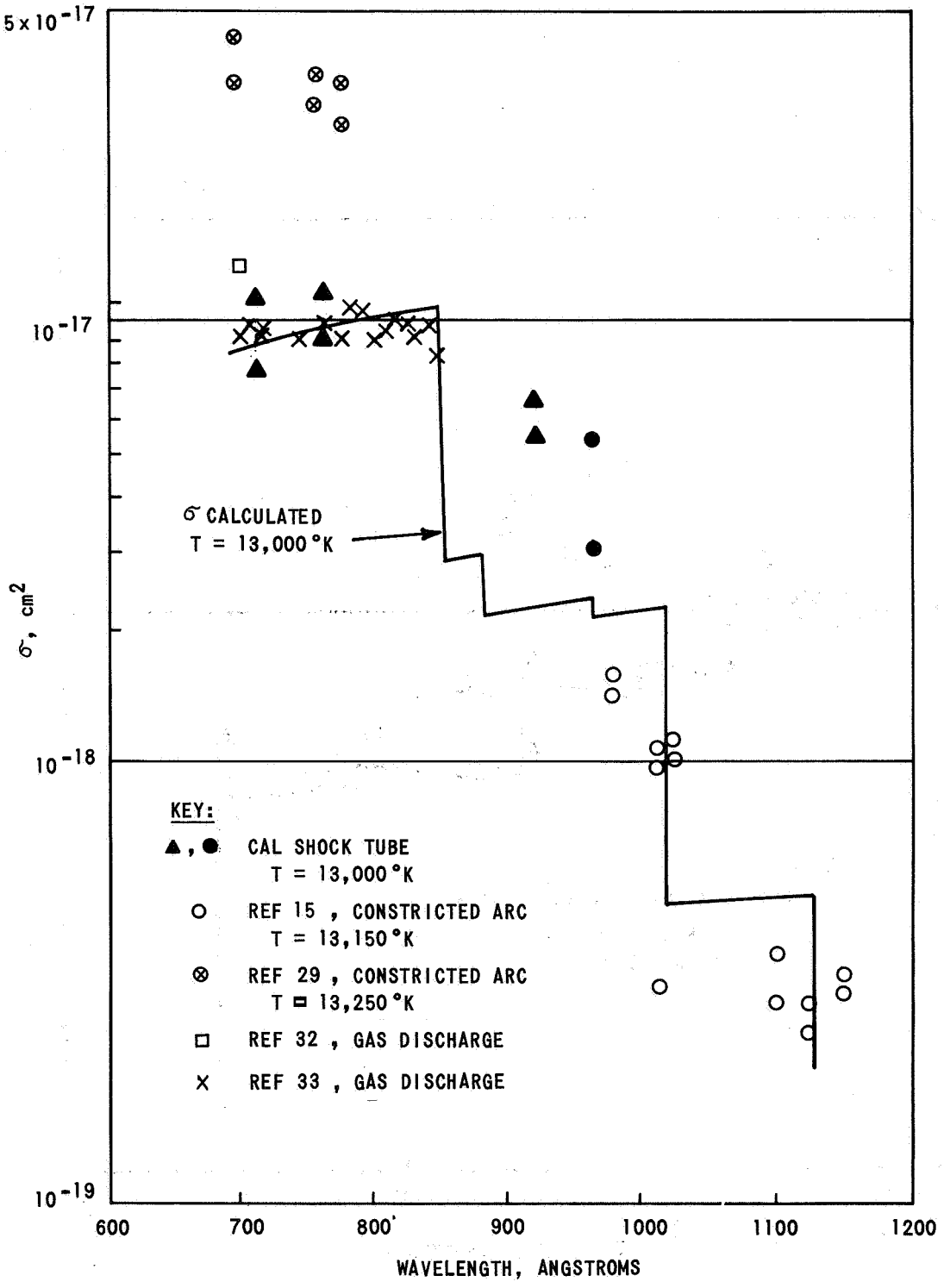

Figure 33 EFFECTIVE PHOTIONIZATION CROSS SECTION FOR NITROGEN ATOMS

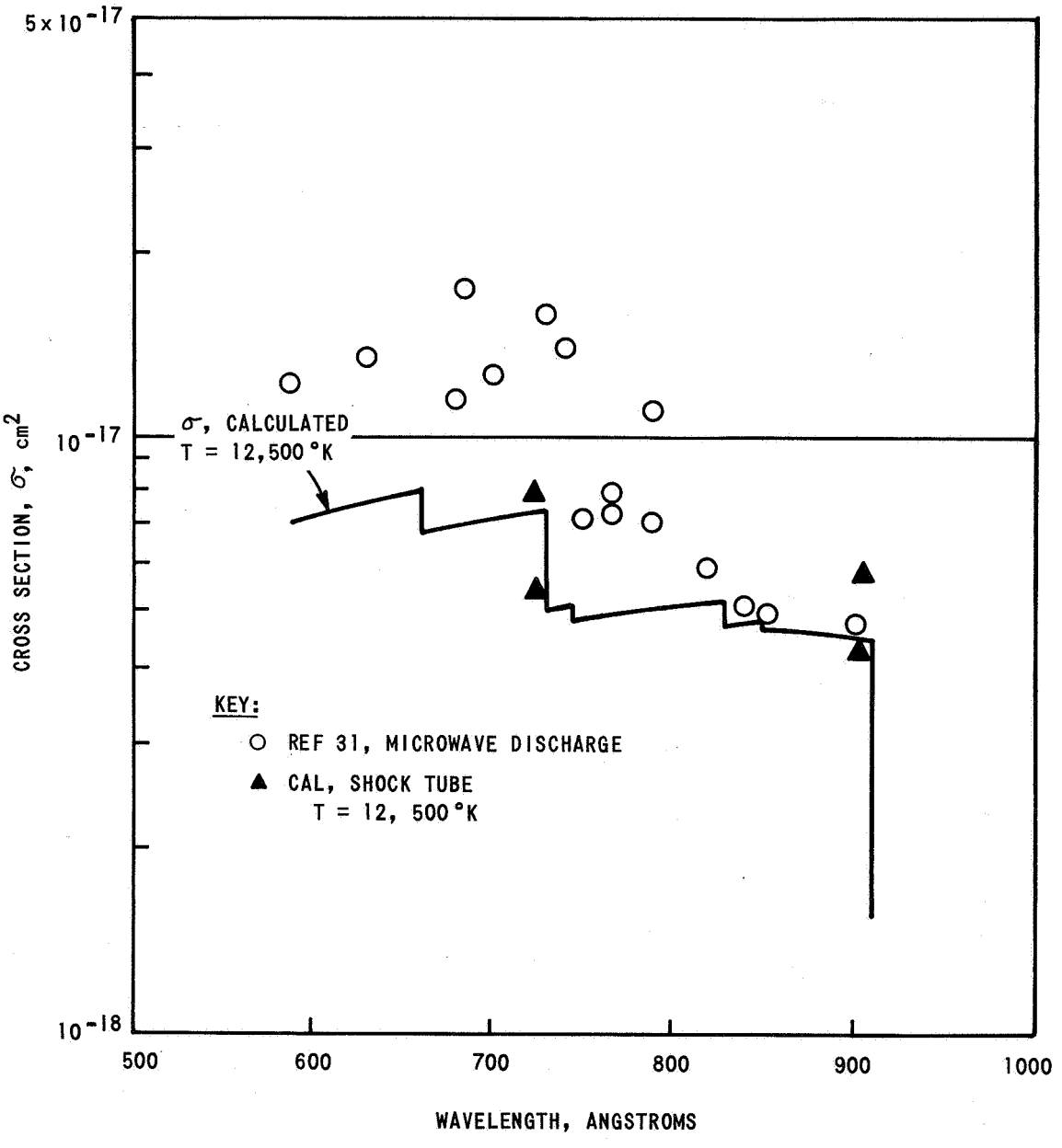

Figure 34 EFFECTIVE PHOTOIONIZATION CROSS SECTION FOR OXYGEN ATOMS